Improved Proximity Assays for Protein Quantitation

by

Jiaming Hu

A dissertation submitted to the Graduate Faculty of
Auburn University
in partial fulfillment of the
requirements for the Degree of
Doctor of Philosophy

Auburn, Alabama
August 3, 2013

Keywords: electrochemical proximity assay, biosensing,
point-of-care diagnostics, secretion sampling

Approved by

Christopher J. Easley, Chair, Assistant Professor of Chemistry
Curtis Shannon, Professor of Chemistry
Vincenzo Cammarata, Associate Professor of Chemistry
Wei Zhan, Associate Professor

Abstract

The work presented in this dissertation is focused on the development of proximity assay formats for biosensor applications in medical diagnostics, biological research, and point-of-care testing. An electrochemical proximity assay (ECPA) was developed for direct detection of a wide variety of target proteins. The detection limit of antibody-based reusable ECPA for insulin was 20 fM, which is lower than commercially available ELISAs, with a dynamic range through 6.25 nM, more than two orders of magnitude wider than the ELISAs. These improvements come with the added benefit of direct electrochemical readout. The measurement of hormone secretion from endocrine tissue via reusable ECPA and characterization by surface plasmon resonance (SPR) permit ECPA to be utilized in secretion sampling or high-throughput screening applications.

Chapter 1 introduces basic concepts and common types of biosensors, the origin of the concept of proximity assay which plays a crucial role in ECPA, the reason of choosing DNA for the development of ECPA model systems, and the properties of apamers and antibodies as bioreceptors in biosensor technologies. In chapter 2, a simple and rapid automated microchip electrophoresis method was developed for measurement of dissociation constants of DNA aptamers against proteins and small molecules. Chapter 3 is mainly focused on the DNA model systems used for the development of asymmetric proximity ligation assay (PLA) and ECPA. Predictions from these model systems greatly promoted improvement of assays for detection of human thrombin,

insulin and other biomolecules. The electrochemical proximity assay is presented in Chapter 4, where the first generation of ECPA is composed of two thrombin aptamers/insulin antibody-oligonucleotide conjugates which form a cooperative complex only in the presence of target molecules, moving a methylene blue (MB)-conjugated oligonucleotide close to a gold electrode. Without washing steps, electrical current is increased in proportion to the concentration of a specific target protein. A faster, easier and reusable ECPA is then introduced in Chapter 5, where regeneration of the base DNA monolayer was accomplished enzymatically. Uracils were incorporated into selected probe strands, and these strands were enzymatically cleaved using a uracil-DNA excision mix. This allows measurement time to be reduced 30-fold for aptamer-based assay, from 90 min to 3 min, without significant loss of sensitivity. The measurement of hormones in blood serum and from secretions by pancreatic islets shows that ECPA could be a powerful tool for fundamental biochemistry, clinical analysis, or high-throughput screening applications. These works are not meant to be final, and proposals to include ECPA into an electronic device or to integrate ECPA with other detection technologies are outlined in Chapter 6.

Acknowledgments

When I crossed the Pacific from China to the United States and entered into Auburn University, fate tied me and this quiet campus tightly together. In the past five years, I have been happy to spend this part of my youth at Auburn University.

I have a grateful heart toward all my teachers, classmates, friends and family. I must admit that I stared at the word “Acknowledgement” on my computer screen for a long time without writing any words, and I don't know whether "Acknowledgement" can express the deep gratitude in my heart. First of all, I would like to thank my advisor, Dr. Christopher J. Easley, a scholar full of wit, an elder of kindness, and a friend of the heart. He uses strict solid research to explain his academic viewpoints, a warm heart to teach me the ways of getting along with people, and a tolerant mind to remind me how to face life with a smile. His unique personality charms, infects, and inspires me. I would like to thank Dr. Curtis Shannon for his funny, open-minded wisdom that has deeply affected me, and acknowledge that this two years’ collaboration has given me a much deeper understanding of electrochemistry. I would like to thank Dr. Vince Cammarata for his carefulness, rigorous persistence, and keen insight, which has let me see a scholar’s infinite love in the academic study. I would like to thank Dr. Wei Zhan, whose experience of life and humble attitude has brought influence and guidance to my study

and my life. And also I would like to acknowledge Dr. David Stanbury for generously providing instrumentation for some of my experiments.

In particular, I would like to offer my sincere gratitude for all members of the Easley group (past and present) (Dr. Joonyul Kim, Dr. William Ashby, Jessica Crumbley, Kennon Deal, Cheryl DeJournette, Leah Godwin, Abdul Sajib, Jean Negou, Subramaniam Somasundaram, Xiangpeng Li, Zac Keenum, Lauren Hoepfner, Louis Jackson, Haley Medlen, Ferdous Torabinejad, Amanda Kelley, Ricky Scheuerle, Rebecca Sollie, Meagan Pilkerton, and Terrance Weeden), I feel very honored to be a member of this big family which has made me feel full of strength in my continuing road of study. And special thanks go to Yajiao Yu and Ferdous Torabinejad, who have accompanied me in finishing my last project, as well as Tanyu Wang who graduated last year, with their help instrumental in the success of the ECPA project.

At last, I would like to acknowledge my family for their generous support. They have been one of the most important sources of encouragement and love. And I would like to express my immeasurable appreciation to my wife, Na Chen, for her unconditional love and constant support during the years of my graduate study. I dedicate this dissertation to the ones I love and respect.

Table of Contents

List of Figures

List of Tables

CHAPTER 1

Introduction

1.1 Motivation for Research

The term "proteome" became popular after the draft of human genome was done in 2003. Although it has long been known that protein levels are of fundamental importance in biological function, technologies for protein separation, detection and quantitation have seen accelerated development with research into the human "proteome."

For protein separation, 2-dimentional gel electrophoresis was the core technology used in 1980s. Even today, it is still a very common separation method in clinic and research laboratories. Sodium dodecyl sulfate polyacrylamide gel electrophoresis (SDS-PAGE) and liquid chromatography (LC) have both progressed in technological development. For protein identification, mass spectrometry (MS) has been a popular choice, and the technology of GC-MS and LC-MS realized the integration of protein separation and detection.[1-3] However, these analytical methods require expensive, bulky, and complicated instruments. Another useful method for protein quantitation is surface plasmon resonance (SPR), the advantages of which are not requiring markers or dyes, reaction process can be monitored in real-time and fast. However, this optical method is sensitive to the environment, such as light and temperature conditions, and also sensitive to the mobile phase composition, such as ion concentration, and contaminants.

In recent years, the frequent exposure of global food safety problems and outbreak of new diseases require more accurate food quality control methods and new diagnostics. Those medical diagnostics and food safety depend on methods that can detect and quantify disease-related proteins and contaminants, often at very low concentrations. In this light, development of improved methods with high-throughput, high sensitivity, and high accuracy is a main direction for protein detection research.

1.2 Commonly used Protein-Based Detection Methods

Western Blotting

The name "Western Blot", like "Northern Blot", came mainly from scientists' sense of humor. In 1975, Edwin Southern introduced a powerful DNA transfer and probing technique,[4] which was named "Southern Blot" after its inventor. In 1977, George Stark and his co-workers successfully transferred cellular RNA to chemically activated cellulose paper.[5] This technique was name "Northern Blot" – as a pun on Southern's name. In 1979, George Stark developed an early protein blotting technique, which relied on capillary transfer from gel to cellulose paper.[6] After that, Harry Towbin developed a faster and simpler technique for electroblotting proteins to nitrocellulose membranes,[7] which is still widely used today. In 1981, W. Neal Burnette[8] first gave a name to Stark and Towbin's technique – "Western Blot". At this point, the "Western Blot" technique is about 32 years old, yet it has changed very little since Towbin's modifications. In 2008, Mathias Mann published a paper entitled "Can Proteomic Retire the Western Blot?".[9] In his view, mass spectrometry can cover most cellular proteins in a quantitative experiment[10] which contains the ones detected by western blotting. However, with the

improvement of gel electrophoresis, membrane technology and increased commercial antibodies, especially the appearance of higher affinity antibodies, the dynamic range of western blotting has been extended. Western blotting has become a simpler, diverse analysis method, and it is a very useful quantitative tool. Because of its cheap equipment and mature technology, the Western Blot will be used for protein detection for a long time, and it already has been applied to detection of HIV, bovine spongiform encephalopathy (BSE), lyme disease, hepatitis and other diseases.[11-13]

More specifically, Western blotting is a technique of protein separation and detection by integrating gel electrophoresis, electrophoretic transfer, and antibody-based probes. It uses gel electrophoresis to separate native proteins by 3-D structure or denatured proteins by the length of the polypeptide. The proteins are then transferred to a solid support, where they are stained with antibodies specific to the target protein, detecting the target proteins from the protein mixture. Thus, the method qualitatively or quantitatively determines target proteins expressed in cell or tissue. There are various protocols for Western blotting, but more or less, it has several basic steps as shown in Figure 1-1A. 1) Sample preparation; as we know, proteins are composed of a variety of amino acids, which have amino, carboxyl groups and charged R groups, so different proteins have different charges. If we want the protein mixture to move towards the same direction, it has to be treated. The commonly used reagent is sodium dodecylsulfate (SDS), which is an anionic detergent that denatures secondary and nondisulfide-linked tertiary structures, thus unfolding and linearizing the proteins completely, and it coats proteins with many negative charges. This way, the proteins can be separated in an electric field strictly by their length or size, respectively. 2) Electrophoresis; the

denatured proteins are placed into the lanes of the stacking site of a polyacrylamide gel, and put into an electric field, so they will move towards the positive pole at different rates. 3) Blotting: transfer to solid support; after proteins separated, they are transferred to a solid membrane to ease labeling and detection steps. 4) Blocking; the used membranes must be treated to block nonspecific binding between probes and the material. 5) Hybridization; adding the antibody-based probes to the blocked membrane. In Western blot, the secondary antibody can be added after the unbound primary antibody is removed by washing the memebrane. 6) Detection; an enzyme linked onto the secondary antibody will catalyze the production of a chemiluminescent or strongly absorbing agent in proportion to the amount of bound protein (Figure 1-1B).

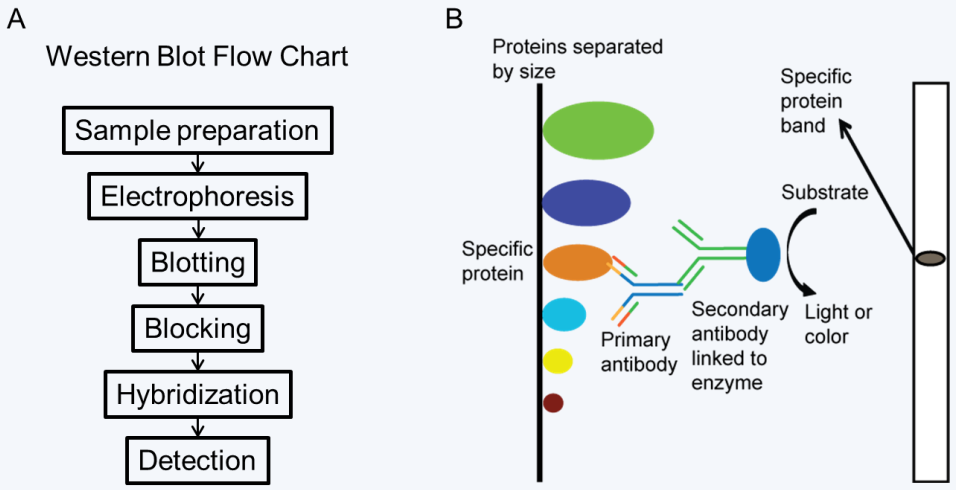

Figure 1-1: Western blot. A) Western blot flow chart. B) Enhanced chemiluminescence detection for blotting analysis.

Enzyme-linked immunosorbent assay (ELISA)

In 1971, Engvall et al. used cellulose and polystyrene tubes as the solid phase carrier for antigen or antibody adsorption, and they established an enzyme-linked immunosorbent assay, referred to as ELISA. Since then, the move to well-plate ELISAs has greatly improved the experimental throughput.[14] ELISA has high flexibility. In the actual operation, people can perform various kinds of ELISA reactions, according to their own needs and materials on hand. Also, the reagents and supplies for ELISA experiments have been commercialized, and the equipment has been more-or-less standardized. Automation has further improved ELISA, which has become the core method for disease diagnostics in clinical laboratories. Many authoritative international organizations list it as one of the priority analysis techniques.[15]

ELISA is an enzyme immunoassay in the stationary phase. For this, there are three important requirements. First, proteins must be adsorbed onto the stationary phase without changing its activity; second, the antigen or antibody must still maintain its activity after crosslinking with an enzyme; and third, after cross-linking, enzymes must efficiently react with the substrate to produce a colored or luminescent substance or generate light in the reaction.

Public opinions on classification of ELISAs are divergent. Different literatures have different opinions about the classification of ELISA from the principle and operation. Here, ELISA is divided into the following three categories, then for each class is explained in detail: (1) direct ELISA; (2) indirect ELISA; (3) sandwich ELISA. (Figure 1-2) Direct ELISA can be regarded as the simplest type of ELISA. In direct ELISA, the antigen is adsorbed to a plastic plate, then an excess of other protein (using bovine serum

albumin) is added to block all the other binding sites. Then an enzyme is linked to an antibody in a separate reaction. The enzyme-antibody conjugate is allowed to adsorb to the antigen, then excess enzyme-antibody conjugate is washed off, leaving enzyme-antibody bound to antigen in proportion to the antigen concentration. By adding the enzyme's substrate, the enzyme is detected and thus the antigen. The advantage of direct ELISA is that it can be performed faster, because only one antibody is being used and fewer washing steps are required. This can be used to test specific antibody-to-antigen reactions, and helps to eliminate cross-reactivity between other antibodies. But, in direct ELISA, the primary antibody must be labeled individually, which can be costly, time-consuming, and inflexible when performing multiple experiments. Additionally, the signal is less amplified, which can be seen as a disadvantage. With a slight modification, indirect ELISA is a two-step method that uses a primary antibody and labeled secondary antibody. The primary antibody is incubated with the antigen followed by the incubation of the secondary antibody and corresponding washing steps. Although containing more steps, this allows more flexibility in operation with different analytes. However, both of these methods require immobilization of the antigen.

One of the most common types of ELISA is the "sandwich ELISA". The "sandwich" type measures the amount of antigen between two layers of antibodies (i.e. capture and detection antibody). The antigen to be measured must contain at least two antigenic sites capable of binding to an antibody, since at least two antibodies act in the sandwich.

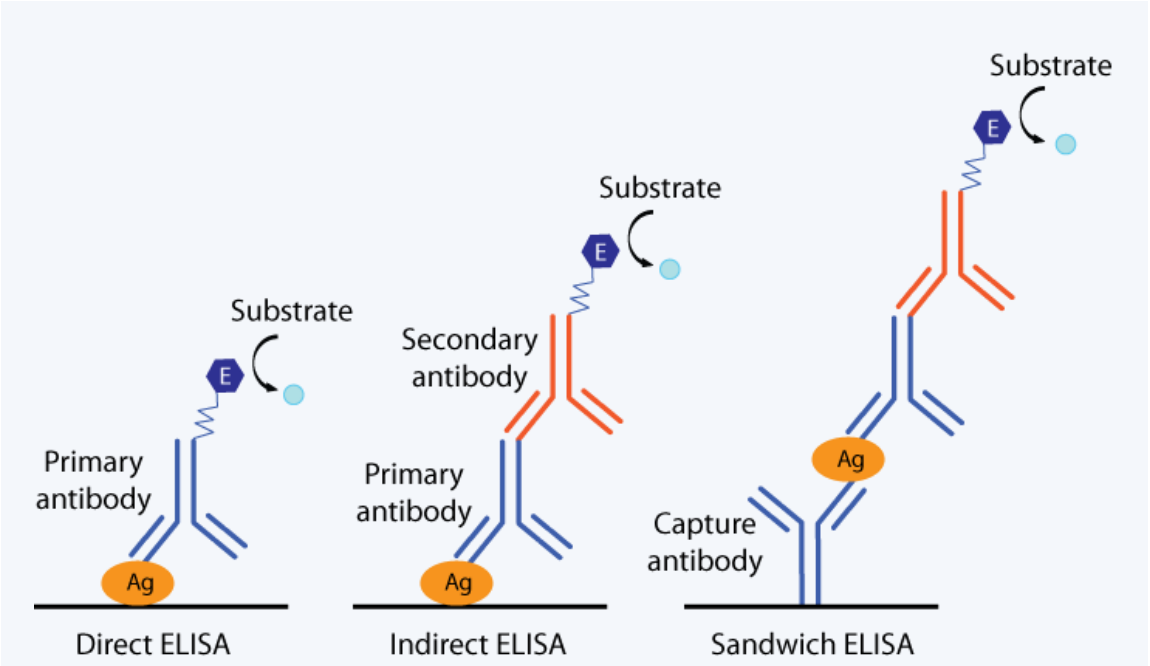

Figure 1-2: Common ELISA formats.

Figure 1-3 describes the protocol of sandwich ELISA: 1) The plate is coated with a suitable capture antibody, and the remaining protein-binding sites on plate are blocked; 2) sample is added to the plate, and any antigen present is bound by the capture antibody; 3) a suitable detection antibody is added to the plate and also binds to any antigen present in well; 4) an enzyme-linked secondary antibody is added, and it binds to the detection antibody; 5) a substrate is added and is converted by the enzyme to a detectable form. The sandwich ELISA has become one of the more popular versions due to its flexibility and propensity for automation. However, a disadvantage to all forms of ELISA is the need for multiple binding, coating, and washing steps, which also requires significant

expertise from the user. These requirements basically limit ELISAs to clinical laboratories rather than point-of-care or on-site measurements.

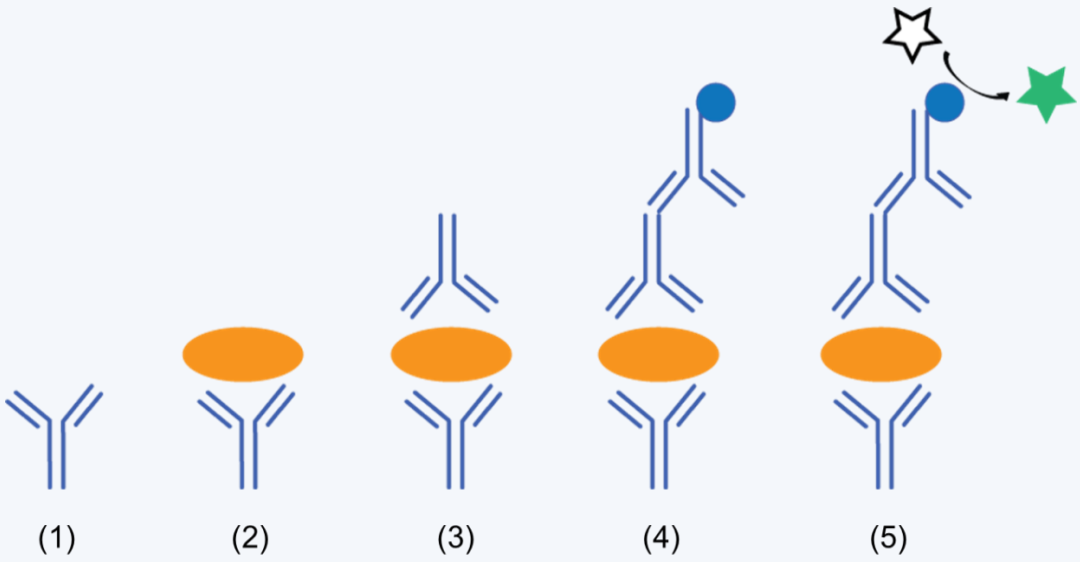

Figure 1-3: Protocol of sandwich ELISA.
Image modified from http://en.wikipedia.org/wiki/File:ELISA-sandwich.svg

Proximity Assay Concept

Advancements in science and technology tend to make complex things more simple over time. Users are never satisfied with the existing technologies. Although Western blots and ELISAs are very good methods for protein detection, the disadvantages are obvious. The operation process in both methods is complicated, and also needs multiple wash steps. So keeping the advantages of Western blots and ELISAs while avoiding the disadvantages becomes a challenge for assay development. In fact, Western blots and ELISAs can be considered the prototype of proximity assays.

Proximity assays have two characteristics: 1) two probes binding target molecule at different binding sites; and 2) signal based on some proximity-driven connection between the two probes. In our systems, taking thrombin as the target molecule for example, two probes can be aptamers or DNA conjugated antibodies binding thrombin at different sites. When pairs of probes bind thrombin, the free ends of their DNA sequence extensions are brought sufficiently close (into "proximity") to hybridize together to a subsequently added connector oligonucleotide. Alternatively, the signal DNA molecule binding to one probe can be brought close to another probe to hybridize together directly.

This coupling of dual-probe to target binding for protein detection was used in both Western blotting and ELISAs, and then developed into sandwich ELISAs. The proximity assay concept was first adopted in a report by Landegren's group. In 2002, their team developed a method for in vitro analysis of proteins and other macromolecules and termed the method proximity ligation assay (PLA).[16,36] By inspection of Figure 1-4, without much thought, one should realize that this assay is similar to the sandwich ELISA, where two probes bind the target molecule at different binding sites. In fact, the proximity ligation assay fundamentally depends on the simultaneous and proximate recognition of target molecules by pairs of probes. When the probes bind the target molecule, the ends of their DNA sequence extensions are brought close—into proximity—to hybridize to an added connector oligonucleotide. Next, the free ends are joined by DNA ligation, and the ligated products can be replicated by the polymerase chain reaction (PCR), giving an amplifiable detection signal in proportion to the original target protein's concentration.

Comparing to sandwich ELISA, based on Landegren's results, PLA has comparable sensitivity and detection limit for thrombin, and also it has a wider dynamic range. More importantly, this assay is homogeneous, does not need washing steps, making it a kind of single tube immunoassay. And in PLA, the sample preparation time is less than one hour, and the automated qPCR assay can be finished in two hours, so the technique is much simpler and faster than sandwich ELISA.

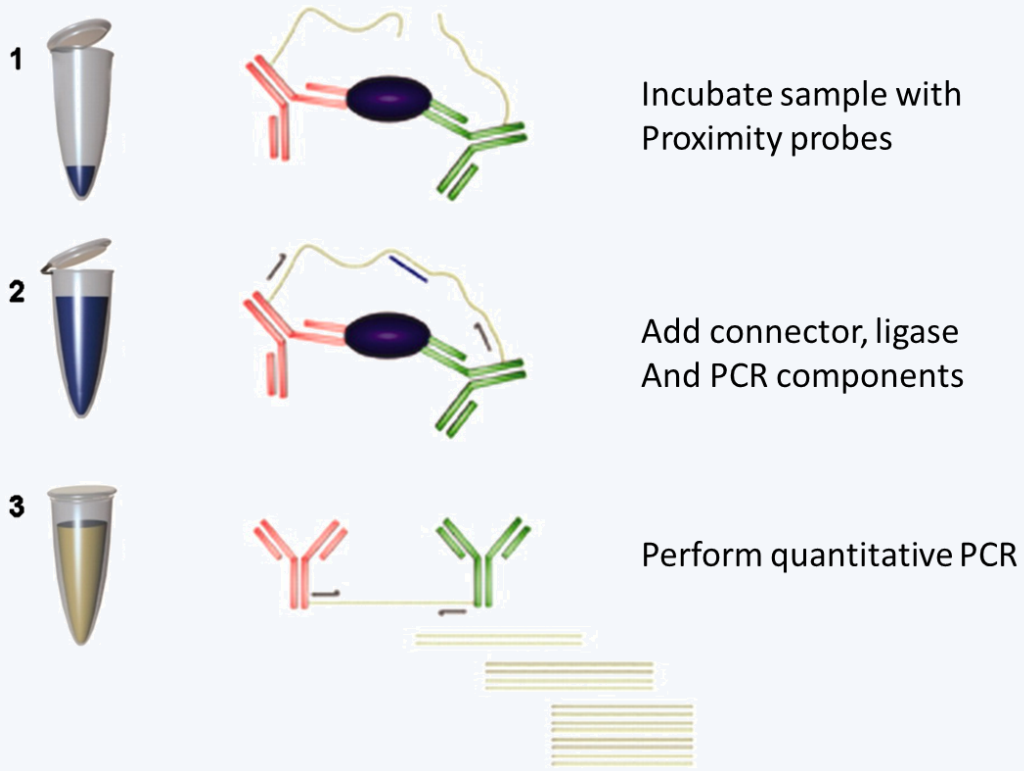

Figure 1-4: The principal steps of the proximity ligation assay (PLA). Step 1, incubation of sample with proximity probe pair; step 2, addition of all components required for ligation and detection by quantitative PCR; step 3, quantitative PCR.[36]

The assay obtains an amplifiable detection signal with a qPCR nuclease assay. A fluorogenic probe is frequently used in the nuclease assay, which contains an oligonucleotide to which a fluorogenic reporter dye and quencher dye are attached. (Figure 1-5) During the annealing phase in PCR, the labeled probe anneals to the target of interest between the forward primer and reverse primer sites. In the extension phase, the primers bind the DNA template, and a new DNA sequence is synthesized by DNA polymerase complementary to DNA template. The labeled probe is cleaved during extension phase, and the reporter dye will be separated from quencher dye, releasing highly fluorescent reporters.

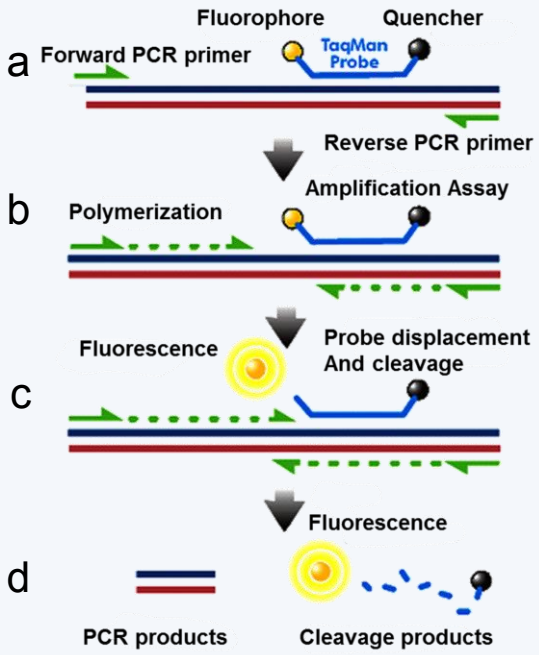

Figure 1-5: Nuclease assay (Taqman). a) annealing phase; b) extension phase I; c) extension phase II; d) end of PCR cycle.
http://upload.wikimedia.org/wikipedia/en/0/07/Taqman.png

In 2005, Tomasz Heyduk and his group developed another assay based on the proximity assay concept, termed "molecular pincers".[17] As shown in Figure 1-6, two different aptamers bind different sites of a protein target, and at the end of each aptamer, short fluorophore-labeled oligonucleotides (which were attached to the aptamers by non-DNA linker) are assembled. In the absence of the target protein, the two aptamer half-sites would not associate, since the number of complementary oligonucleotides was too

small to promote efficient annealing. When the half-sites of aptamers are bound to the target protein, it would bring the two signaling oligonucleotides close to each other, into relative proximity, increasing their local concentrations. This results in the annealing of the signaling oligonucleotides, which brings the fluorophore and the quencher (or FRET pair) into proximity, resulting in a change of fluorescence signal.

The development of proximity assays successfully overcomes some limitations of Western blots and ELISAs. It makes three breakthroughs: first, the assays are homogeneous, such that no wash steps are needed and measurement time and complexity can be greatly reduced. Second, the binding probes can be aptamers, not just antibodies. Third, the reaction can be done in a smaller tube, saving significant amounts of reagents. In PLA, these benefits were realized without loss of sensitivity compared to ELISA.

Figure 1-6: Molecular beacons for detection proteins. Molecular beacons for detecting proteins based on aptamers directed to two different epitopes of the protein.[17]

Reprinted with permission from Heyduk, E.; Heyduk, T. Anal. Chem. 2005, 77, 1147-1156. Copyright © (2013) American Chemical Society.

1.3 DNA as a Bioengineering Material

Due to in the following chapters, multiple DNA sequences are used in the model systems for assay development. For this reason, it is necessary to mention the basic concepts of DNA and its interactions.

DNA biotechnology, arising in the 1980s, is defined bytechnical developments, which are improving at a rate as fast or faster than improvements in computing technology. “Carlson’s Law” shows that the prices of DNA synthesis and sequencing are dropping exponentially in time (Figure 1-7).

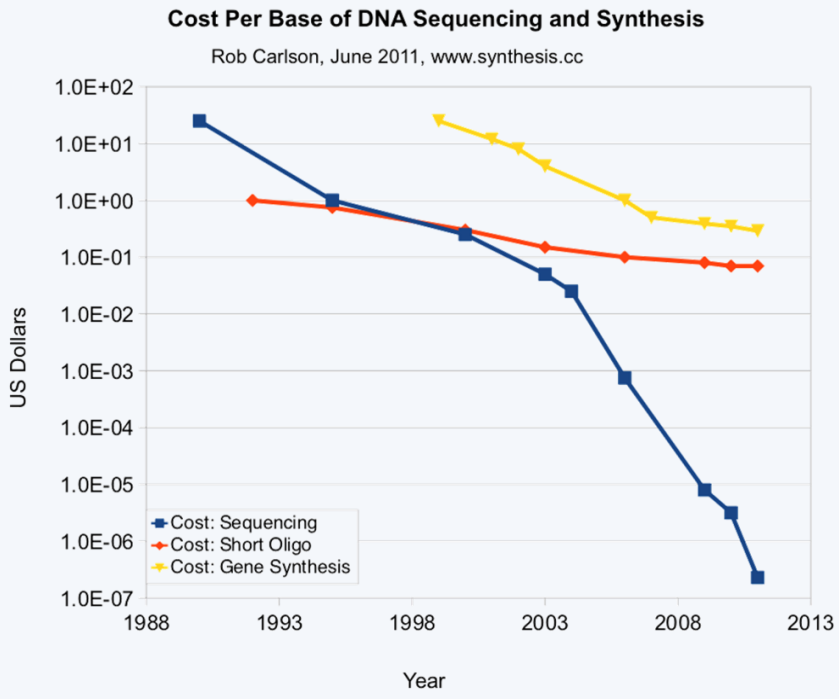

Figure 1-7: Carlson’s Law. The price of DNA oligonucleotide and gene synthesis has been dropping exponentially over the past 25 years.
Image by Robert Carlson, http://www.synthesis.cc/carlson_cost%20per_base_june_2012.png

The use of biological objects in ways different from their naturally intended use is not a new concept. One could argue that this idea traces back to ancient times, when people used animal bones as a rigid material for axes and other tools. Similarly, materials

have been constantly refined through advancements in science and technology and the progression of time. Similarly, DNA and other nucleic acids are likely not the best materials with which we can make biosensors or nanoscale tools. At some point in the future, it is likely that DNA will be replaced by synthetic molecules with superior properties. However, DNA is material that can be cheaply and widely used today, and it does have well-understood interaction properties. DNA can form defined secondary and tertiary structures with specific properties and can bind with molecules to allow biosensor studies and diagnostic research.

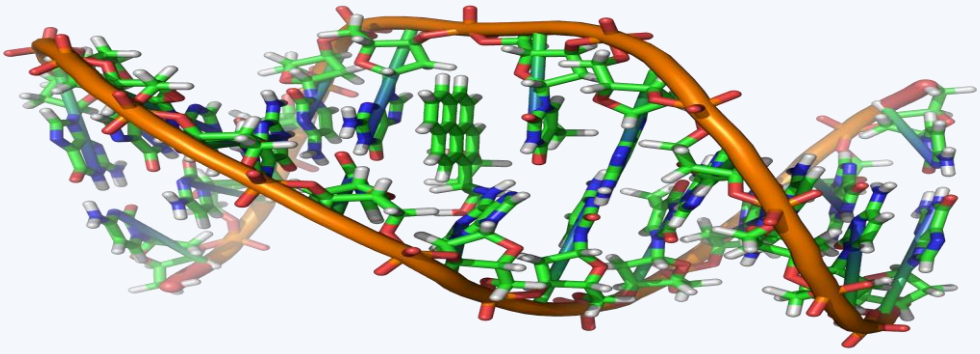

Figure 1-8: The structure of DNA.
http://upload.wikimedia.org/wikipedia/commons/d/d8/Benzopyrene_DNA_adduct_1JDG.png

Most people understand that DNA plays an important role in inheritance ("I have my dad's nose and my mom's hair."). Figure 1-8 presents a molecular view of DNA, showing that it has three components: a sugar, a nitrogen-containing base, and a phosphoric acid. Described by the Watson - Crick structural model, a DNA molecule consists of two polynucleotide strands coiled around each other in helical "twisted ladder"

structure. However, there are many more structural intricacies in DNA, not just a double helix.

In Dr. David Yu Zhang's thesis,[18] he explained the biophysical properties of DNA in very vivid way by analogy to Velcro and magnets. In DNA, there are four nucleotide bases: adenine, cytosine, guanine, and thymine (A, C, G and T) which can hybridize to form a stable duplex (double helix) bound together by hydrogen bonds between complementary base pairs (A-T and C-G). Table 1-1,[18] quoted from Zhang's thesis, shows the names and definitions of frequently used concepts in DNA nanotechnology.

Preferred term	Synonyms	Definition
strand	oligonucleotide molecule oligo	A continuous linear nucleic acid polymer covalently joined by phosphodiester bonds, typically less than 200 nucleotides.
complex	molecule tile	A non-covalently linked structure of several strands joined by Watson-Crick base pair interactions.
domain	Subsequence tract section	Several continuous nucleotides in a strand that act as a unit in hybridization, branch migration, dissociation, structure, or (deoxy) ribozyme function.
toehold	sticky end	A particular type of domain that serves to colocalize nucleic acid strands and complexes. Toeholds are typically short (4 to 10 nt).

Table 1-1: Common terms and their synonyms and definitions.[18]

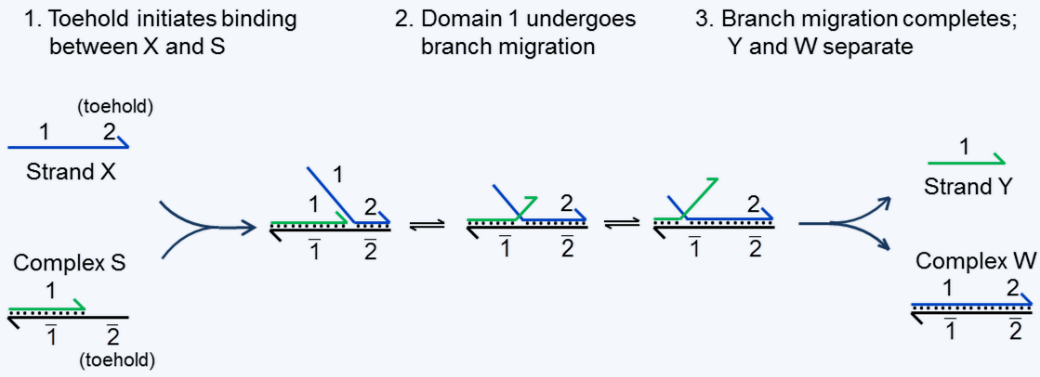

Figure 1-9: DNA strand displacement overview. Panel shows one example of this reaction. Single stranded DNA molecule X reacts with multi-stranded DNA complex S to release strand Y and complex W. This reaction is facilitated by the "toehold" domains 2 and $\bar{2}$: The hybridization of these single-stranded toeholds colocalizes S and X, and allows the 1 domain to branch migrate. Branch migration is the random walk process in which one domain displaces another of identical sequence in binding to a complementary domain, via a series of single nucleotide dissociation and hybridization steps. At the completion of branch migration, complex W is formed and strand Y is released.[18]
Image modified from David Yu Zhang's Thesis: Dynamic DNA Strand Displacement Circuits, California Institute of Technology, Pasadena, California, 2010.

Also covered in Zhang's thesis are DNA strand displacement reactions. When one single-stranded nucleic acid molecule hybridizes to a partially double-stranded DNA, it can cause strand displacement. This reaction starts at the single-stranded "toehold" domains and progresses through a branch migration process.[18] This way, the originally bound DNA strand is released. An overview of the DNA strand displacement process is given in Figure 1-9. In Chapter 2 of this dissertation, a competitor oligonucleotide was used to bind with ATP aptamer to unfold its hairpin structure in the measurement of

aptamer-small molecule dissociation constants. In Chapter 4, the standard electrochemical proximity assay (ECPA) adopted a short DNA competitor strategy, where the DNA competitor has 9 bases complimentary to thiolated-DNA, and a one-base toehold from thiolated-DNA can bind with methylene blue labeled DNA (MB-DNA) permitting strand displacement with the help of the proximity effect.

1.4 Basic concepts of Electrochemical Biosensors

Detection systems frequently used in medical diagnostics are mainly based on optical methods and electrochemical methods.[19-26] With optical approaches, light sources and optical sensors are typically expensive, and measurements are sensitive to local light and temperature. Comparing to the optical methods, electrochemical detection can offer greater signal stability and consistency, high sensitivity, simple instrumentation, and great compatibility with miniaturization technologies[21,22]. From the beginning of this century, electrochemical biosensors were used in many aspects in diagnostics.[27,28] In addition, electrochemical biosensors are easier to be developed into portable devices with microfluidic technologies.[29] These are the main reasons that we chose to combine electrochemical detection with the proximity assay concept for assay development

Electrochemical biosensors measure the changes in the electrical properties of a sample solution based on the chemical reactions which cause production or consumption of ions or electrons. Typically, an electrochemical biosensor comprises of 1) a bioreceptor specifically binding to the analyte; 2) a transducer which transduces the change taking place on the interface with bioreceptor to the electronic system; and 3) an electronic system to transfer this electrical signal to computer software that converts it to

a meaningful physical parameter presented to the operator. (Figure 1-10) The electrochemical biosensors, based on the measured parameters, can be classified as conductimetric, potentiometric, and amperometric. Usually, conductimetric biosensors measure electrical conductance or resistance.[21,30,31] Potentiometric biosensors measure the potential of electrochemical cells in the absence of appreciable currents.[32-34] Amperometric biosensors measure current.[21] Generally, if the current is measured at a constant potential, it is referred to as amperometry, and if the current is measured in a controlled range of potential, it is referred to as voltammetry.[30]

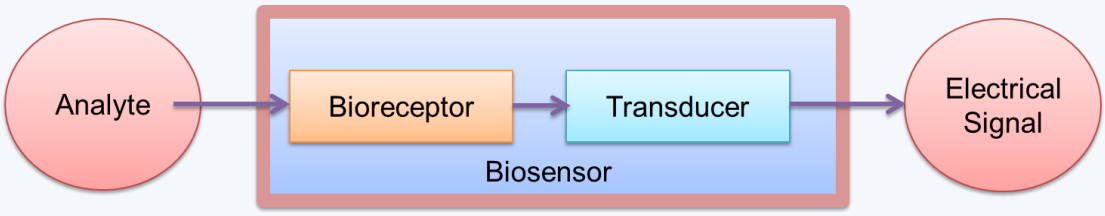

Figure 1-10: A schematic representation of biosensors

In the following electrochemical proximity assay (ECPA) and reusable ECPA, methylene blue (MB) is the reporter molecule, and square-wave voltammetry (SWV) is used to measure the current change caused by electrons transferring between MB and gold electrode. SWV is a kind of pulse polarography, which can offer great speed and high sensitivity. The great sensitivity of SWV can be attributed to two reasons. First, it can enhance the faradaic current; second, it can decrease the nonfaradaic charging current. In SWV, the current is measured twice during each cycle, once at the end of the forward pulse, and again at the end of reverse pulse. (Figure 1-

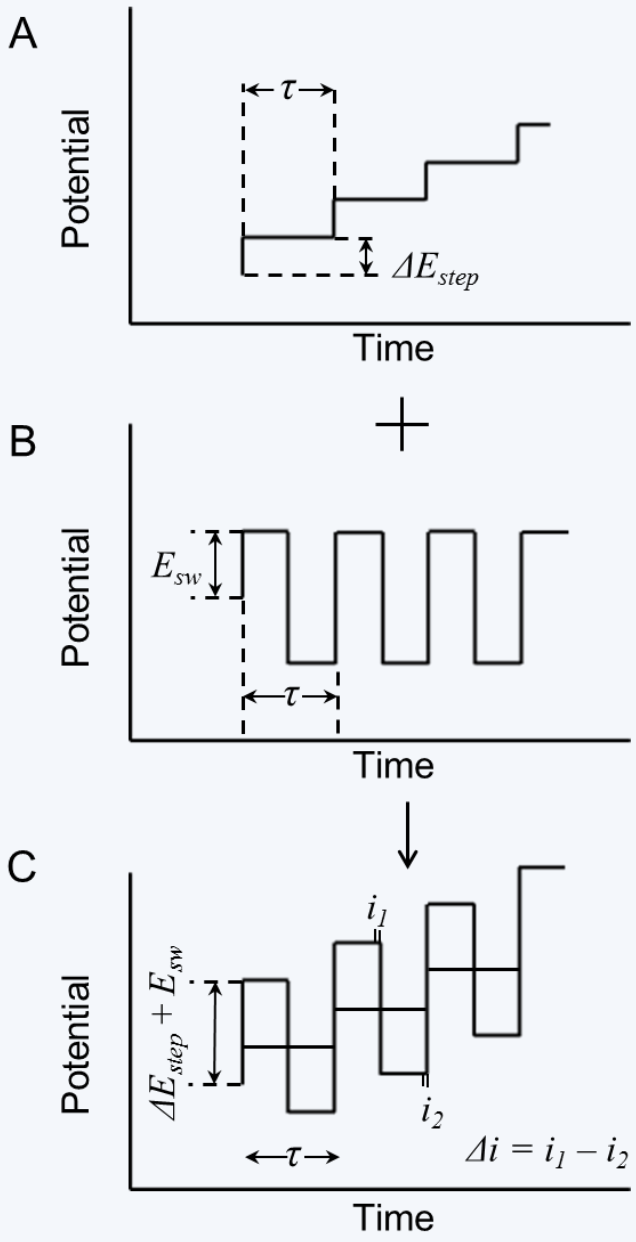

Figure 1-11: Applied excitation in square-wave voltammetry. The staircase signal in (A) is added to the symmetrical square wave in (B) to give the square-wave excitation signal in (C).

11C) Taking our experiment as an example, let us consider the events that occur on the electrode surface as the potential is suddenly increased by 50 mV. If a MB molecule is present near the electrode surface, there will be a surge of current that lowers the concentration of reduced MB molecules to that demanded by the new potential. When the potential pulse is first applied to the gold electrode, a surge in the nonfaradaic current (charging current) also occurs. However, the charging current decays exponentially with time. By measuring the current at the end of each pulse, the charging current is greatly reduced, and signal-to-noise ratio is larger, thus enhancing sensitivity. Figure 1-11 shows the excitation signal in SWV, which is obtained by super-imposing a symmetrical square wave onto the stair case signal. The magnitude of each pulse, E_{sw}, is one-half of the peak-to-peak amplitude of the signal. The duration of each pulse is one-half the staircase period, $\tau/2$. The frequency of the signal is the reciprocal of the staircase period: $f = 1/\tau$. And the scan rate for a SWV experiment can be defined as:

$$\text{Scan Rate (mv/sec)} = \frac{E_{step}\ (mV)}{\tau\ (\text{sec})} \qquad (1)$$

The currents are measured during the last few microseconds of each pulse and the current measured on two pulses of the same step is recorded as:

$$\Delta I = i_1 - i_2 \qquad (2)$$

1.5 Aptamers and Antibodies as Bioreceptors

Biomolecules are very commonly used as bioreceptors for biosensors in detection and quantitation of target proteins in clinical and biomedical research.[21,22,35] Bioreceptors

are the key to specificity for biosensor technologies. Aptamers and antibodies are two bioreceptors used commonly, due to the development of SELEX (systemic evolution of ligands by exponential enrichment) and monoclonal technology. Both methods have reduced the selection time and price and give these types of probes diversity and specificity.

Aptamers are short single-stranded oligonucleotides, either RNA or DNA, that fold into secondary or tertiary structures to specifically bind to their targets (e.g. small molecules, peptides and proteins) with high affinity and specificity. Antibodies are proteins consisting of varied amino acids and have very specific binding capabilities for the target of interest.

Particularly, aptamers have several advantages compared to antibodies: first, aptamers can be selected in vitro for any given target, from small molecules to large proteins and even cells. Second, aptamers can be synthesized with high reproducibility and purity from commercial sources. Third, aptamers are usually highly chemically stable, and once denatured under high temperature, they can reform their specific structure reversibly when the temperature is decreasing. Third, aptamers often undergo significant conformational changes upon target binding. However, the binding affinities of aptamers to target molecules are not as strong as that of antibodies, and the existing number of aptamers is still much lower than that of antibodies.

1.6 Additional Comments

In Chapter 2 of this dissertation, two different types of aptamers are chosen, which specifically bind to small molecules (ATP) or large proteins (thrombin, human IgE).

There, we introduce a method to measure the dissociation constant (K_d) of DNA aptamers to these target molecules. Because the dual-antibody recognition concept has served as a guide to various alternative strategies in the past few years,[36-39] in Chapter 3, a proximity ligation assay (PLA) is introduced and optimized using DNA model systems. As noted before, PLA is a simpler and more sensitive assay format for protein detection and quantitation comparing to standard sandwich ELISA. We show in Chapter 3 that with careful engineering of DNA strands, experimental model systems can be developed to accurately describe trends in PLA and to ease optimization of assay conditions. In Chapters 4 and 5, the electrochemical proximity assay (ECPA) is introduced, which cleverly combines the proximity assay concept with electrochemical detection. Both aptamers and antibody-oligonucleotide conjugates are used as assay probes in ECPA. Compared to antibodies, nucleic acids are easily modified with a variety of reporter molecules, such as methylene blue and ferrocene. The DNA "tails" of the pairs of probes have complementary bases to the DNA sequences forming a DNA monolayer on the electrode surface and to methylene blue labeled DNA. So in the presence of target molecules, the antibody part of the probes would specifically bind to the target, and the DNA hybridization would bring the methylene blue molecule close to the electrode surface, giving an electric current signal. Finally, general conclusions from this work, along with future possibilities, are presented in Chapter 6.

1.7 References

(1) Salm, P.; Taylor, P. J.; Roberts, D.; Silva, J. D. J. *Chromatogr*. **2009**, *877*, 568.
(2) Silva, C. J.; Onisko, B. C.; Dynin, I.; Erickson, M. L.; Requena, J. R.; Carter, J. M. *Anal. Chem.* **2011**, *83*, 1609-1615.
(3) Silva, C. L.; Passos, M.; Camara, J. S. *Talanta* **2012**, *89*, 360-368.
(4) Southern, E. *J Mol Biol* **1975**, *98*, 503–517.
(5) Alwine, J.; Kemp, D.; Stark, G. *Proc Natl Acad Sci USA* **1977**, *74*, 5350–5354.
(6) Renart, J.; Reiser, J.; Stark, G. *Proc Natl Acad Sci USA* **1979**, *76*, 3116–3120.
(7) Towbin, H.; Staehelin, T.; Gordon, J. *Proc Natl Acad Sci USA* **1979**, *76*, 4350–4354.
(8) Burnette, W. *Anal Biochem* **1981**, *112*, 195–203.
(9) Mann, M. J. *Proteome Research*. **2008**, *7*, 3065
(10) Cox, J.; Mann, M. *Cell* **2007**, *130*, 395-398.
(11) Papadoupulos-Eleopulos, E.; Turner, F.; Papadimitriou, M. *Bio/Technology* **1993**, *11*, 696-707.
(12) Porcario, C.; et al. *BMC Research Notes*, **2011**, *4*, 376.
(13) Li, D.; et al. *J. Addiction Medicine*, **2012**, *6*, 311-317.
(14) Engvall, E.; Perlmann, P. *Immunochemistry* **1971**, *8*, 871-874.
(15) Conaway, J. *J AOAC Int*. **1991**, *74*, 715 -717
(16) Fredriksson, S.; Gullberg, M.; Jarvius, J.; Olsson, C.; Pietras, K.; Gústafsdóttir, S. M.; Östman, A.; Landegren, U. *Nature Biotechnol*. **2002**, *20*, 473-477.
(17) Heyduk, E.; Heyduk, T. *Anal. Chem*. **2005**, *77*, 1147-1156.
(18) Zhang, D. Y. Thesis: Dynamic DNA strand displacement circuits, California Institute of Technology, **2010**.
(19) Bau, L.; Tecilla, P.; Mancin, F. *Nanoscale* **2011**, *3*, 121-133.
(20) Dey, D.; Goswami, T. *J. Biomed Biotechnol*. **2011**, *348218*, 7.
(21) Grieshaber, D.; MacKenzie, R.; Voros, J.; Reimhult, E. *Sensors* **2008**, *8*, 1400-1458.
(22) Kimmel, D. W.; LeBlanc, G.; Meschievitz, M. E.; Cliffel, D. E. Anal.
(23) Lu, L.-M.; Zhang, X.-B.; Kong, R.-M.; Yang, B.; Tan, W. *J. Am. Chem. Soc.* **2011**, *133*, 11686-11691.
(24) Reches, M.; Mirica, K. A.; Dasgupta, R.; Dickey, M. D.; Butte, M. J.; Whitesides, G. M. *ACS Appl. Mater. Inter*. **2010**, *2*, 1722-1728.
(25) Shang, J.; Cheng, F.; Dubey, M.; Kaplan, J. M.; Rawal, M.; Jiang, X.; Newburg, D. S.; Sullivan, P. A.; Andrade, R. B.; Ratner, D. M. *Langmuir* **2012**, *28*, 3338-3344.
(26) Yang, Y.-C.; Lu, H.-H.; Wang, W.-T.; Liau, I. *Anal. Chem.* **2011**, *83*, 8267-8272.
(27) Pemberton, R. M.; Hart, J. P.; Foulkes, J. A. *Electrochimica Acta* **1998**, *43*, 3567-3574.
(28) Velasco-Garcia, M. N.; Mottram, T. *Trends in Biotechnology* **2001**, *19*, 433.
(29) Aytur, T.; Foley, J.; Anwar, M.; Boser, B.; Harris, E.; Beatty, P. R. *Journal of Immunological Methods* **2006**, *314*, 21-29.

(30) Chaubey, A.; Malhotra, B. D. *Biosens. Bioelectron*. **2002**, *17*, 441-456.
(31) Blanco-Lopez, M. C.; Lobo-Catanon, M. J.; Miranda-Ordieres, A. J.; Tunon-Blanco, P. *Trends Anal. Chem*. **2004**, *23*, 36-48.
(32) Eggins, B. Analytical Techniques in the Sciences. John Wiley & Sons, West Sussex, **2002**.
(33) Chaubey, A.; Malhotra, B. D. *Biosensors & Bioelectronics* **2002**, *17*, 441–456.
(34) D'Orazio, P. *Clinica Chimica Acta* **2003**, *334*, 41–69.
(35) Ispas, C. R.; crivat, g.; Andreescu, S. *Anal. Lett*. **2012**, *45*, 168-186.
(36) Gullberg, M.; et al. *Proc. Natl. Acad. Sci. USA* **2004**, *101*, 8420-8424.
(37) Heyduk, E.; Dummit, B.; Chang, Y. H.; Heyduk, T. *Anal. Chem.* **2008**, *80*, 5152-5159.
(38) Kim, D.; Daniel, W. L.; Mirkin, C. A. *Anal. Chem*. **2009**, *81*, 9183-9187.
(39) Konry, T.; Hayman, R. B.; Walt, D. R. *Anal. Chem*. **2009**, *81*, 5777-5782.

CHAPTER 2

Dissociation Constants (K_d) Measurement of DNA Aptamers

2.1 Introduction

Aptamers are RNA or single stranded DNA molecules that have been isolated from random-sequence nucleic acid libraries by *in vitro* selection [1, 2] and which fold into unique tertiary structures, allowing them to bind targets with high affinity and specificity. As such, aptamers have attracted attention for their potential as pharmaceutical lead compounds or diagnostic agents. To date, numerous aptamers have been selected against a broad range of targets, such as small molecules [3, 4], proteins [5, 6], and even entire cells [7, 8]. Due to their similar affinity and selectivity, aptamers draw obvious comparisons with antibodies [9], yet aptamers exhibit a number of advantages over antibodies as molecular recognition elements, especially for diagnosis. First, the relative ease of *in vitro* aptamer isolation eliminates the need for animal hosts, chemical modification of nucleic acids is highly flexible and well-developed, and aptamer binding affinity can be tailored or manipulated. Furthermore, aptamers can be selected against virtually any molecule, even those that are toxic or do not stimulate an immune response. Lastly, aptamers will refold to regain functionality after exposure to denaturing conditions such as extreme pH or

temperature. Due to these advantages over antibodies, aptamers have now infiltrated much of analytical chemistry [4].

DNA aptamers against thrombin, human IgE, and ATP were among the first selected, thus they have been thoroughly characterized [10-12]. Commonly used thrombin aptamers include two G-quartet conformations that selectively bind to α -thrombin: a 29-nucleotide ligand, 60-18(29) (a modified version is named 'THRaptA' herein) [10], and a 15-nucleotide aptamer, known as G15D ('THRaptB' herein) [10]. For human IgE, often used is a 37-nucleotide aptamer, D17.4 ('IgEapt' herein,) [12], and a commonly used ATP aptamer is DH25.42 ('ATPapt' herein) [13]. In the original reports, these aptamers were isolated from pools of random-sequence, single-stranded DNA molecules by *in vitro* selection, and all have been characterized to bind their targets in solution with dissociation constants in the nanomolar or micromolar ranges.

Dissociation constant (K_d) measurements of aptamers against their target molecules have been achieved previously using techniques such as filter binding [10, 12, 14, 15], fiber-optic microarrays [16], affinity capillary electrophoresis (ACE) [11], capillary electrophoresis (CE) [17, 18], nonequilibrium capillary electrophoresis of equilibrium mixtures (NECEEM) [19], micro free flow electrophoresis (μFFE) [20], microchip CE [21], optical biosensors using fluorescence anisotropy [22], and affinity chromatography [13, 23]. A common characteristic of many of these approaches is the requirement of a separation step, namely rinsing or washing. For example, washing of unbound DNA and elution of DNA complexes is required during selection cycles in filter binding, washing of beads is needed during DNA immobilization in fiber-optic microarrays, and rinsing steps are needed during aptamer coupling in the optical biosensor method. The approaches that do

not require a washing step prior to measurement (ACE, CE, NECEEM, μFFE) are advantageous due to their low reagent consumption, but these methods are not applicable to measuring dissociation constants of aptamer-small molecule binding. Measurable binding with these methods generally requires a large shift in size or charge-to-size ratio. Thus, there is a need for a method that combines low reagent consumption, homogeneous measurement (no separation or washing required), and the ability to measure binding of small and large molecules.

In this chapter, we describe two approaches based on automated microchip electrophoresis for aptamer-target effective dissociation constant ($K_{d,eff}$) measurement. These approaches, which allow $K_{d,eff}$ measurements on aptamers against large or small molecules, are both based on a microchip version of the DNA mobility shift assay. The methods offer typical advantages of the microfluidic platform, including minimized reagent use, reduced cost, and reduced analysis time. Additionally, there is no need for labor-intensive, tedious washing steps. The first approach applies to large molecule (protein) targets, where non-denaturing microchip gel electrophoresis separations of DNA could be used to resolve unbound from target-bound aptamers. This approach is similar to previously reported CE methods [17, 18], yet requires even less starting material for measurement. The second approach adds a level of flexibility that is novel to this work, in which an aptamer/competitor strategy was used to extend the technique to small molecules targets such as ATP. Finally, we provide evidence that our approach could be used during aptamer selection (e.g. SELEX) by accurately measuring aptamer $K_{d,eff}$ in the presence of a large background of randomized DNA sequences.

2.2 Reagents and Experimental Methods

2.2.1 Reagents and Materials

All solutions were prepared with deionized, ultra filtered water (Fisher Scientific). Human thrombin, IgE, and ATP were obtained from Sigma Aldrich. All oligonucleotides were obtained from Integrated DNA Technologies (IDT; Coralville, Iowa), with purity and yield confirmed by mass spectrometry and HPLC, respectively. Nucleotide sequences of DNA aptamers used in experiments are given in Table 2-2. Buffer reagents were purchased from VWR. The binding buffer used for THRaptA-thrombin or THRaptB-thrombin incubations consisted of 50 mM Tris-HCl, 100 mM NaCl, and 1 mM $MgCl_2$ at pH 7.5; the IgE aptamer buffer consisted of 1x PBS (138 mM NaCl, 2.7 mM KCl, 8.1 mM Na_2HPO_4, 1.1 mM KH_2PO_4, at pH 7.4) with 1 mM $MgCl_2$; and the ATP aptamer binding buffer consisted of 10 mM Tris–HCl, 150 mM NaCl, and 5 mM $MgCl_2$ at pH 7.5.

Table 2-1. Oligonucleotide sequences used for $K_{d,eff}$ measurements of aptamer binding to large or small molecules by automated microchip electrophoresis.

Name	* Sequence
THRaptA	5′ - TCG TAC CAG CTG ATG CAC TTC **AGT CCG TGG TAG GGC AGG TTG GGG TGA CT**T CGT GGA ACT ATC TAG CGG TGT ACG TGA GTG GGC ATG TAG CAA GAC C-3′
THRaptB	5′ - TCA GCC ATT CGA ATC GTA CTG CAA TCG GGT ATT AGG CTA GTG A CTA CT**G GTT GGT GAG GTT GG**G TAG TCA CAA AGT GAC GCG ACT AG TTA CGG A -3′
IgEapt	5′ - TCG TAC CAG CTG ATG CAC TT**G GGG CAC GTT TAT CCG TCC CTC C TA GTG GCG TGC CCC** TCG TGG AAG CGG TGT AGT GGG CAT GTA G CA AGA CC -3′
ATPapt	5′ - A**CC TGG GGG AGT ATT GCG GAG GAA GG**T -3′
competitor	5′ - ACC TGG GAA TAC TCC CCC AGG TGA AGA AGA AAG AGA GAG AAA AGA AGA AA -3′
C_{26}	5′ - TTT CTT CTT TTC TCT CTC TTT CTT CT -3′
library	5′ - TCA GCC ATT CGA ATC GTA CTG CAA TCG GGT ATT AGG CTA - N_{41} - G TGA CGC GAC TAG TTA CGG A -3′

* Blue text represents aptamer consensus sequences, which were previously determined during selection.
N = random nucleotide sequence generated by hand-mixing of reagents during synthesis

2.2.2 Automated Microchip Electrophoresis

In order to form the aptamers' functional secondary and tertiary structure, solutions of THRaptA, THRaptB, and IgEapt were heated to 95 ℃, then cooled slowly to room temperature (22 ℃) at speed of −3 ℃ min^{-1} using a Mastercycler-EP gradient thermal cycler (Eppendorf). Microchip electrophoresis was performed on an Experion automated electrophoresis system (Bio-Rad). According to the manufacturer's protocol, the microchip used in the experiment was an Experion DNA 1K chip, in which 11 sample wells and 1 DNA sizing ladder well are included. Titration sets (11 points) were carried out in triplicate. Fixed amounts of THRaptA, THRaptB, or IgEapt strands were incubated

with variable amounts of thrombin or IgE for 2 h at room temperature, in a total volume of 5 mL, prior to loading into the chip. 1 mL aliquots of these reaction mixtures (samples), or standards, or ladder were loaded into each sample well, and the manufacturer's protocol was followed for injection, separation, and fluorescence-based detection using DNA intercalating dyes. The overall analysis time was ~30 min for separation of all 11 samples and the sizing ladder, inferring that each separation (including heating and transition times) required approximately 2.5 min. The intercalating dye used in the Experion system binds to both double- and single-stranded DNA, with approximately 5-fold higher sensitivity toward double-stranded DNA. Since aptamer structure is comprised of both double- and single stranded DNA segments, these dyes are appropriate for detection of folded aptamers in solution. As discussed in detail below, the presence of intercalating dyes may affect aptamer–target binding affinities to some extent. Note that the Experion DNA 1K loading buffer is of low ionic strength, but its composition and the intercalating dye identity remain proprietary.

2.2.3 Dissociation Constant Determination

The effective dissociation constants ($K_{d,eff}$) were determined using nonlinear least-squares fitting to the Hill equation (eqn (1)), with the Hill coefficients (n) set as variable.

$$S = S_i + (S_f - S_i)\frac{[T]^n}{(K_{d,eff})^n + [T]^n} \quad (1)$$

Where S is the fluorescence signal measured as a function of [T], the titrant concentration (target is typically used as the titrant); S_i and S_f are the initial and final signals, respectively; and $K_{d,eff}$ represents the effective dissociation constant of the complex of interest. Intensities of peaks of interest in microchip electropherograms were fit to the

Hill equation after titration experiments. This simple model, which has found widespread use in biochemistry, physiology, and pharmacology to analyze binding equilibria,[53-55] provides flexibility in measuring systems of unknown stoichiometry. Without information on stoichiometry, this approach results in an effective dissociation constant ($K_{d,eff}$) measurement rather than a strict dissociation constant (K_d) with known stoichiometry. $K_{d,eff}$ measurement is proper in the current work, since in most cases little is known about the stoichiometry of aptamer-target interactions. For large molecule–aptamer $K_{d,eff}$ measurements (Figure 2-1A), we chose to measure the decrease in the free aptamer peak.[11,17,20] In some cases, it should be possible to simplify the $K_{d,eff}$ measurements using the ratios of bound and free aptamers to determine the average $K_{d,eff}$ value.[21] However, this methodology would be less flexible than using the free aptamer peak, since it would only apply to special cases where the complex peak could be detected. Furthermore, the response of aptamer-target complexes in our system will vary greatly depending on the extent to which target displaces DNA intercalating dyes. For small molecule-aptamer $K_{d,eff}$ measurements, an aptamer-competitor scheme (Figure 2-6B and C) was used to extract binding constants, as discussed in detail below.

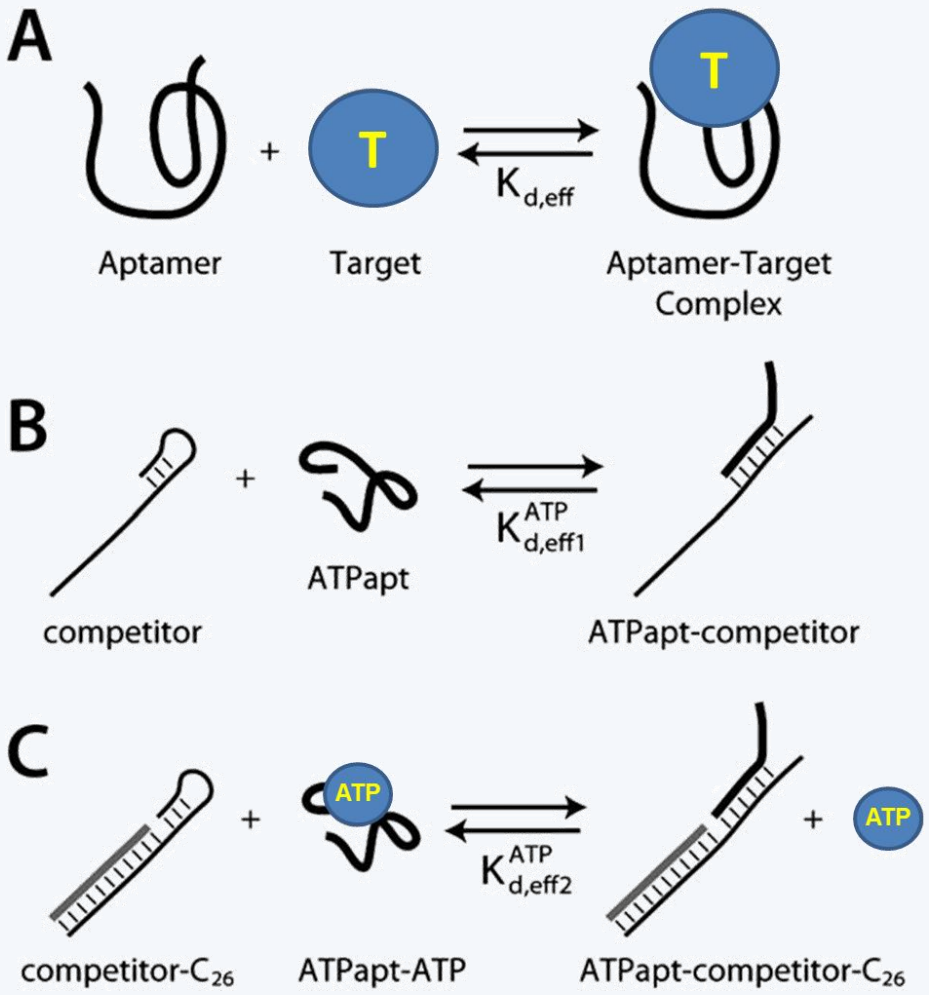

Figure 2-1: Schematic representations of aptamer–target binding equilibria during $K_{d,eff}$ measurements. (A) Protein–aptamer $K_{d,eff}$ measurements were straightforward, where the decrease in the amount of free aptamer could be followed with microchip electrophoresis as the concentration of target (T) was varied. Small molecule aptamer $K_{d,eff}$ measurements relied upon (B) aptamer–competitor equilibria in the absence of target as well as (C) the complete system in the presence of target.

2.3 Validation of Method by Measurement of Aptamer-Protein Dissociation Constants

As depicted by the first scheme in Figure 2-1A, aptamer-protein dissociation constants ($K_{d,eff}$) were measured using the microchip ssDNA mobility shift assay. Upon binding to a protein or large molecule target (T), the electrophoretic mobility of the bound fraction of the aptamer was altered, and the decreased height or area of the free aptamer peak (or increase in the complex peak) was monitored as a function of target concentration to obtain a binding curve. Since we utilize automated microchip gel electrophoresis rather than zone electrophoresis as the separation mechanism, it is necessary to validate that this approach can be used to obtain aptamer-protein dissociation constants that are comparable to previous reports. The microchip electropherograms of THRaptA complexed with thrombin at different ratios are shown in Figure 2-2A. The concentration of THRaptA was fixed at 300 nM while thrombin was varied from 0 to 2.88 mM in separate 5 mL incubation mixtures. 1 mL aliquots of each mixture were loaded into the 11 sample wells of the electrophoretic microchip along with 5 mL of the Experion DNA 1K loading buffer (Bio-Rad), lowering the concentrations of all components by 6-fold (THRaptA fixed at 50 nM; thrombin varied from 0 to 480 nM). By monitoring the THRaptA peak at ~50 s (filled blue peak in Figure 2-2A), a consistent trend was observed in which the peak intensity decreased as the thrombin concentration in the incubation mixture was increased. This decrease was a result of the mobility shift of the ssDNA aptamer as it formed a complex with thrombin.[11,20] The peaks at ~39 s corresponded to a 15-base pair internal standard for DNA sizing and concentration measurements. The peak intensities at ~50 s were used to generate a binding curve as a

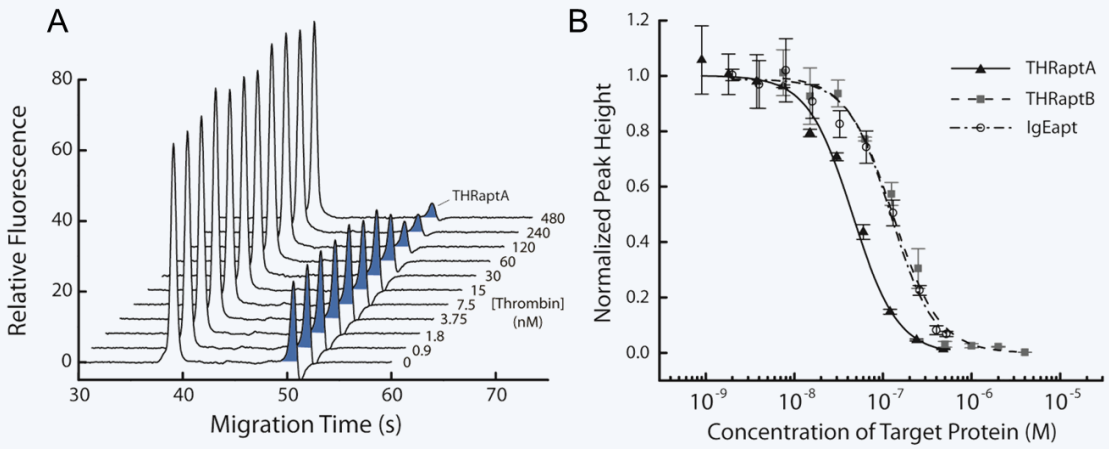

Figure 2-2: ssDNA mobility shift assay for protein–aptamer $K_{d,eff}$ measurements. (A) Example microchip electropherograms of THRaptA during titration with thrombin. The THRaptA peak around 50 s was observed to decrease proportionally as thrombin formed complexes with a fraction of the aptamer pool. (B) Binding curves generated from electropherograms for aptamer–target binding of THRaptA (solid line, filled triangles), THRaptB (dashed line, filled gray squares), and IgEapt (dash-dotted line, open circles) against their respective targets. Nonlinear least squares analyses revealed $K_{d,eff}$ values of 25.6 ± 2.9, 128 ± 27, and 112 ± 7 nM, respectively.

function of concentration of thrombin (Figure 2-2B; solid line, filled triangles), with error bars representing standard deviations of triplicate measurements (3 microchips). Using nonlinear least squares fitting of this data to the Hill equation, we determined the $K_{d,eff}$ of THRaptA binding to thrombin to be 25.6 ± 2.9 nM at 30 ℃ (running temperature of the microchip electrophoresis system). This value is higher than previous measurements, likely due to the increased temperature or other effects such as aptamer sequence

differences (Table 2-2; discussion below). Essentially the same $K_{d,eff}$ value, albeit with larger error, was obtained when using the presumed aptamer-protein complex peak at 107 s (data not shown). It is noteworthy that only 28.8 and 16.5 pmol of thrombin and thrombin aptamer, respectively, were required for a single-point $K_{d,eff}$ measurement (one microchip, 11 sample wells), which represents a major advantage of this microchip electrophoresis based approach (Table 2-2). If duplicate or triplicate runs are desired, these amounts must be doubled or tripled.

For further validation, this method was used to measure the $K_{d,eff}$ values of THRaptB and IgEapt against their respective targets. The fixed concentrations of THRaptB and IgEapt in the final dilution on-chip were 200 and 50 nM in these sets of experiments, respectively. As shown by the binding curves in Figure 2-7B, the $K_{d,eff}$ values of THRaptB binding thrombin (dashed line, filled gray squares) and IgEapt binding to IgE (dash-dot line, open circles) were 128 $\pm$ 27 and 112 $\pm$ 7 nM, respectively (triplicate incubations, 3 microchips). The THRaptB $K_{d,eff}$ measurement was in good agreement with previous reports, which vary by about an order of magnitude depending on the methodology (Table 2-2). The IgEapt $K_{d,eff}$ measurement was slightly higher than previous reports, again likely due to the increased temperature of measurement (30 ℃; discussed in detail below). The total amounts of thrombin, THRaptB, IgE, and IgEapt required for single-point versions of these measurements were 239, 66.0, 28.8, and 16.5 pmol, respectively.

Table 2-2. Method comparisons for $K_{d,eff}$ measurements of the four aptamers analyzed in this work. The microchip electrophoresis approach is the only one listed that can interrogate aptamer–small molecule binding without requiring a washing step; the amount of consumedDNAreagent is also small for this approach

Method	Dissociation Constant, K_d (nM)				Small molecule binding?	Washing step	*Analysis time (h)	*DNA used (pmol)	Temp. (°C)
	THRaptA	THRaptB	IgEapt	ATPapt					
Nitrocellulose Filter Binding	0.5 - 1	100-200	10		yes	required	> 2	~0.6	RT
Fiber Optic Microarray		300			yes	required	> 3	~100 000	NR
Affinity Capillary Electrophoresis		450	8, 64		no	none	> 1	~1 700	RT
NECEEM		240			no	none	~2	NR	RT
Micro Free Flow Electrophoresis			48		no	none	~0.25	~2**	RT
Optical Biosensor		50			no	required	> 1	~17 000	20
Affinity Chromatography				< 50 000	yes	required	> 1	~6 000	RT
Automated Microchip Electrophoresis	25.6	128	112	70 900	yes	none	~0.5	17-170	30

* For equal comparison, time and amount estimates were generated by assuming an equal number of points of titration (11 points here).
** Value was estimated using flow rate and time, since syringe volumes were not reported.
NR = not reported; RT = room temperature; NECEEM = nonequilibrium capillary electrophoresis of equilibrium mixtures

2.4 Measurement of Aptamer-Small Molecule Dissociation Constants

With small molecule targets such as ATP, the charge-to-size ratios—and hence the electrophoretic migration times—of target-bound aptamers are not significantly altered compared to that of the unbound aptamers, thus the peaks cannot be distinguished. This problem limits the flexibility of our approach or any other electrophoretic approach, as well as for fluorescence anisotropy-based methods. To remedy the issue, an aptamer/competitor strategy was utilized, in which a DNA competitor complementary to

the aptamer could be displaced by ATP (Figure 2-1B and C). The equilibrium between ATPapt (thick bold line) and competitor (thinner line) is depicted in Figure 2-1B, where a competitor sequence with a designed 7-base-pair hairpin loop possesses a 15-base region that is complementary to ATPapt. This equilibrium between ATPapt and competitor is defined by the dissociation constant, $K_{d,eff\,1}^{ATP}$. In Figure 2-1C, this aptamer–competitor equilibrium is combined with the ATPapt binding to its target, ATP. As small molecules of ATP displace the competitor from ATPapt, the competitor hairpin reanneals, promoting an equilibrium shift to the left where ATP is then bound to its aptamer, ATPapt. This equilibrium is defined by dissociation constant, $K_{d,eff\,2}^{ATP}$. Note also that an additional region was added in Figure 2-1C, namely a 26-nucleotide region complementary to the competitor, C_{26} (gray bold line) for the purpose of enhancing separation. For measurement of $K_{d,eff\,1}^{ATP}$ (Figure 2-6B), solutions of competitor only were heated to 95 ℃, then cooled slowly to room temperature (22 ℃) at −3 ℃ min^{-1} using a thermal cycler. Fixed amounts of competitor were incubated with variable amounts of ATPapt for 2 h at room temperature prior to loading into the chip. To measure $K_{d,eff\,2}^{ATP}$ (Figure 2-1C), ATPapt–competitor–C26 complex was heated to 95 ℃, then cooled slowly to room temperature (22 ℃) at −3 ℃ min^{-1}. The ratio of ATPapt : competitor : C26 was maintained at 1 : 1 : 1. Fixed amounts of ATPapt–competitor–C26 complex (0.5 mM) were incubated with variable amounts of ATP for 2 h at room temperature prior to loading into the chip.

From Figure 2-1B, we define the effective dissociation constant of aptamer–competitor complex as:

$$K_{d,eff\,1}^{ATP} = \frac{[\text{competitor}][\text{ATPapt}]}{[\text{ATPapt} - \text{competitor}]} \quad (2)$$

Now, we define the effective dissociation constant of the competitive equilibrium shown in Figure 2-1C, which is a unitless constant:

$$K_{d,eff\,2}^{ATP} = \frac{[\text{competitor} - \text{C}_{26}][\text{ATPapt} - \text{ATP}]}{[\text{ATPapt} - \text{competitor} - \text{C}_{26}][\text{ATP}]} \quad (3)$$

$K_{d,eff\,2}^{ATP}$ can also be defined as below, since the C26 strand is stably complexed with competitor and does not participate significantly in this equilibrium:

$$K_{d,eff\,2}^{ATP} = \frac{[\text{competitor}][\text{ATPapt} - \text{ATP}]}{[\text{ATPapt} - \text{competitor}][\text{ATP}]} \quad (4)$$

It is from these two measurable equilibria that we can extract the effective dissociation constant of interest, $K_{d,ATPapt}$:

$$K_{d,\,ATPapt} = \frac{[\text{ATPapt}][\text{ATP}]}{[\text{ATPapt} - \text{ATP}]} = \frac{K_{d,eff\,1}^{ATP}}{K_{d,eff\,2}^{ATP}} \quad (5)$$

Thus, we can separately measure $K_{d,eff\,1}^{ATP}$ and $K_{d,eff\,2}^{ATP}$ using microchip DNA mobility shift assays (Figure 2-3A and B) with the systems depicted in Figure 2-1B and C, then we can extract $K_{d,ATPapt}$ from this data using eqn (5). In this way, from binding curves (Figure 2-3C), we determined $K_{d,eff\,1}^{ATP}$ and $K_{d,eff\,2}^{ATP}$ to be 16.1 $\pm$ 1.9 nM and 2.27 $\pm$ 0.05 $\times$ 10^{-4}, respectively. Using eqn (5), $K_{d,ATPapt}$ was then determined to be 70.9 $\pm$ 8.5 mM at

30 ℃. This extracted value also agrees well with the published value of ~50 mM,[13,23] especially considering the increased temperature (Table 2-2).

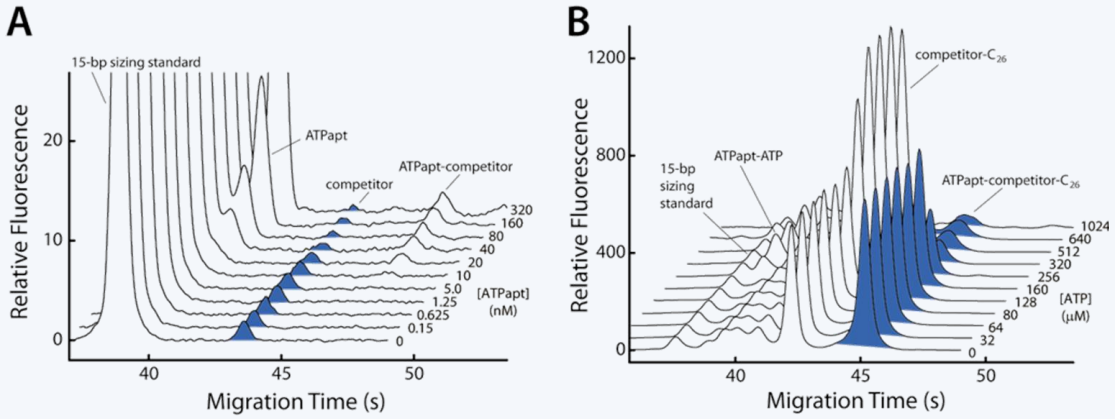

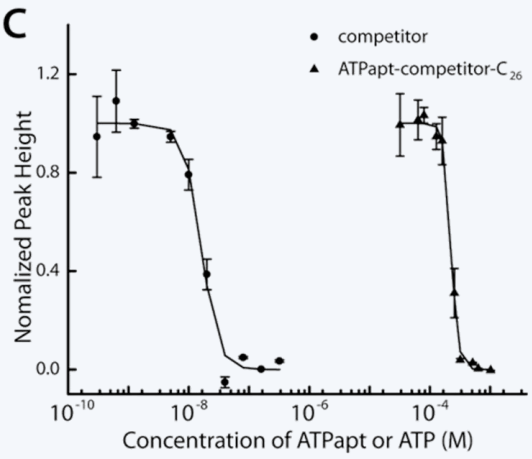

Figure 2-3: ssDNA mobility shift assay for protein–small molecule $K_{d,eff}$ measurements. (A) Microchip electropherograms of the system shown in Fig. 2-5B, as competitor is titrated with ATPapt. The competitor peak (43 s, filled gray peaks) was observed to decrease in height as it hybridized with ATPapt, shifting the equilibrium shown in Fig. 2-5B to the right. (B) Electropherograms of the system in Fig. 2-5C during titration with ATP. The ATPapt–competitor–C_{26} peak (~45 s, filled gray peaks) decreased in height as ATP complexed with ATPapt, shifting the equilibrium in Fig. 2-5C to the left. (C) Binding curves generated from decreases in the competitor peak (filled circles) and the ATPapt–competitor–C_{26} peak (filled triangles) gave $K_{d,eff1}^{ATP}$ =16.1 ± 1.88 nM and $K_{d,eff2}^{ATP}$ = 2.27 ± 0.05 ×10^4, respectively. By eqn (5), $K_{d,ATPapt}$ = 70.9 ± 8.5 μM at 30 °C.

It is feasible that $K_{d,eff}$ measurements can be made in this way for aptamers against any small molecule target, greatly enhancing the flexibility of our automated microchip electrophoresis approach for aptamer–target $K_{d,eff}$ measurements. In doing so, one must first develop a similar aptamer–competitor strategy for each aptamer to be assayed, inferring an increased experimental commitment. As long as the aptamer sequences are known, it should be relatively straightforward to design similar hairpin-forming competitors for other small-molecule binding aptamers, but the energetics of competitor–aptamer binding will need to be optimized empirically.

2.5 Method and Dissociation Constant Comparisons

The measured $K_{d,eff}$ values of THRaptA, THRaptB, IgEapt, and ATPapt were 25.6 ± 2.9 nM, 128 ± 27.0 nM, 112 ± 7 nM, and 70.9 ± 8.5 mM, respectively (Table 2-2). These values agreed reasonably well with previously published numbers, especially considering the differences in temperature and solution conditions. The measured $K_{d,eff}$ values for THRaptB (128 ± 27.0 nM) and ATPapt (70.9 ± 8.5 mM) were in agreement with the published values of 50–450 nM[21,22,25-27,30] and ~50 mM,[24,34] respectively. The measured dissociation constants for both THRaptA (25.6 ± 2.9 nM) and IgEapt (112 ± 7 nM) were higher than the published values of 0.5 – 1 nM[21] and 8 – 48 nM.[23,28,31,32] There are several possibilities that could cause this discrepancy. Most importantly, the running temperature in our experimental setup is fixed at 30 ℃, which is higher than that used in the other methods. A temperature increase can cause a significant increase in measured K_d value, with the magnitude of the shift dependent on the thermodynamics of binding for each system. Second, the salt concentrations and buffer constituents are

different among measurements, which can also significantly affect the binding constants. Third, the nucleotide sequences of THRaptA and IgEapt (as well as THRaptB) used in this paper were slightly different than those used in other measurements. Our sequences (Table 2-1) include the consensus sequences from selection (bold text), but also include additional sections at the 5' and 3' ends for use in proximity ligation assays.[55,57] With the nitrocellulose filter binding method,[21,23,25,26] the authors used only the consensus sequences of THRaptA and IgEapt, shown in bold in Table 2-1. German et al.[22] used different versions of the IgE aptamer, namely the unlabeled aptamer (bold sequences in Table 2-1) and a labeled aptamer, with a fluorescent label at the 5'-end using an ethylene glycol linker. Their dissociation constants were determined to be 64 nM for labeled aptamer and 8 nM for unlabeled aptamer. It is obvious that the added fluorescent label caused a significant decrease in binding affinity. Likewise, our extended sequences at the 3' and 5' ends of aptamers may have affected the binding with target molecules. Finally, since DNA intercalating dyes were used to label the free aptamer in this work, these dyes may have competed to some extent with target binding, increasing the measured $K_{d,eff}$. It is noteworthy that order of magnitude differences are often observed when comparing K_d measurements reported in the literature (e.g. 'THRaptB' column in Table 2-2), due to the lack of consistency in buffer conditions, temperature, labeling, etc. Nonetheless, our aptamer affinity measurements were in reasonably good agreement with previous reports, and our approach is greatly simplified compared to others.

Perhaps equally important is the fact that the microchip electrophoresis-based approach requires much less time and reagent consumption than other methods (Table 2-2). As shown in Table 2-2, our approach provides a 2- to 6-fold reduction in analysis time

compared to all other methods except the μFFE method,[31] which provides ~2-fold faster analysis than our approach. In this comparison, 'analysis time' refers to the time required for completion of washing and measurement steps, but excluding preparation and incubation times for titrations, which should be essentially equal among the methods. The automated microfluidic system also requires only 1 mL sample volumes in each of 11 sample wells, allowing 5 mL incubation volumes for our experiments. In order to provide equal comparisons, the time and amount estimates shown in Table 2-2 were generated by assuming an equal number of points of titration (11 used here) and scaling the values reported for individual incubations. By comparison to all but the filter binding and μFFE methods, our approach provides a 10- to 6000-fold reduction in DNA consumption, with only 17–170 pmol of DNA used for 11 of the 5 mL incubations. Although less DNA was required, the filter binding approach requires washing steps and specialized equipment for dealing with radioactive reagents. Specialized equipment and training will also be required for the μFFE method,[31] since the method is still in the development stage. On the other hand, this method is promising and would likely find much success if made widely available. A significant advantage of our approach is the commercial availability and ease of use of the automated instrumentation. Furthermore, the automated and homogeneous nature of our method reduces instances of human error and avoids repetitive washing steps.

As a final point of comparison, our approach provides an added level of flexibility in comparison to other homogeneous methods based on electrophoresis[22,28,31] or fluorescence anisotropy.[33] The scheme developed for measurement of aptamer–small molecule dissociation constants (Figure 2-1B and C and 2-3) is a novel extension of

electrophoretic affinity measurements which allows the flexibility of our method to rival filter binding and affinity chromatography. In fact, our approach is the only one listed in Table 2-2 that can interrogate aptamer–small molecule binding without requiring a washing step. By exploiting the inherent nature of DNA aptamers to coexist in their target binding form (with tertiary structure) and in their duplex form with complementary sequences (e.g. antidotes for aptamer-based drugs), a competitive equilibrium was developed (Figure 2-1B and C). This system imparts large, measurable electrophoretic mobility shifts that are triggered by aptamers binding to small molecules (Figure 2-3). The approach combines the power of DNA-based computing or structure-switching with aptamer–target interactions to significantly improve the flexibility of our mobility shift assays. Moreover, the use of DNA-based competitors could also be applied to the other homogeneous methods shown in Table 2-2, such as μFFE, ACE, NECEEM, or to optical biosensors to improve their flexibility of application.

2.6 Feasibility for K_d Monitoring during Aptamer Selection

To provide proof-of-principle that the microchip DNA mobility shift assays could be useful for monitoring dissociation constants during aptamer selection processes (e.g. SELEX[5,6]), a mock-SELEX process was carried out. A known DNA aptamer was spiked into a random sequence DNA library at increasing ratios to mimic enrichment within the library, and our approach was used to measure the bulk dissociation constant of these mixtures. Solutions of increasing percentages of THRaptA in a random DNA library were prepared (0, 1, 5, 10, 25, 75, 90, and 100%). Fixed total DNA concentrations of each THRaptA/library mixture were then incubated in 5 mL volumes (300 nM total

DNA, or 1.5 pmol) with variable amounts of thrombin (11 thrombin concentrations and 1 microchip for each mixture) for 2 h at room temperature prior to loading into the microchip, injection, and separation. Since the DNA library and THRaptA were of approximately equal length (100 and 97 bp, Table 2-1), only one peak in the electropherogram was monitored. The THRaptA/library peak was observed to decrease with the addition of thrombin for all samples except the 0% THRaptA control (Figure 2-4A). Data shown in this figure are peak heights of free THRaptA/library pool, normalized to the peak height with no thrombin added. The shape of the binding curve became more pronounced with increasing percentage of THRaptA in the pool. As shown in Figure 2-4B, nonlinear least squares analysis revealed that the known $K_{d,eff}$ of THRaptA could be extracted from this data at concentrations as low as 5% of the pool (75 fmol THRaptA + 1425 fmol library in each incubation tube). Error bars in this data represent fitting errors in the least squares analysis. The $K_{d,eff}$ of the 1% mixture was determined to be 24.6 $\pm$ 70.2 nM. Although this value was coincidentally near the true value of 25.6 nM, with such large error, a one-parameter t-test showed that it was significantly different from the true value of 25.6 nM ($p < 0.05$). In the same way, mixtures with 5% THRaptA or more were shown to be statistically equal to the true value ($p > 0.2$). In essence, the measured $K_{d,eff}$ of the pools converged on the true value of the THRaptA $K_{d,eff}$ as the fraction of THRaptA in the library pool increased (Figure 2-4B). In a true SELEX process, the bulk $K_{d,eff}$ should decrease with each round as higher affinity ligands succeed in the evolutionary competition, rather than continuously converging toward a single value. Nonetheless, these results suggest that our approach could be used as an automated, homogeneous route for monitoring $K_{d,eff}$ values during each round of the SELEX

process, requiring only ~825 fmol (11 incubation tubes with 75 fmol each) of binding sequences (THRaptA) in a background of random DNA.

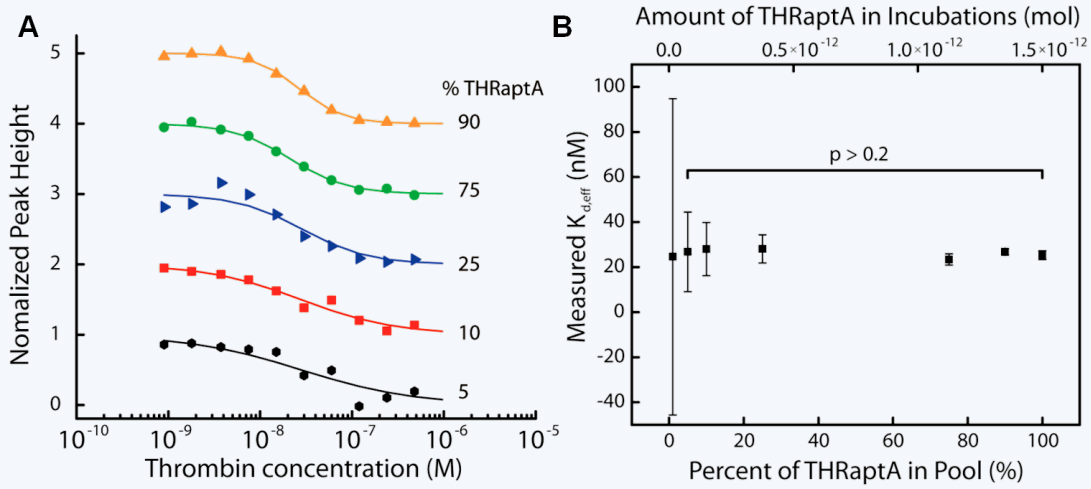

Figure 2-4： Mock-SELEX process in which THRaptA was spiked into a random sequence DNA pool at different concentrations. (A) Microchip electrophoresis binding curves for pools from 5 to 90% THRaptA. (B) Measured $K_{d,eff}$ values of the pool converged to the true value with increasing THRaptA fraction, and our system was able to detect aptamers spiked into a random sequence pool at as low as 5% population (75 fmol THRaptA). A one sample t-test showed no difference from the previously measured value of 25.6 nM ($p > 0.2$) for all samples other than the 1% sample ($p < 0.05$).

2.7 Conclusions

In this work, we have demonstrated that automated microchip electrophoresis is a useful method for measurement of aptamer–target $K_{d,eff}$ measurements. The approach is homogeneous, requires minimal time and reagent consumption, and can be applied to aptamer–protein or aptamer–small molecule binding. To achieve this flexibility, an aptamer–competitor strategy, akin to DNA-based logic operations, was used to extract $K_{d,eff}$ values for aptamer–small molecule interactions. This aspect should be applicable to any electrophoretic affinity assays[22,28,31] or fluorescence anisotropy assays[33] developed to date, which should greatly improve the flexibility of the assays. The approach was also proven feasible for $K_{d,eff}$ monitoring of DNA pools during SELEX processes. For a typical SELEX process, only one microchip electrophoresis run can be carried out between selection rounds to preserve precious material and time. This would still provide 11 points on the titration curve to extract binding constants, while only consuming ~825 fmol of DNA between rounds. In this respect, the advantage provided by the microfluidic platform in reducing reagent consumption should be particularly useful.

2.8 References

(1) Jones, S.; et al. *Nucl. Acids Res.* **2001**, *29*, 943-954.
(2) Jones, S.; et al. *J. Mol. Biol.* **1999**, *287*, 877-896.
(3) Morozova, N.; et al. *BIoinformatics* **2006**, *22*, 2746-2752.
(4) Nagai, K. *Curr. Opin. Struct. Biol.* **1996**, *6*, 53-61.
(5) Ellington, A. D.; Szostak, J. W. *Nature* **1990**, *346*, 818-822.
(6) Tuerk, C.; Gold, L. *Science* **1990**, *249*, 505-510.
(7) Osborne, S. E.; et al. *Curr. Opin. Chem. Biol.* **1997**, *1*, 5-9.
(8) Famulok, M.; et al. *Chem. Rev.* **2007**, *107*, 3715-3743.
(9) Navani, N. K.; Li, Y. F. *Curr. Opin. Chem. Biol.* **2006**, *10*, 272-281.
(10) Jiang, Y. X.; et al. *Anal. Chem.* **2003**, *75*, 2112-2116.
(11) Griffin, L. C.; et al. *Gene* **1993**, *137*, 25-31.
(12) Ferreira, C. S.; et al. *Anal. Bioanal. Chem.* **2008**, *390*, 1039-1050.
(13) Balogh, Z.; et al. *FASEB* **2010**, *24*, 4187-4195.
(14) Shangguan, D.; Li, Y.; Tang, Z.; Cao, Z. C.; Chen, H. W.; Mallikaratchy, P.; Sefah, K.; Yang, C. J.; Tan, W. *PNAS* **2006**, *103*, 11838-11843.
(15) Li, J. W.; et al. *Biochem. Biophys. Res. Commun.* **2002**, *292*, 31-40.
(16) Gutsaeva, D. R.; et al. *Blood* **2011**, *117*, 727-735.
(17) Lu, C.; et al. *Cancer Biol. Ther.* **2010**, *9*, 176-182.
(18) Wu, Y.; Sefah, K.; Liu, H.; Tan, W. *PNAS* **2010**, *107*, 5-10.
(19) Huang, Y. F.; et al. *Langmuir* **2008**, *24*, 11860-11865.
(20) Chu, T. C.; et al. *Nucl. Acids Res.* **2006**, *34*, e73.
(21) Tasset, D. M.; Kubik, M. F.; Steiner, W. *J. Mol. Biol.* **1997**, *272*, 688-698.
(22) German, I.; Buchanan, D. D.; Kennedy, R. T. *Anal. Chem.* **1998**, *79*, 4540-4545.
(23) Wiegand, T. W.; et al. *J. Immunol.* **1996**, *157*, 221-230.
(24) Huizenga, D. E.; Szostak, J. W. *Biochemistry* **1995**, *34*, 656-665.
(25) Bock, L. C.; Griffin, L. C.; Latham, J. A.; Vermaas, E. H.; Toole, J. *J. Nature* **1992**, *355*, 564-566.
(26) Macaya, R. F.; Waldron, J. A.; Beutel, B. A.; Gao, H.; Joesten, M. E.; Yang, M.; Patel, R.; Bertelsen, A. H.; Cook, A. F. *Biochemistry* **1995**, *34*, 4478-4492.
(27) Lee, M.; Walt, D. R. *Anal. Biochem.* **2000**, *282*, 142-146.
(28) Mendonsa, S. D.; Bowser, M. T. *Anal. Chem.* **2004**, *76*, 5387-5392.
(29) Mosing, R. K.; Bowser, M. T. J. *Sep. Sci* **2007**, *30*, 1420-1426.
(30) Berezovski, M.; Nutiu, R.; Li, Y.; Krylov, S. N. *Anal. Chem.* **2003**, *75*, 1382-1386.
(31) Turgeon, R. T.; Fonslow, B. R.; Jing, M.; Bowser, M. T. *Anal. Chem.* **2010**, *82*, 3636-3641.
(32) Gong, M.; Wehmeyer, K. R.; Limbach, P. A.; Heineman, W. R. *Electrophoresis* **2007**, *28*, 837-842.
(33) Potyrailo, R. A.; Conrad, R. C.; ellington, A. D.; Hieftje, G. M. *Anal. Chem.* **1998**, *70*, 3407-3412.
(34) M. Sassanfar; Szostak, J. W. *Nature* **1993**, *364*, 550-553.

(35) Walt, D. R. *Chemical Society Reviews* **2010**, *39*, 38-50.
(36) Drabovich, A.; Berezovski, M.; Krylov, S. N. *J. Am. Chem. Soc* **2005**, *127*, 11224-11225.
(37) Berezovski, M.; Drabovich, A.; Krylova, S. M.; Musheev, M.; Okhonin, V.; Petrov, A.; Krylov, S. N. *J. Am. Chem. Soc* **2005**, *127*, 3165-3171.
(38) Dolnik, V. *Electrophoresis* **2008**, *29*, 143-156.
(39) Heller, C. *Electrophoresis* **2001**, *22*, 629-643.
(40) Kostal, V.; Arriaga, E. *Electrophoresis* **2008**, *29*, 2578-2586.
(41) Barrolier, V.; Watzke, E.; Gibian, H. *Naturforschung* **1958**, *13B*:754.
(42) Hannig, K. Z. *Anal. Chem.* **1961**, *181*, 244-254.
(43) Roman, M.; Brown, P. *Anal. Chem.* **1994**, *66*, 86-94.
(44) Pruski, Z.; et al. *Electrophoresis* **1990**, *11*, 932-986.
(45) Zeiller, K.; et al. *Hoppe-Syler's Z Physiol Chem.* **1975**, *356*, 1225-1244.
(46) Rodkey, L. *Appl. Theor. Electrophor.* **1990**, *1*, 243-247.
(47) Kessler, R.; Manz, H. *Electrophoresis* **1990**, *11*, 979-980.
(48) Hoffstetter-Kuhn, S.; Wagner, H. *Electrophoresis* **1990**, *11*, 451-456.
(49) Nath, S.; Schutte, H.; Weber, G.; Hustedt, H.; Deckwer, W. *Electrophoresis* **1990**, *11*, 937-941.
(50) Knisley, K.; Rodkey, L. *Electrophoresis* **1990**, *11*, 927-931.
(51) Clifton, M.; Jouve, N.; de Balmann, H.; Sanchez, V. *Electrophoresis* **1990**, *11*, 913-919.
(52) Poggel, M.; Melin, T. *Electrophoresis* **2001**, *22*, 1008-1015.
(53) Hill, A. V. *Physiology* **1910**, *40*, 190-224.
(54) Weiss, J. N. *FASEB J.* **1997**, *11*, 835-841.
(55) Kim, J.; Hu, J.; Sollie, R. S.; Easley, C. J. *Anal. Chem.* **2010**, *82*, 6976-6982.
(56) Li, N.; Ho, C. *J. Am. Chem. Soc.* **2008**, *130*, 2380-2381.
(57) Fredriksson, S.; Gullberg, M.; Jarvius, J.; Olsson, C.; Pietras, K.; Gústafsdóttir, S. M.; Östman, A.; Landegren, U. *Nature Biotechnol*. **2002**, *20*, 473-477.

CHAPTER 3

DNA Models for Development of Proximity Assays

3.1 DNA Models for Asymmetric Proximity Ligation Assays

The proximity ligation assay (PLA) is one of the most sensitive and simple protein assays developed to date, yet a major limitation is the relatively narrow dynamic range compared to other assays such as enzyme-linked immunosorbent assays. In this work, the dynamic range of PLA was improved by 2 orders of magnitude and the sensitivity was improved by a factor of 1.57. To accomplish this, asymmetric DNA hybridization was used to reduce the probability of target-independent, background ligation. An experimental model of the aptamer-target-connector complex (aptA-T-aptB-C_{20}, PLA) in PLA was developed to study the effects of asymmetry in aptamer-connector hybridization. Connector base pairing was varied from the PLA standard of 20 total bases (C_{20}) to an asymmetric combination with 15 total bases (C_{15}). The results of this model suggested that weakening the affinity of one side of the connector to one aptamer would significantly reduce target-independent ligation (background) without greatly affecting target-dependent ligation (signal).

3.1.1 Background of Proximity Ligation Assay (PLA)

The proximity ligation assay[1] (PLA) is among the most sensitive protein assays developed to date. PLA can be considered a descendent of immuno-PCR methods,[2] in which antibodies are attached to oligonucleotides to allow the coupling of target binding with exponential amplification by polymerase chain reaction (PCR). The term "proximity ligation" was first named in Landegren's paper,[1] the method depends on the simultaneous and proximate recognition of target molecules by pairs of affinity probes, giving rise to an amplifiable detection signal. In that paper, the molecule they targeted was the homodimer of the platelet-derived growth factor B-chain (PDGF-BB). A DNA aptamer with affinity for PDGF-BB was extended by additional sequence elements at either the 5' or the 3' end, forming a proximity probe pair. When pairs of probes bind PDGF-BB, the free ends of their sequence extensions are brought close to hybridize together to a subsequently added connector oligonucleotide, allowing the ends to be connected by enzymatic DNA ligation. So, the detected protein molecules promote the ligation reaction by bringing together the free ends of the proximity probe pairs. The ligation products can then be replicated by nucleic acid amplification through PCR (Figure 1-4).

In the beginning stages of PLA method development, Landegren and co-workers determined the optimal concentrations of each proximity probe and the connector oligonucleotide that maximize the cooperative effect induced by target binding,[1] (Figure 3-1) and they further proved that this cooperative effect was inversely related to the K_d of the proximity probes.[3] Major advantages of PLA are sensitivity, selectivity, and ease of use. Furthermore, the assay requires no washing steps due to its homogeneous nature.

However, PLA has the limitation of a relatively narrow dynamic range. The reason for this flaw is the necessity to use very low amounts of proximity probes to minimize a target-independent hybridization and ligation (background).

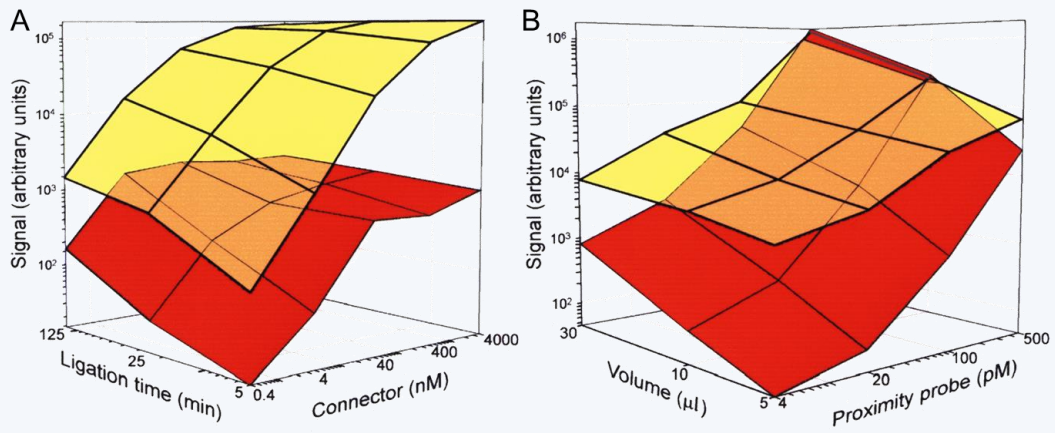

Figure 3-1: Optimization of reaction conditions for the proximity ligation assay. (A) Effect of connector oligonucleotide concentration and time of ligation on signal and background. (B) Influence of preincubation volume and probe concentration. The upper, yellow layers connect the signals recorded in reactions with 5.6 attomoles of PDGF-BB, while the lower, red layers represent the target-independent background, expressed in arbitrary units.
Adapted by permission from Macmillan Publishers Ltd: Nature biotechnology (Fredriksson, S.; Gullberg, M.; Jarvius, J.; Olsson, C.; Pietras, K.; Gústafsdóttir, S. M.; Östman, A.; Landegren, U. Nature Biotechnol. 2002, 20, 473-477.), copyright© (2013)

3.1.2 Improvement of Sensitivity and Dynamic Range in PLAs by Asymmetric Connector Hybridization

As shown in Figure 3-2A, the mode of action of PLA results in a four-part complex composed of the targeted protein analyte (T), two proximity probes (DNA-conjugated antibodies or oligonucleotide aptamers; apt_A and apt_B), and a connector oligonucleotide ($C_{20,PLA}$). The three separate DNA molecules (or moieties) are designed to hybridize into

a structure that promotes a DNA ligase enzyme to covalently couple the two proximity probes. In the presence of target, the four-part complex is preferred over target-independent hybridization (three-part complex) due to a cooperative "proximity effect" that essentially increases the local concentration of the oligo-nucleotide tails.[4-6] Thus, the amount of ligation products is proportional to the amount of protein analyte, and these products can be made recognizable by PCR for exponential amplification and highly sensitive quantitation by qPCR. Due to its simplicity and sensitivity, PLA has found much interest of late and has been successfully utilized in a variety of applications, such as sensitive protein detection,[1,3] in situ analysis of protein localization,[7] DNA-protein interactions,[8] clinical diagnostics,[9] and protein-protein interaction assays.[10]

Our goal in this study was to improve the dynamic range of PLA without sacrificing LOD. To address this issue, we made two hypotheses: (1) target-independent hybridization (background; Figure 3-2A, bottom) is inversely proportional to the K_d of the connector oligonucleotide at a given concentration of proximity probes, and (2) the width of the dynamic range is proportional to the amount of a proximity probe to be used. If confirmed, these hypotheses suggest that dynamic range and signal to background could be improved by simply reducing the number of bases in the connector. To test these hypotheses, first we developed and tested an experimental model of the proximity effect. This model suggested that asymmetric connectors with higher K_d values could significantly decrease target-independent hybridization (background; Figure 3-2A, bottom). In turn, this would lead to higher signal-to-background ratios and allow the use of more proximity probes, which should increase the dynamic range of PLA.

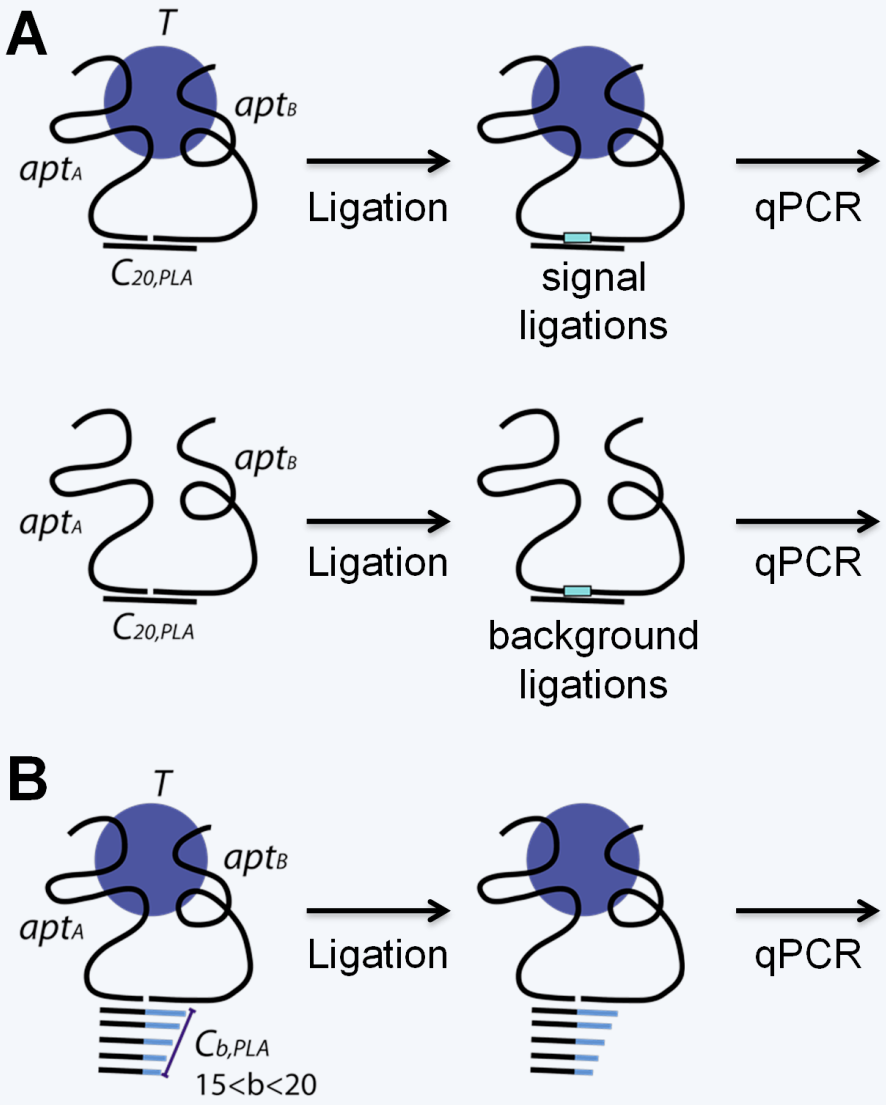

Figure 3-2. Schematics of PLA and model systems described in the text. (A) Standard PLA, in which a connector length of 20 bases ($C_{20,PLA}$, or b = 20) is used. Ligated signal or background complexes are not differentiated by qPCR. (B) Asymmetric PLA, in which connector lengths of 15-19 bases ($C_{b,PLA}$, where $15 \leq b < 20$) are tested.

3.1.3 Reagents and Experimental Methods

3.1.3.1 Reagents and Materials

All solutions were prepared with deionized, ultrafiltered water (Fisher Scientific). T4 DNA ligase was purchased from New England BioLabs. Human thrombin was obtained from Sigma-Aldrich. All oligonucleotides except the Taqman probe were obtained from Integrated DNA Technologies (IDT; Coralville, Iowa), with purity and yield confirmed by mass spectrometry and HPLC, respectively. Sequences of ssDNA strands used in the experimental model are given in Table 3-1. Sequence $Free_A$ was labeled at its 5′-end with Iowa black FQ quencher (IABkFQ; absorbance maximum at 531 nm). Sequence $Free_B$ was labeled at its 5′-end with a phosphate group (Phos) and at its 3′-end with 5(6)-carboxyfluorescein (6-FAM, mixed isomer; emission maximum at 520 nm). Loop strands (Table 3-1) were synthesized by ligation of $Free_A$ and $Free_B$ using T4 DNA ligase; Sequences (listed 5′ to 3′) for PLA or asymmetric PLA were as follows. Thrombin aptamer A, apt_A, CAG TCC GTG GTA GGG CAG GTT GGG GTG ACT TCG TGG AAC TAT CTA GCG GTG TAC GTG AGT GGG CAT GTA GCA AGA GG; thrombin aptamerB, apt_B, /5Phos/GT CAT CAT TCG AAT CGT ACT GCA ATC GGG TAT TAG GCT AGT GAC TAC TGG TTG GTG AGG TTG GGT AGT CAC AAA; symmetric connector, $C_{20,PLA}$, AAG AAT GAT GAC CCT CTT GCT AAA A; asymmetric connector, $C_{18,PLA}$, TTA TGA TGA CCC TCT TGC TAA AA; asymmetric connector, $C_{16,PLA}$, TAG ATG ACC CTC TTG CTA AAA; forward PCR primer, GTG ACT TCG TGG AAC TAT CTA GCG; reverse PCR primer, AAT ACC CGA TTG CAG TAC GAT TC; Taqman probe (Applied Biosystems, ABI), 4-chlorofluorescein-TGT ACG TGA GTG GGC ATG TAG CAA GAG G-carboxytetramethylrhodamine.

Table 3-1. Oligonucleotide Sequences Used in the Experimental Model of Proximity Hybridizationa

name	sequence[b]
C_{20}	5′-TAATACTTGCTGAGGAATAA-3′ (similar to thatused in standard PLA)
C_{19}	5′-TAATACTTGC**TGAGGAATA**-3′
C_{18}	5′-TAATACTTGC**TGAGGAAT**-3′
C_{17}	5′-TAATACTTGC**TGAGGAA**-3′
C_{16}	5′-TAATACTTGC**TGAGGA**-3′
C_{15}	5′-TAATACTTGC**TGAGG**-3′
$Free_A$	5′-/IABkFQ/GCA AGT ATT ATT TTT TTT TTT TTT TTT TTT TTT TTT TTC TCT TTT TC-3′
$Free_B$	5′-/Phos/TCT TCT CTC TCT CTC TTT TTT TTT TTT TTT TTT TTT TTT ATT CCT CA/6-FAM/-3′
linker	5′-GAG AGA GAG AGA AGA GAA AAA GAG AAA AAA-3′
Loop	5′-/IAbFQ/GCA AGT ATT ATT TTT TTT TTT TTTTTT TTT TTT TTT TTC TCT TTT TC TCT TCTCTC TCT CTC TTT TTT TTT TTT TTT TTT TTT TTTTTT ATT CCT CA/6-FAM/-3′

[a]Bases in bold depict the variable segments of the connectors usedto alter connector affinity (see Table 2 for affinities). [b]Notes: IABkFQ,Iowa black FQ; Phos, phosphorylated end; 6-FAM, 5(6)-carboxyfluorescein(mixed isomer).

3.1.3.2 Fluorescence Measurements for Model Titrations

Fluorescence measurements were conducted using a Nanodrop 3300 fluorospectrometer (Thermo Scientific). The intensity of FAM emission was measured at 520 nm with LED excitation at 485 nm. The buffer used for titrations was 50 mM Tris-HCl (pH 7.5), 100 mM NaCl, 1 mM $MgCl_2$. Titrations sets (14-16 points) were carried out in duplicate, and each fluorescence measurement was repeated six times. Fixed

amounts of Loop or $Free_A$ and $Free_B$ strands were incubated with variable amounts of C_b overnight at room temperature prior to fluorescence measurements.

3.1.3.3 Synthesis of Loop strands

Loop strands (Table 3-1) were synthesized by ligation of $Free_A$ and $Free_B$ using T4 DNA ligase. The Linker strand was used to hybridize with and adjacently position the strands for ligation. Ligation was carried out by T4 DNA ligase (New England Biolabs) in a total volume of 100 μL for 3 h at 16 ℃ with a Linker:$Free_{A,/B}$ molar ratio of 20:1. Ligated products were further concentrated to 20 μL total volume and mixed with 100μl of 1.2x DNA loading dye (0.5mg/ml bromophenol blue, 8M urea, 1% (v/v) NP-40, 1mM Tris-HCl pH 8;)[11]. Then, samples were denatured at 90 ℃ for 5 min, and quickly loaded onto 1 M urea containing TAE 5% agarose gel. Gel electrophoresis was run on a VWR Mini Gel apparatus at 70 volts for 5 h with a 100 nt ssDNA as well as the 50 nt $Free_A$ and $Free_B$ strands for markers (Figure 3-3). Under UV light, the ligated product bands were excised and eluted using Wizard® SV Gel and PCR Clean-Up Systems (Promega) under the manufacturer's protocol. Ligated products were quantified using both UV absorbance at 260 nm and FAM absorbance at 490 nm with a Nanodrop 1000 small-volume spectrophotometer (Thermo Scientific).

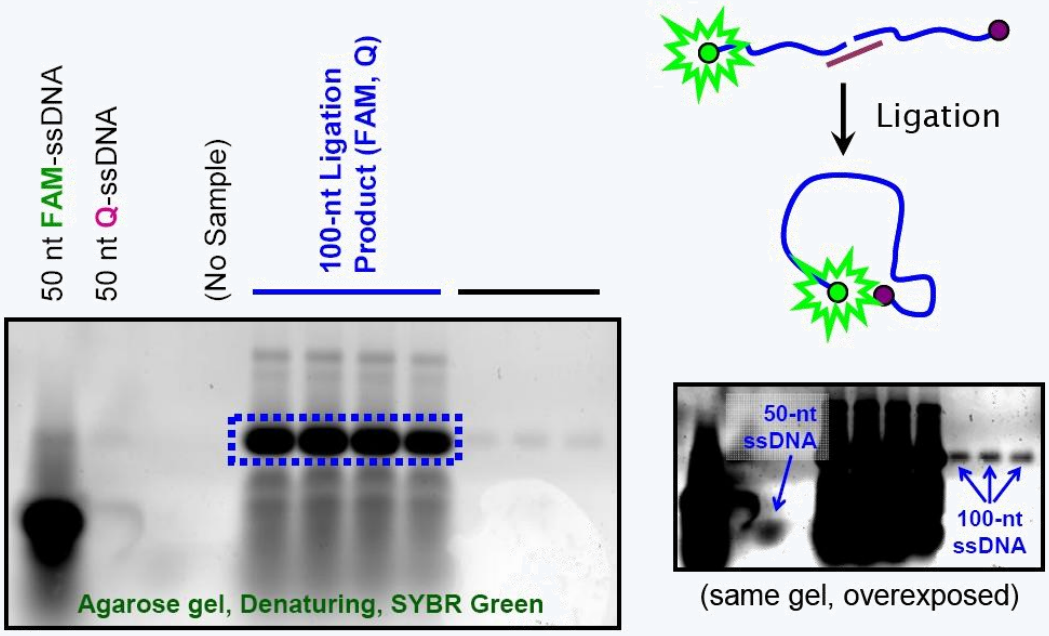

Figure 3-3: Schematic of *Loop* strand synthesis by ligation. ssDNA separation by agarose gel electrophoresis was used to purify ligation products.

3.1.3.4 Proximity Ligation Assays

Temperature control was achieved using a Mastercycler-EP gradient thermal cycler (Eppendorf). Thrombin and oligonucleotide solutions were made as described.[1] An amount of 4 µL of a reaction mixture containing human thrombin, apt_A, and apt_B was incubated at 37 ℃ for 15 min before adding 1 µL of connector ($C_{16,PLA}$, $C_{18,PLA}$, or $C_{20,PLA}$). An additional 30 min of incubation at 22 ℃ was performed to stabilize complexes. These 5 µL samples were then brought to a total volume of 55 µL for the

ligation and amplification mixture, which contained 50 mM KCl, 10 mM Tris-HCl, pH 8.3, 1.9 mM $MgCl_2$, 0.4 Weiss unit T4 DNA ligase, 73 μM ATP, 0.18 mM dNTPs, 0.45 μM forward and reverse PCR primers, 45 nM Taqman probe for the 5′ nuclease assay, and 1.5 units of AmpliTaq Gold polymerase (ABI). The reactions were transferred to a real-time PCR instrument (CFX96, Bio-Rad) for temperature cycling: 5 min at 22 ℃ for ligation, 10 min at 95 ℃, and then cycling for 15 s at 95 ℃ and 60 s at 60 ℃, repeated 45 times. Signal-to-background (S/BG) values were calculated from the relative number of ligation products detected in a sample with thrombin to that in a sample without thrombin. The relative quantity of the ligated products was calculated by using the comparative threshold cycle (Ct) method.[12] For measurements of PLA background, 15 pM apt_A and 20 pM apt_B were used, with different connector concentrations as follows: $C_{16,PLA}$) 178 nM; C18,PLA) 112 nM; $C_{20,PLA}$) 45 nM. For asymmetric PLA, 900 pM apt_A and 1200 pM apt_B were used with 480 nM $C_{16,PLA}$; and for symmetric PLA, 15 pM apt_A and 20 pM apt_B were used with 400 nM $C_{16,PLA}$ (same conditions as previously reported[1]).

3.1.3.5 Connector K_d Calculations

Base-pairing dissociation constants for the invariable segment ($K_{d,A}$) and for each variable segment ($K_{d,B}$) of the connectors were calculated using the well-established, thermodynamic nearest-neighbor model.[13] Dissociation constants were derived from thermodynamic parameters calculated via the BioPHP melting temperature calculator (http://insilico.ehu.es/tm.php), a free online service that uses SantaLucia's method.[13] Source code is freely downloadable at http://www.biophp.org/. $K_{d,B}$ values were also

experimentally confirmed; in Table 3-2, the column labeled "$K_{d,B}$" shows the calculated values, and the column labeled "$K_{d,eff}^{BG}$" shows the experimentally confirmed values.

Table 3-2. Analysis of Connector Sequences Used in the Experimental Model of Proximity Hybridization[a]

connector Cb	length (bases)	Kd,B (nM)	$K_{d,eff}^{BG}$ (nM)	$K_{d,eff}^{S}$ (nM)	S/BG	$[C_n]_{opt}$ (nM)
C20	20	16	18.6 ± 2.7	3.25 ± 0.48	5.72	45
C19	19	135	149 ± 11	5.54 ± 0.93	26.9	80
C18	18	539	446 ± 59	9.52 ± 1.33	46.8	110
C17	17	3370	2550 ± 220	7.12 ± 1.67	358	170
C16	16	28 600	7100 ± 740	8.47 ± 0.38	838	480
C15	15	297 000		17.5 ± 6.3		20 000

[a] Notes: $K_{d,B}$, calculated dissociation constant for variable segment of connector in 100 mM salt and 1 mM Mg^{2+}; $K_{d,eff}^{BG}$ and $K_{d,eff}^{S}$, measured effective dissociation constants of background and signal, respectively; $[C_n]_{opt}$, optimal connector concentration for PLA; unvaried $K_{d,A}$ = 14.8 nM.

3.1.3.6 DNA Melting Curve Measurement

The melting temperatures (T_m) of DNA oligomers C_{16} through C_{20} (sequences in Table 3-1) were determined using a Bio-Rad CFX96 qPCR instrument (Figure 3-4). Working solutions consisted of varying concentrations of oligomers and 200 nM of the DNA intercalating dye PicoGreen (em ~520 nm; Invitrogen) in 50 mM Tris-HCl (pH 7.5), 100 mM NaCl, and 1 mM $MgCl_2$. Oligomer concentrations were intentionally adjusted to approximately 3 × $K_{d,B}$ from Table 3-2 (calculated values). In this way, a constant T_m for C_{16} through C_{20} inferred accuracy of SantaLucia's[13] thermodynamic

nearest-neighbor modeling approach for estimating $K_{d,B}$ values. Fluorescence was measured as a function of temperature, and the derivative of the fluorescence was fit to Gaussian functions using nonlinear least squares fitting to determine Tm values (peak center).

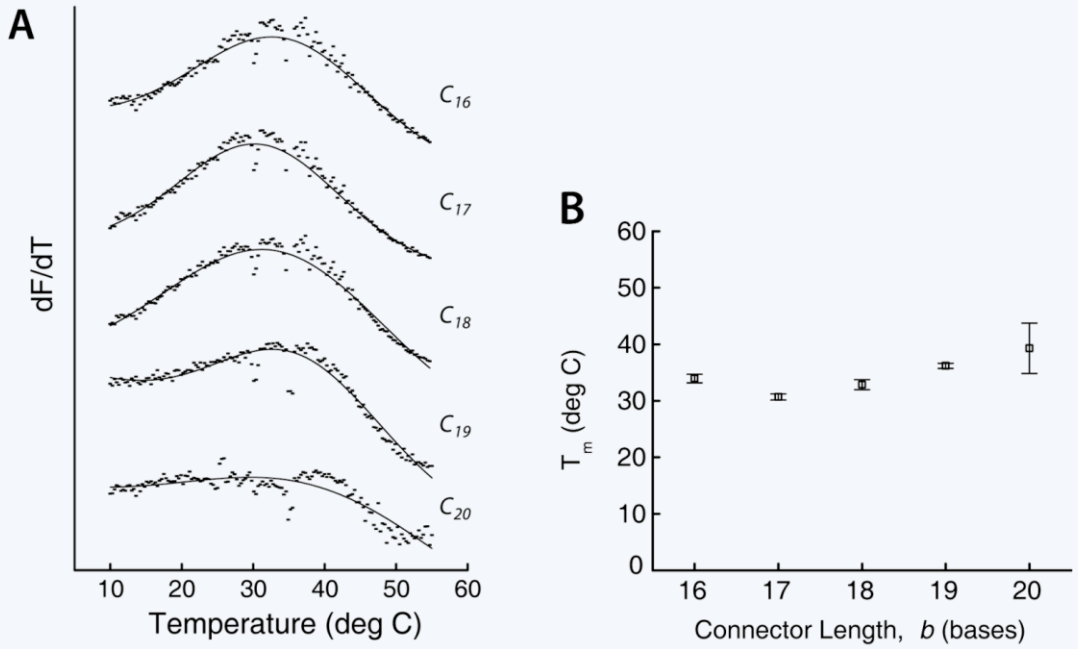

Figure 3-4: (A) Fluorescence melting curves of DNA oligomers from Table 3-1. (B) Melting temperatures (Tm) were kept essentially constant using variable oligomer concentrations of 3 × $K_{d,B}$.

3.1.4 Signal and Background in Proximity Ligation

A schematic of the original, aptamer-based PLA[1,3] is shown in Figure 3-2A, in the context of protein detection with aptamer probes. The quantitative capability of PLA is most heavily dependent upon two steps: the cooperative hybridization of the four-part complex, aptamer A−target−aptamer B−connector (apt_A−T−apt_B−$C_{20,PLA}$), followed by the proximity-dependent ligation of the two aptamers using a DNA ligase. This process results in an amount of ligated product that is proportional to the original amount of protein analyte ("signal" ligations), albeit with some analyte-independent ligation products present ("background" ligations). Although qPCR does not differentiate signal from background ligations, under optimized conditions[1,3] the signal will be dominant over background to allow highly sensitive, indirect detection of the protein analyte. Signal enhancement over background in PLA is based on the proximity effect. The effective concentrations of two aptamers are significantly increased due to their proximity, afforded by simultaneous binding to the same protein.[4-6]

The chief interference in PLA is target-independent, background ligation (Figure 3-2A, bottom). This background ligation has been reported to result from two sources.[1,3,14] First, based simply on binding equilibria, a fraction of aptamers will always hybridize with the 20-base connector sequences ($C_{20,PLA}$), even in the absence of protein analyte, resulting in target-independent ligations that increase the background levels in the assay.[1,3] Second, the T4 DNA ligase is capable of ligating a small fraction of ssDNA sequences, even in the absence of a connector sequence.[14,15] This will also increase assay background. Importantly, the presence of this background limits the amount of usable aptamer (or antibody) probes, which affects the sensitivity and partially defines the upper

limit of the dynamic range.[3] Methods to widen dynamic range would address a major weakness of PLA and significantly improve the applicability of the assay.

3.1.5 Design of Experimental Model of Proximity Hybridization

We hypothesized that by decreasing connector binding affinities for aptamers using an asymmetric connector (Figure 3-2B), the amount of background ligation products would be greatly reduced compared to signal ligation products. In turn, this should allow the use of higher aptamer concentrations, which can increase the upper limit of dynamic range and improve sensitivity. This hypothesis was based on the inherent signal enhancement given by cooperative binding in the proximity effect,[4-6] which does not apply to background. To understand the impact of connector binding affinity on S/BG ratio in PLA, we developed a simple experimental model using DNA hybridization and fluorescence quenching (Figure 3-5). First, we define an "asymmetric connector" in the model system as a connector with one side shortened, compared to the original PLA connector, $C_{20,PLA}$. Herein, model connector sequences are represented by C_b, where b is equal to the total number of bases in the connector that are complementary to the Loop sequence. For example, the symmetric connector used in the model is represented by C_{20}, similar to the 20-base connector used in the original PLA work,[1,3] whereas an asymmetric connector with only six bases in the variable region is represented by C_{16}. Sequences are noted in Table 3-1, with variable regions in bold. (Note that connectors used later for PLA or asymmetric PLA are differentiated from model connectors using the subscript "PLA," such as $C_{20,PLA}$ or $C_{16,PLA}$.) In our model system, signal and background were treated separately. The equilibria shown in Figure 3-5 represent signal complex formation

with a sequential binding mode and background complex formation with an independent binding mode. These are not blind assumptions but are based upon Hill coefficients which were determined by nonlinear least-squares fitting of our experimental data (discussed in detail below).

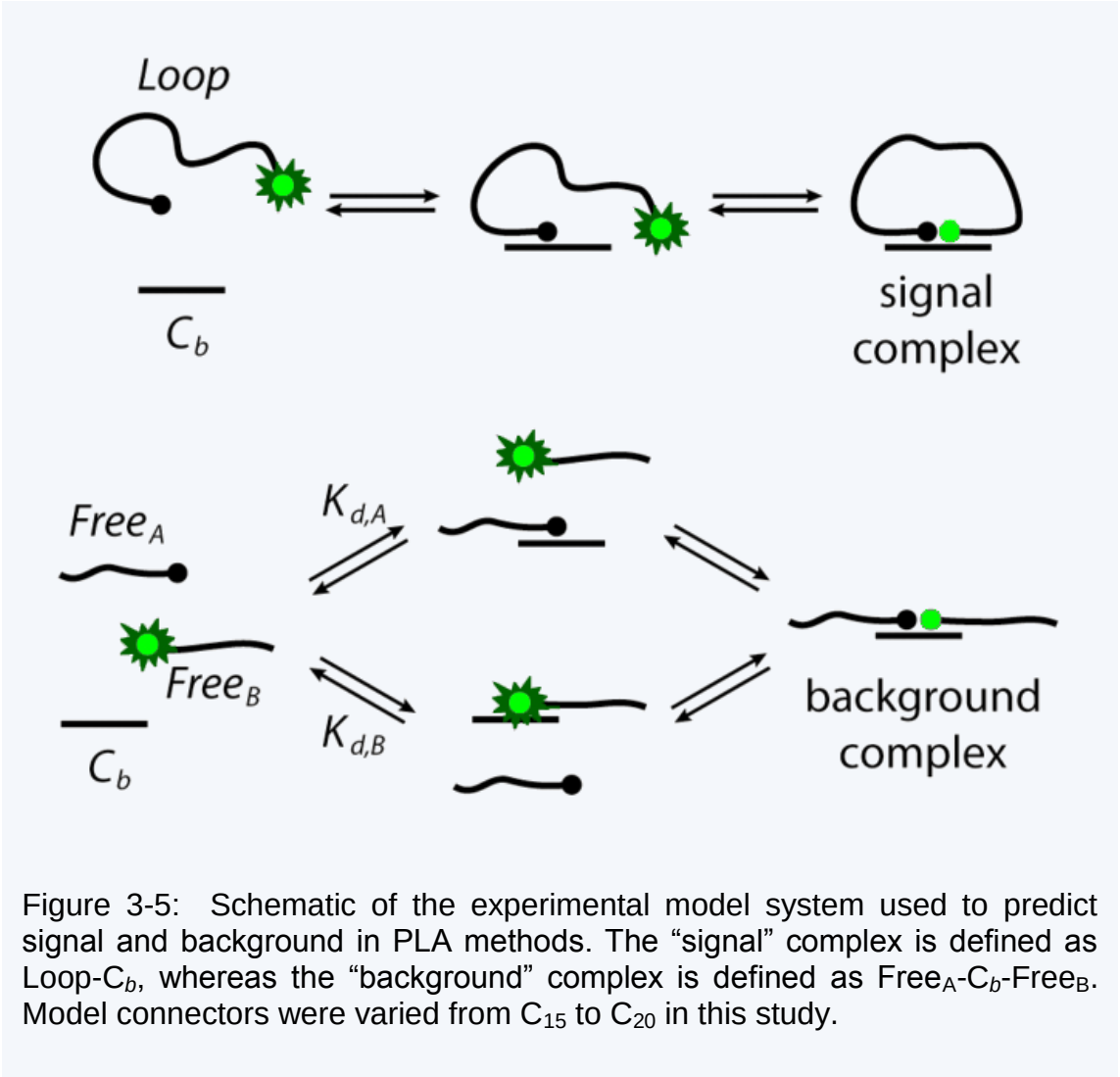

Figure 3-5: Schematic of the experimental model system used to predict signal and background in PLA methods. The "signal" complex is defined as Loop-C_b, whereas the "background" complex is defined as $Free_A$-C_b-$Free_B$. Model connectors were varied from C_{15} to C_{20} in this study.

To model target-dependent signal in PLA, a single DNA loop was hybridized with connector sequences (Figure 3-5, top). The $apt_A{-}T{-}apt_B$ complex in PLA was modeled using a 100-nucleotide DNA loop (Loop) that is capable of hybridizing with a connector sequence at both ends, representing the ideal case in which aptamers possess infinite affinities for their protein analyte (K_d's $\approx$ 0). To measure the extent of hybridization, the Loop was covalently labeled with IABkFQ quencher at the 5′-end (black circle) and with FAM at the 3′-end (green circle). Quenching of FAM fluorescence ensued when both the 5′- and 3′-ends of the Loop were hybridized to a connector sequence, mimicking the proximity hybridization complex in PLA (i.e., $Loop{-}C_b$ represents $apt_A{-}T{-}apt_B{-}C_{20,PLA}$). Thus, a decrease in Loop fluorescence was referred to as "signal" in this case. The model of background ligations in PLA (Figure 3-5, bottom) follows from the model of signal. The FAM- and IABkFQ-labeled Loop sequence was essentially split into two free strands ($Free_A$ and $Free_B$), representing aptamers unbound by protein analytes. Upon combination of both free strands and a connector sequence, the extent of fluorescence quenching represented target-independent hybridization in PLA and was proportional to the amount of background ligation products that would be expected (i.e., $Free_A{-}C_b{-}Free_B$ represents $apt_A{-}C_{20,PLA}{-}apt_B$). Thus, a decrease in fluorescence was referred to as "background" in this case.

3.1.6 Complex Formation with Asymmetric Connectors

Moving toward our goal of reduced background in PLA, the experimental model (Figure 3-5) was used to determine effective dissociation constants ($K_{d,eff}$) of signal and background complexes at different connector lengths (C_b, where $15 \leq b < 20$). The

assumption was that the $K_{d,eff}$ values could represent the relative amounts of signal and background. Separate titrations of the Loop and Free strands with the C_b strand gave the corresponding $K_{d,eff}$ values of the complexes. The S/BG was then calculated as

$$\text{S/BG} = \frac{K_{a,eff}^{S}}{K_{a,eff}^{BG}} = \frac{K_{d,eff}^{BG}}{K_{d,eff}^{S}} \quad (1)$$

This S/BG represents the ideal case in which aptamers have infinite affinities for the target (K_d's $\approx$ 0).

Connectors' affinities for the $Free_B$ strand (or for one arm of the Loop) were reduced by decreasing the number of complementary bases to $Free_B$ or the Loop arm (blue segments in Figure 3-1B; blue text in Table 3-1). Base-pairing dissociation constants for the invariable segment ($K_{d,A}$) and for each variable segment ($K_{d,B}$) of the connectors were calculated (Table 3-2) using the well-established, thermodynamic nearest-neighbor model.[13] Starting with the 20-base connector (C_{20}) similar to that used in standard PLA, the variable segment was decreased in length, resulting in five different asymmetric connectors (C_{15} through C_{19}). Titrations with these asymmetric connectors and the symmetric control connector (C_{20}) were carried out on both the signal and background models (Figure 3-5), and the decrease in fluorescence was used to assay stability.

3.1.7 Background Reduction in the Experimental Model

Modeling of cooperative complex formation has proven difficult, particularly in the realm of predicting the affinity of bivalent ligands based on known affinities of each individual ligand.[4-6] Rather than attempting to develop an extensive model of the system shown in Figure 3-5, titration data was analyzed using the Hill equation,[16] a simplified

model that has found wide use in biochemistry, physiology, and pharmacology to analyze binding equilibria and ligand-receptor interactions.[17] According to Weiss,[17] the Hill coefficient is best described as an "interaction coefficient" that reflects the extent of cooperativity among multiple ligand binding sites. Since it is expected that cooperativity is inherent to the formation of the apt_A−T−apt_B−C_{20} complex in PLA, or the Loop−C_b complexes in our model, we employed nonlinear least-squares (NLLS) fitting of our data to the Hill equation (eq 2) to assay this cooperativity and to determine $K_{d,eff}$ values.

$$S = S_i + (S_f - S_i)\frac{[C_b]^n}{(K_{d,eff})^n + [C_b]^n} \qquad (2)$$

where S is the fluorescence signal measured as a function of [C_b], the connector concentration, S_i and S_f are the initial and final signals, respectively, and $K_{d,eff}$ represents the effective dissociation constant of the Loop−C_b complex ($K_{d,eff}^{S}$) or the $Free_A$−C_b−$Free_B$ complex ($K_{d,eff}^{BG}$). In this way, fluorescence measurements during titration with increasingly higher [C_b] could be fit to the Hill equation (eq 2) and the $K_{d,eff}$ values could be extracted. Furthermore, each extracted Hill coefficient, n, represented the extent of cooperativity in that particular system. Our expectation was that the Loop−C_b complexes (signal) would have significantly increased cooperativity (higher n) compared to the $Free_A$−C_b−$Free_B$ complexes (background).

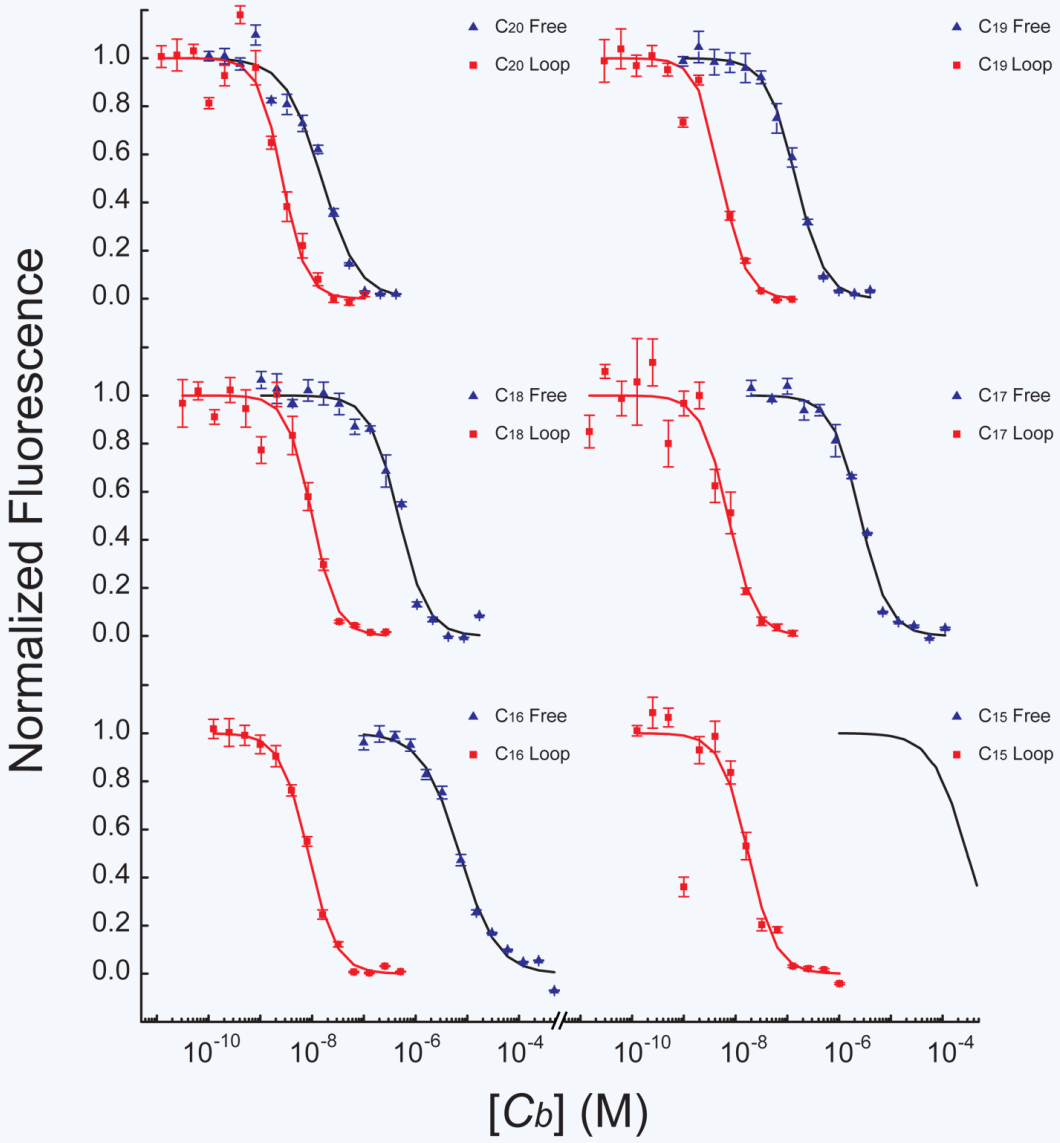

Figure 3-6: Results of experimental model of proximity hybridization. Fluorescence response curves for the signal (*Loop*, red squares) and background (*Free*, blue triangles) complexes when titrated with C_{15} through C_{20}. NLLS fits to the Hill equation (Eq. 2) are shown as solid curves. It is clear from this depiction that as the connector affinity decreases, the background stability is drastically decreased, while the signal stability is only moderately decreased.

Example data sets from these titrations are shown in Figure 3-6, with error bars representing standard deviations of the triplicate measurements. Figure 3-6 shows that the Loop−C_b complex (red squares) is more thermodynamically favored compared to the $Free_A$−C_b−$Free_B$ complex (blue triangles). All titrations were fit to eq 2 via NLLS fitting to determine $K_{d,eff}$ values and S/BG (via eq 1) for each asymmetric connector (C_b); measured and calculated values are shown in Table 3-2. This figure clearly shows that the relative stability of the signal complex (Loop−C_b, red squares) over the background complex ($Free_A$−C_b−$Free_B$, blue triangles) is increasing with decreasing connector length through C_{20} to C_{15}. With the use of the symmetric connector, C_{20}, the S/BG value was determined to be 5.72, the S/BG value using C_{16} was determined to be 838. Thus, a 146-fold increase in S/BG was achieved by simply decreasing the connector length in an asymmetric manner. As shown in Figure 3-7A, the background levels with C_{20} were 382-fold larger than the background with C_{16}, whereas the signal differed by only 3.16-fold. These large decreases in background and only modest decreases in signal gave the expected increase in S/BG with decreasing connector affinity (Figure 3-7B). The agreement between measured $K_{d,eff}^{BG}$ and calculated $K_{d,B}$ values was also encouraging (Figure 3-7C). It must be noted that the background complex titration experiment for C_{15} was impractical, due to the expense involved in working with millimolar concentrations of DNA. Although, using nearest-neighbor calculations,[13] it is predicted that the S/BG could be as high as 1.7×10^4 for C_{15}. These results provided a first step toward confirmation of our hypothesis. Also shown in Figure 3-7B is a curve (dashed line) calculated from data presented by Tian and Heyduk,[6] who developed a similar experimental model using bivalent ligands of various affinities. It is clear that the general

trend observed in our data matches with that seen by Tian and Heyduk with an obvious offset in magnitude. This offset is likely due to the model differences, in which Tian and Heyduk used a 6 nm spacer between their binding sites, whereas our model has essentially no spacer between the binding sites. Inclusion of an equivalent spacer in our system would be unreasonable, since PLA requires subsequent ligation of the aptamers after hybridization of the signal complex. Nonetheless, the similarities were encouraging.

Figure 3-7B presents the relationship between S/BG and the affinities of the variable segments of the connectors, which are represented by the calculated $K_{d,B}$ values[13] (Table 3-2). This analysis is useful, since $K_{d,B}$ will ultimately become the independent variable in the asymmetric PLA approach. As shown in the figure, S/BG increases proportionally with $K_{d,B}$. In theory, one could increase $K_{d,B}$ even further. In the extreme example, one could use C_{11} (only one base pair in the variable segment). However, the S/BG parameter is not useful if there is insufficient signal present with respect to the noise of measurement, and it is likely that the amount of either signal or background (or both) complexes using C_{11} would be negligible. The connector length, b, could be considered an alternative for the independent variable (shown as upper axis in Figure 3-7, parts A and B), but care must be taken, since b remains dependent upon base composition, making it less precise than $K_{d,B}$.

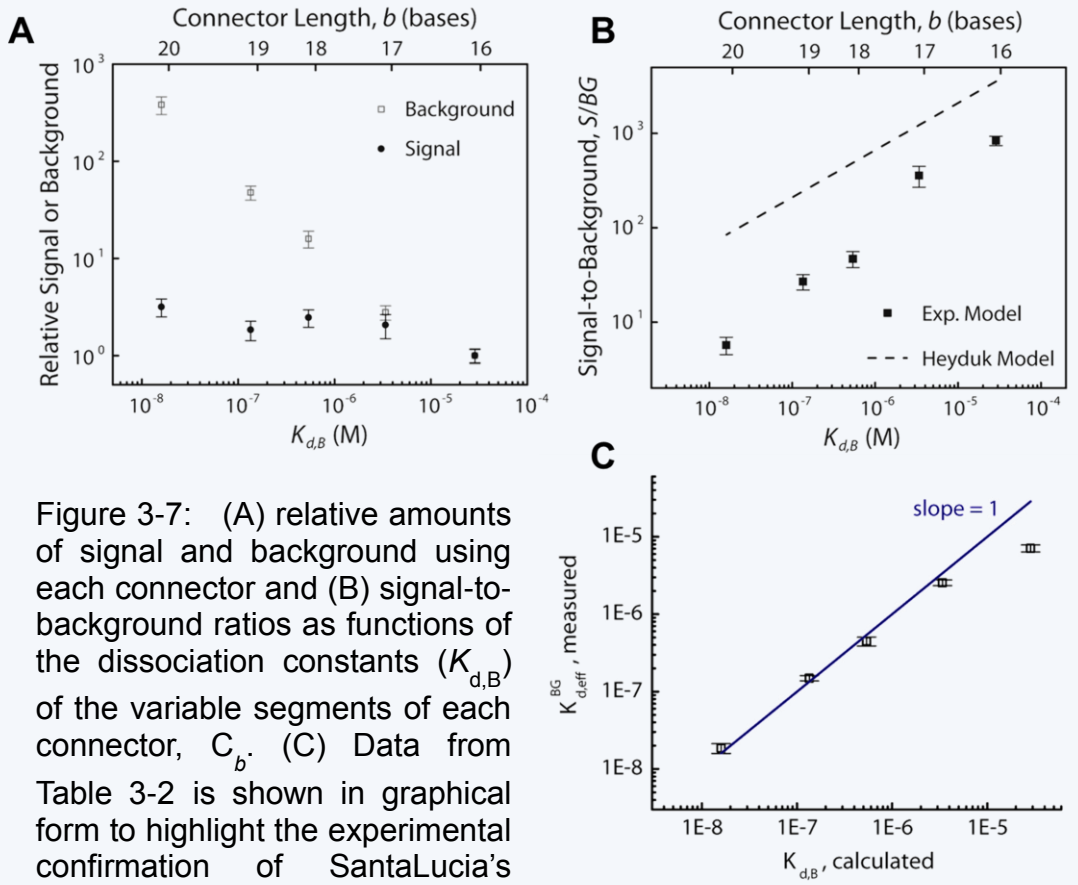

Figure 3-7: (A) relative amounts of signal and background using each connector and (B) signal-to-background ratios as functions of the dissociation constants ($K_{d,B}$) of the variable segments of each connector, C_b. (C) Data from Table 3-2 is shown in graphical form to highlight the experimental confirmation of SantaLucia's nearest-neighbor calculations of $K_{d,B}$. Ideally, $K^{BG}_{d,eff}$ should equal $K_{d,B}$. Since the majority of the points follow a slope of unity (black line), the measured and calculated values are shown to be well correlated.

Hill coefficients (n) were also determined by NLLS fitting of the data to eq 2. The mean n values for formation of all of the background ($Free_A{-}C_n{-}Free_B$) and signal ($Loop{-}C_n$) complexes were 1.42 $\pm$ 0.19 and 1.76 $\pm$ 0.11, respectively. These values were shown to be statistically different ($p < 0.01$). Cooperativity enhancement in the

signal complex was expected, since this effect gives PLA the ability to discriminate signal from background. Furthermore, as reported by Weiss,[17] these Hill coefficients suggest that the signal complex forms in a sequential manner, whereas the background complex forms in an independent manner, as reflected in Figure 3-5.

In summary, the improvements in S/BG in the experimental model is derived from the more than 2 orders-of-magnitude increase in $K_{d,eff}^{BG}$ (reduced affinity) that is achieved using asymmetric connectors, whereas $K_{d,eff}^{S}$ is increased by less than 1 order of magnitude (Table 3-2, Figure 3-7A); thus, by eq 1, S/BG is increased significantly (Figure 3-7B). However, application of asymmetric connectors to PLA requires experimental confirmation, as given below, since we began our model with the assumption of infinite aptamer affinities.

3.1.8 Confirming the Experimental Model in Asymmetric PLA

3.1.8.1 Design of Asymmetric PLA

A schematic of asymmetric PLA is shown in Figure 3-2B. Since decreased background was achieved in the experimental model (Figure 3-6, 3-7), the next step was to confirm that this approach was useful for PLA. The real assay is inherently more complicated than the experimental model, requiring not only a four-part complex formation but also ligation of apt_A to apt_B, followed by qPCR.[1,3] Furthermore, aptamer affinities are finite in the real system, compared to the assumption of infinite affinities in the model. On the basis of these factors, we expected that the observations from the model would be less pronounced in the real system. Asymmetric PLA (Figure 3-2B) is based on the formation of the complex $apt_A{-}T{-}apt_B{-}C_{b,PLA}$, where $b < 10$ is achieved by

decreasing connector lengths on the side complementary to apt_B. Shorter connectors, therefore, have higher $K_{d,B}$ (Table 3-2), or lower affinity.

For the standard PLA system ($C_{20,PLA}$, b = 20), the optimal connector concentration was determined to be > 40 nM.[1] This correlates well with the model results shown in Figure 3-6. At $C_{20,PLA}$ = 40 nM, the stability of the signal complex is near maximal, whereas the stability of the background complex is minimized as much as possible. Working on this principle, the results from the titrations in the experimental model (Figure 3-6, 3-7) were used to estimate the optimal connector concentrations, $[C_n]_{opt}$, for each model connector of different length. These values are reported in the rightmost column of Table 3-2 and were used for all asymmetric PLA experiments to follow. This approach allowed the interrogation of each asymmetric PLA system at its optimal values of signal and background.

3.1.8.2 Background Reduction Using Asymmetric PLA

Starting with the identical reagents used by Landegren and co-workers[1,3] for sensitive detection of human thrombin, connector lengths were systematically decreased from the initial $C_{20,PLA}$ sequence. Background ligation levels were measured by carrying out the assay without the target protein (human thrombin) present. As shown in Figure 3-8A, the background levels in asymmetric PLA were significantly reduced by increasing $K_{d,B}$ (or decreasing length, b), matching well with the experimental model (Figure 3-7A). Background levels in asymmetric PLA with $C_{16,PLA}$ were 46.7-fold lower than with standard, symmetric PLA ($C_{20,PLA}$), thus confirming our hypothesis. It should, therefore,

be possible to use higher concentrations of aptamer probes with asymmetric PLA to improve the dynamic range and sensitivity.

3.1.8.3 Dynamic Range and Sensitivity Enhancement with Asymmetric PLA

A major limitation of standard PLA is the relatively narrow dynamic range. This disadvantage is directly related to the generation of background ligations. The original work in PLA for human thrombin detection determined the optimal concentrations of aptamer probes to be 15 and 20 pM for apt_A and apt_B in the 5 μL incubation mixture, respectively.[1] At higher probe concentrations, increased background ligations were shown to be detrimental to the S/BG of the assay. Since the assay relies on the simultaneous binding of two aptamers to the same target, simple probability theory shows that the population of signal complexes (apt_A−T−apt_B−$C_{b,PLA}$) will first increase then decrease as the concentration of target is increased. The upper limit of the dynamic range is thus positively related to both the concentrations and the K_d's of the aptamer probes. Gullberg et al.[3] showed that target at 10 times higher concentration than probes could not be assayed with probe K_d < 0.4 nM but could be assayed with a probe K_d = 2.5 nM, albeit with relatively low S/BG. This implies that in standard PLA, a lower LOD is achievable with higher affinity probes at the expense of narrow dynamic range.

Previous publications using standard, aptamer-based PLA for thrombin detection did not report the LOD or the dynamic range.[1,3] However, by analyzing the presented data, the reported LOD was determined to be 16 amol (significantly different from background, $p < 0.05$), with a dynamic range from 16 to 400 amol. In our laboratory, with the standard PLA system using $C_{20,PLA}$, we obtained a detection limit about 3-fold

higher than 16 amol, but we were able to achieve a significantly wider dynamic range compared to the previous reports. As shown in Figure 3-8B (open blue squares), our standard PLA detection limit was 50 amol, and our dynamic range was from 50 to 3000 amol (7.68-fold wider than previous reports).

With significant reductions in background using asymmetric PLA (Figure 3-8A), we hypothesized that the dynamic range could be improved using higher aptamer concentrations with connector $C_{16,PLA}$. This hypothesis was confirmed by titration of the system with human thrombin (Figure 3-8B). Asymmetric (closed black circles) and standard (open blue squares) PLA were carried out under the following optimal conditions in the 5 μL incubation mixture: asymmetric, $[C_{16,PLA}]$ = 480 nM, $[apt_A]$ = 0.9 nM, and $[apt_B]$ = 1.2 nM; standard, $[C_{20,PLA}]$ = 45 nM, $[apt_A]$ = 15 pM, and $[apt_B]$ = 20 pM. Using asymmetric PLA, the dynamic range was increased by 2 orders of magnitude, and the sensitivity was improved by a factor 1.57 compared to the standard system with $C_{20,PLA}$ (Figure 3-8, parts B and C). In addition, the maximum achievable S/BG was larger by a factor of 3.15. These improvements were accomplished with an additional 3-fold improvement in LOD to 5.0 amol of thrombin. When compared to previously reported data,[1,3] our dynamic range was improved by an even larger factor of 323. In Figure 3-8B, horizontal bars mark the dynamic ranges (blue line is for asymmetric PLA, orange line is for standard PLA), with the upper bounds defined as the highest concentration with a statistically higher ($p < 0.05$) value of signal-to-background ratio compared to the adjacent lower concentration. Error bars represent standard errors of quadruplicate runs of qPCR.

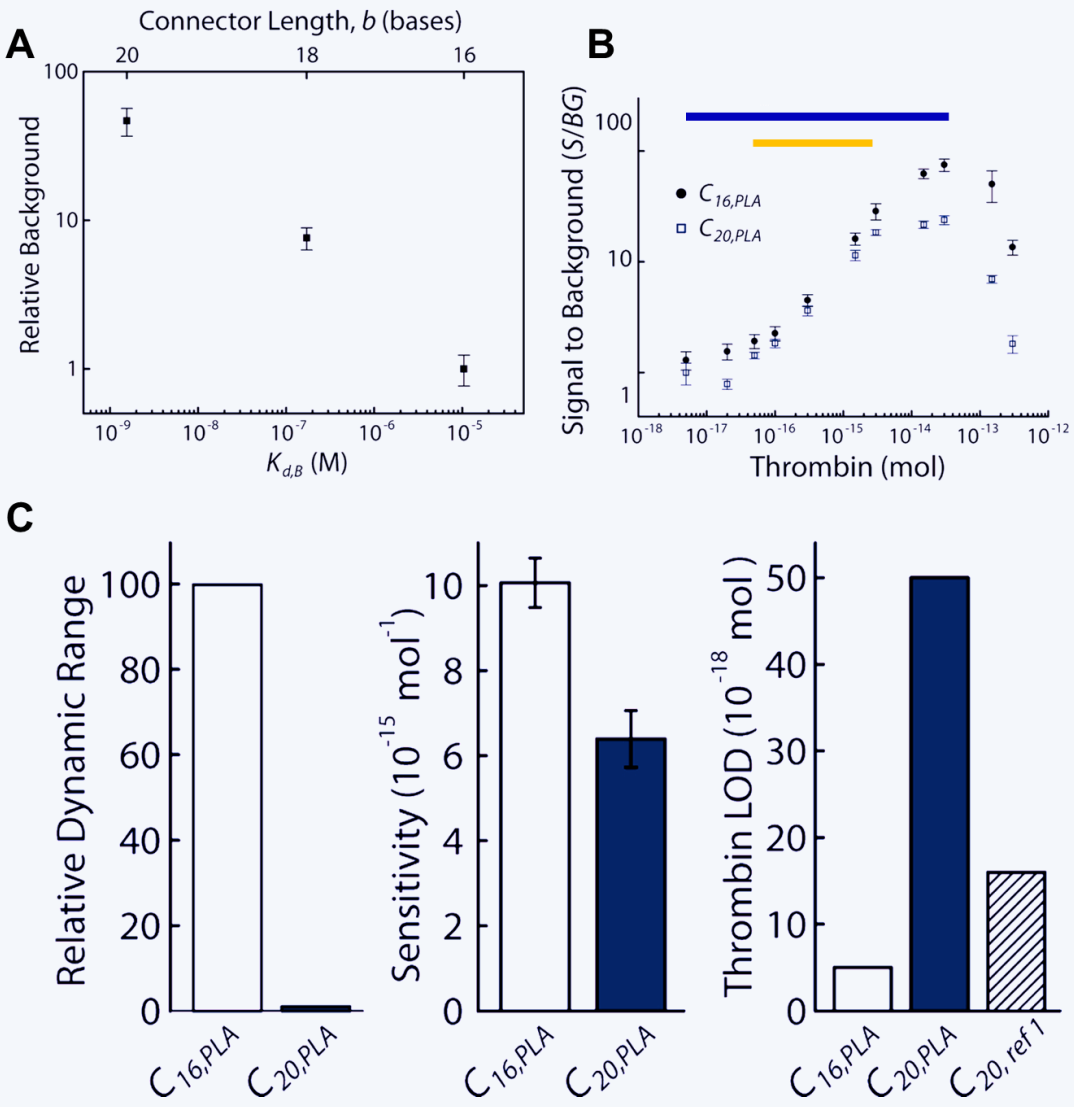

Figure 3-8: Asymmetric PLA. (A) Amount of background ligations vs dissociation constant ($K_{d,B}$) of the variable segments of each connector, $C_{b,PLA}$, in the absence of target protein. (B) Titration with human thrombin. Asymmetric connector $C_{16,PLA}$ (filled black circles) and symmetric connector C20,PLA (open blue squares) were used for comparison. Error bars represent the standard error of quadruplicate qPCR measurements. Horizontal bars define the assay dynamic ranges. (C) Linear scale comparisons of dynamic range, sensitivity, and limit of detection (LOD) improvements using asymmetric connector $C_{16,PLA}$ (white bars) compared to the standard connector $C_{20,PLA}$ (blue bars). Error bars depict standard deviations of linear sensitivities. The cross-hatched bar represents the LOD obtained in the original reports of PLA.

Since logarithmic scales were used in Figure 3-8B, linear scale comparisons of dynamic ranges, sensitivities, and limits of detection are shown in Figure 3-8C. Sensitivities were determined as the slopes of the linear regressions of both data sets in the range from the LOD to 3000 amol. This figure helps to clarify the significant advantages provided by asymmetric PLA, in comparison to standard PLA. Most notably, our approach of using asymmetric connectors has allowed a significant improvement in one of the major limitations of the assay, dynamic range. This improvement should be generally applicable to any of the previously developed PLA methods.[1,3-11]

3.2 DNA-Based Experimental Model of Electrochemical Proximity Assay (ECPA)

3.2.1 Background

Sandwich immunoassays are now widely adopted for bioanalytical quantitation of a multitude of proteins in various fields, and there are numerous assay kits available for purchase. The assays possess both high sensitivity and selectivity, due in large part to the requirement of simultaneous binding of two high-affinity antibodies, and they are highly scalable. However, from a biosensing perspective, sandwich immunoassays still have room for improvement. These heterogeneous assays cost ~$10 per sample and require washing steps, making protocols tedious and time-consuming, with significant user intervention and reagent volumes required. Point-of-care analysis is difficult to envision using sandwich ELISAs.

Proximity ligation assays (PLA) (Figure 3-9A) are some of the most simple-to-use and sensitive protein assays developed to date. PLA is homogeneous and can achieve protein detection limits in the zeptomole range (fM in 1 μL). A key concept in PLA is the "proximity effect," i.e. when two oligonucleotide-conjugated antibodies are bound to target, the local concentration of the oligos is largely increased, making weak interactions with connectors more kinetically feasible. Probes are then enzymatically ligated, and the products are PCR amplifiable. PLA can be used with aptamers or with antibodies. A modified version of this assay is the molecular pincer assay (Figure 3-9B).[19] Although this assay will have lower sensitivity, it can achieve highly specific, homogeneous protein detection (pM detection limits), with direct readout using fluorescence resonance energy transfer (FRET) between dyes attached to the oligo arms, making it amenable to point-of-care analysis.

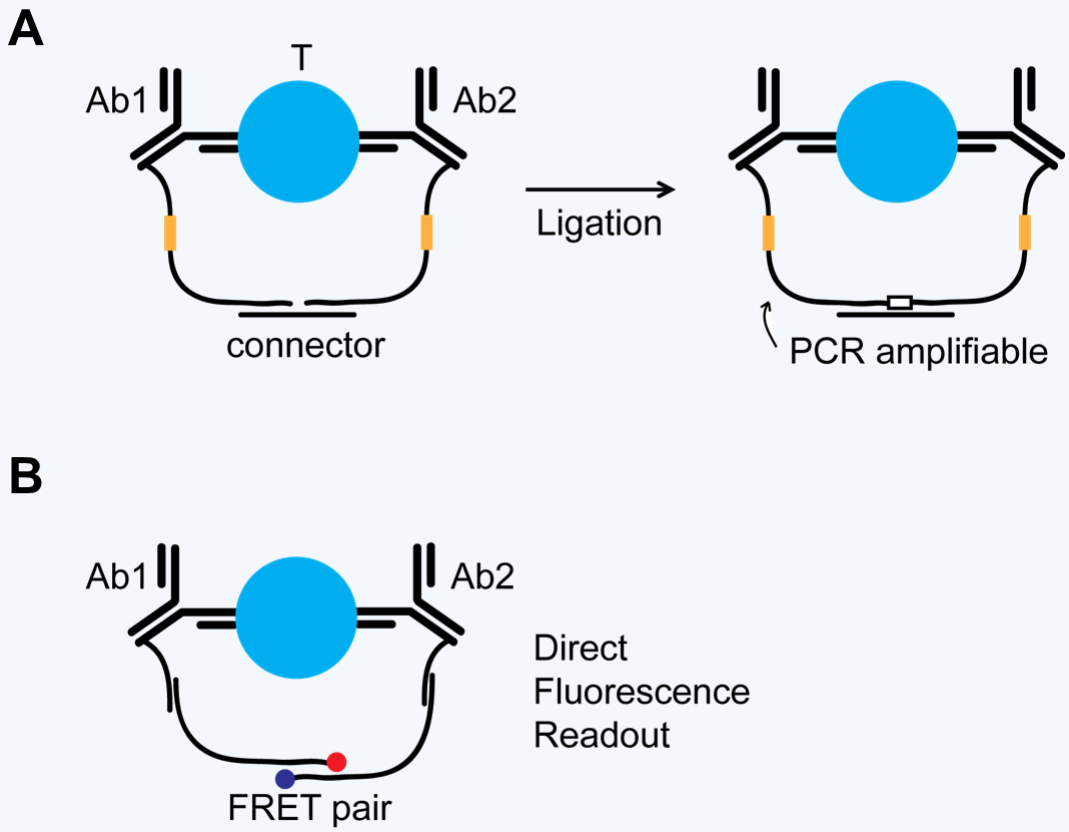

Figure 3-9: (A) Proximity ligation assays (PLA) and (B) molecular pincer assays.

A disadvantage of the aforementioned assays is that purification of the Ab-oligo conjugate is a determining factor for sensitivity. Use of aptamers in these assays has the potential to significantly improve performance. Aptamers are RNA or single stranded DNA (ssDNA) molecules that have been isolated from random-sequence nucleic acid libraries and selected for high affinity against a target protein, small molecule, or even

whole cells. Aptamers exhibit a number of advantages over antibodies as molecular recognition elements, especially for diagnosis. Their in vitro isolation eliminates the need for animal hosts, chemical modification of nucleic acids is highly flexible and well-developed, and aptamer binding affinity can be tailored. Furthermore, aptamers can bind virtually any molecule, even toxic or non-immunogenic targets. Lastly, aptamers will refold into functional structures after exposure to extreme conditions (pH, temperature, etc.), making them amenable to reusable biosensors. Thus, SELEX has opened a new and promising field of research, giving more than mere alternatives to antibodies.

Our proposed approach will combine the proximity effect (Figure 3-9) with an electrochemical approach recently proven feasible by the Revzin group. They used a structure-switching aptamer to move an electrochemically active species away from a gold electrode as target was bound, providing homogeneous, electrochemical (EC) detection of interferon gamma with 0.06 nM detection limit. However, the flexibility of this approach is severely limited due to the requirement of a structure-switching aptamer, which will not exist against many targets.

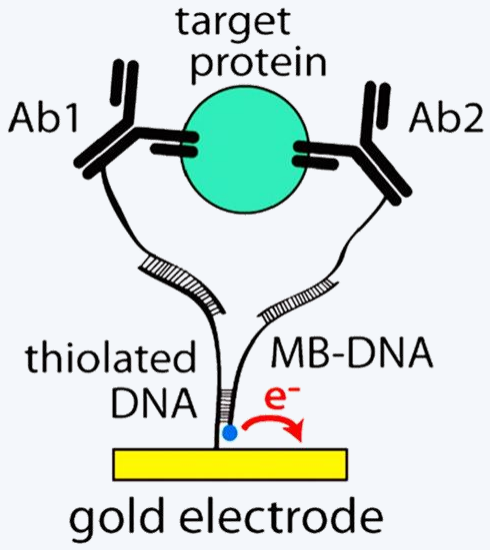

Figure 3-10: The electrochemical proximity assay (ECPA). In the presence of the target protein, this five-part complex moves the redox-active methylene blue (MB) near the gold surface, thus increasing current in proportion to the protein analyte.

As shown in Figure 3-10, we propose to use the proximity effect to move the EC-active methylene blue (MB) closer to a gold electrode upon binding of two antibody-oligo conjugates to protein targets. This novel combination of proximity-dependent assays with EC current enhancement allows wash-free, highly-sensitive, and highly selective detection of target molecules, in a format amenable to point-of-care use. The assay format will be extremely flexible, since any target with two antibodies could be assayed.

3.2.2 Model Systems of ECPA

As in our previous work with PLA,[18] here we utilized a DNA loop to model the probe-target complex in ECPA (Figure 3-11), making the assumption that probe affinity for the target protein is infinite. The 80-nucleotide DNA loop mimics formation of the ECPA complex, bringing MB near the gold surface and increasing redox current. The background was modeled using only the thiolated DNA and MB-DNA (Figure 3-11). This experimental model greatly simplified the optimization of experimental parameters. Since the surface-dependent ECPA involves a different type of cooperative complex formation compared to homogeneous PLA, we devised two new strategies for minimizing background in ECPA.

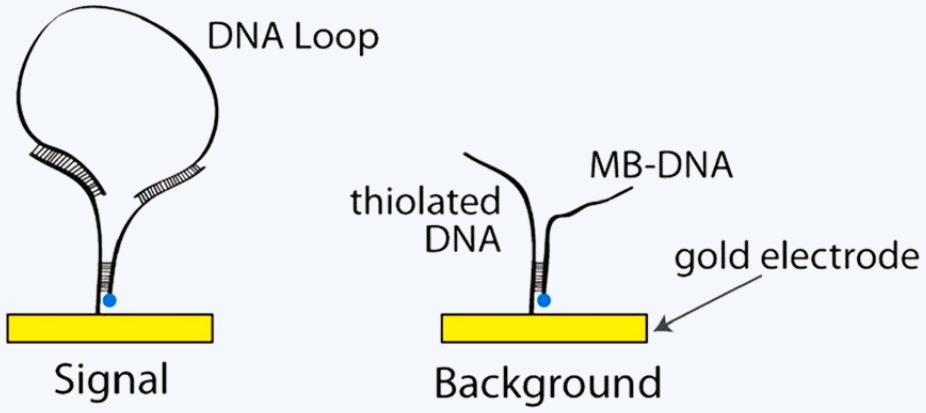

Figure 3-11: DNA-based model for ECPA. A continuous DNA loop is used to model the Signal complex shown in Figure 3-10. Background is modeled by simply adding MB-DNA without the loop.

The first strategy was to decrease the binding affinity between thiolated DNA and MB-DNA by reducing the number of complementary bases in the thiolated DNA (Figure 3-12A). The hypothesis was that the amount of background hybridization between thiolated DNA and MB-DNA would be greatly reduced, thereby reducing background current greatly without a large decrease in signal current. However, the background reduction was accompanied by a large decrease in signal (more detail is shown in chapter 4), since the weakened connection also weakened hybridization of the DNA Loop (model of signal). In an attempt to reduce background without such a large signal reduction, our second strategy was to utilize a short DNA competitor with the thiolated DNA. We hypothesized that when using a competitor sequence, background hybridization would occur more slowly than signal hybridization, since both signal and background

complexes must displace the short competitor prior to current enhancement by the MB-DNA strand. Figure 3-12B shows a representation of the delayed background formation over time, mediated by competition with competitor strands. This way, signal should form rapidly, while background would be delayed kinetically by the competitor.

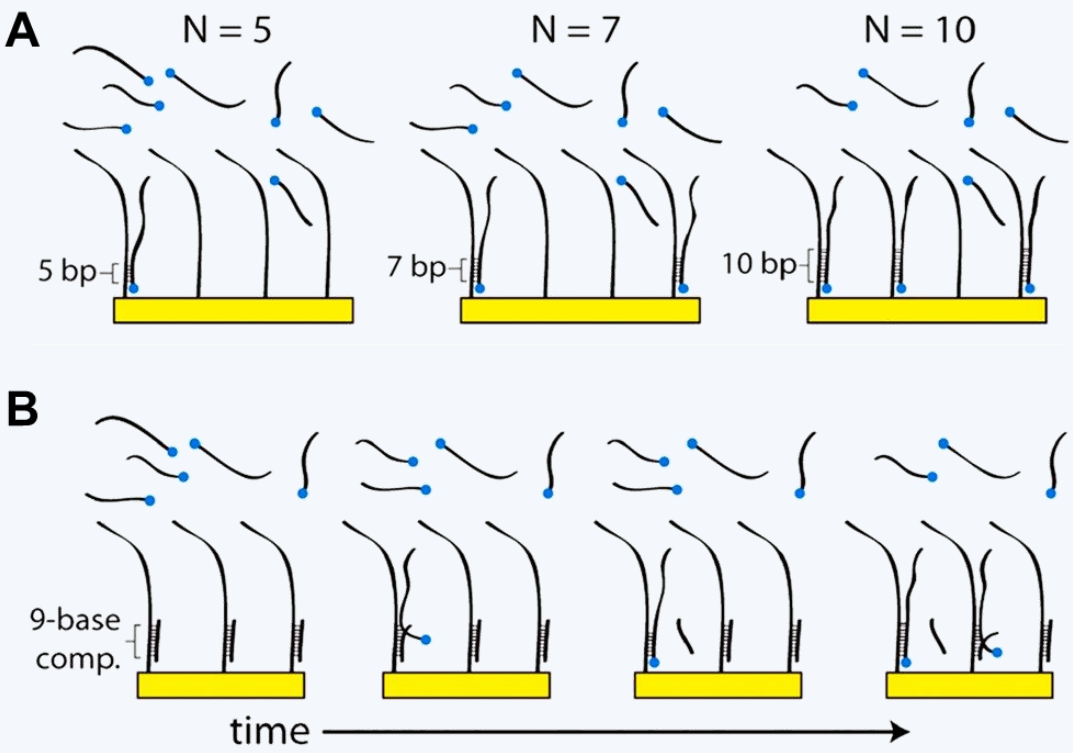

Figure 3-12: Model system strategies. (A) Depiction of background reduction in strategy 1. Fewer base pairs (weaker hybridization) between thiolated DNA and MB-DNA results in lower background current. (B) Depiction of background reduction in strategy 2, where a competitor strand prevents or slows background formation over a given time window.

3.3 Conclusions

This chapter describes experimental models of proximity hybridization that were successfully developed and tested. The first part of the chapter describes modeling and use of asymmetric connectors to significantly improve the dynamic range of PLA, thereby addressing a major limitation of the assay. Learning from the DNA-based models, sensitivity, LOD, and maximum S/BG were also improved in the real assay. By enhancing its already successful predecessor, this asymmetric PLA method approaches an ideal assay system, providing a homogeneous and highly specific protein assay with the capability to detect very small quantities of protein in free solution, at high throughput, and with good dynamic range.

This DNA-based experimental model system ultimately improved our understanding of the proximity effect and its inherent cooperative assembly in PLA or any other proximity assay, highlighting the importance of the interplay between connector-to-aptamer affinities and aptamer-to-target affinities in maximizing S/BG and dynamic range. Generally speaking, low connector affinities can be paired with high probe affinities (aptamers or antibodies) to achieve this goal.

The second part of this chapter reports the use of our DNA model systems to study ECPA. We compared two strategies, in order to decrease background current and widen the gap between background and signal current. The DNA model system design and experimental results provided very important information for the aptamer-based and antibody-based ECPA tests discussed in later chapters.

3.4 References

(1) Fredriksson, S.; Gullberg, M.; Jarvius, J.; Olsson, C.; Pietras, K.; Gu´stafsdo´ttir, S. M.; Ostman, A.; Landegren, U. *Nat. Biotechnol.* **2002**, *20*, 473–477.
(2) Adler, M.; Wacker, R.; Niemeyer, C. M. *Analyst* **2008**, *133*, 702–718.
(3) Gullberg, M.; Gu´stafsdo´ttir, S. M.; Schallmeiner, E.; Jarvius, J.; Bjarnegård, M.; Betsholtz, C.; Landegren, U.; Fredriksson, S. *Proc. Natl. Acad. Sci. U.S.A.* **2004**, *101*, 8420–8424.
(4) Zhou, H. X. *Biochemistry* **2001**, *40*, 15069–15073.
(5) Zhou, H. X. *J. Mol. Biol.* **2003**, *329*, 1–8.
(6) Tian, L.; Heyduk, T. *Biochemistry* **2009**, *48*, 264–275.
(7) Söderberg, O.; Leuchowius, K. J.; Gullberg, M.; Jarvius, M.; Weibrecht, I.; Larsson, L. G.; Landegren, U. *Methods* **2008**, *45*, 227–232.
(8) Gustafsdottir, S. M.; Schlingemann, J.; Rada-Iglesias, A.; Schallmeiner, E.; Kamali-Moghaddam, M.; Wadelius, C.; Landegren, U. *Proc. Natl. Acad. Sci. U.S.A.* **2007**, *104*, 3067–3072.
(9) Nordengrahn, A.; Gustafsdottir, S. M.; Ebert, K.; Reid, S. M.; King, D. P.; Ferris, N. P.; Brocchi, E.; Grazioli, S.; Landegren, U.; Merza, M. *Vet. Microbiol.* **2008**, *127*, 227–236.
(10) Gustafsdottir, S. M.; Wennström, S.; Fredriksson, S.; Schallmeiner, E.; Hamilton, A. D.; Sebti, S. M.; Landegren, U. *Clin. Chem.* **2008**, *54*, 1218–1225.
(11) Hegedüs, E.; Kókai, E.; Kotlyar, A.; Dombrádi, V.; Szabó, G. *Nucleic Acids Research* **2009**, *37*, e112.
(12) Livak, K. J. User Bulletin No. 2: ABI PRISM 7700 Sequence Detection System; PE Applied Biosystems: Foster City, CA, **1997**; pp 11-15.
(13) SantaLucia, J. *Proc. Natl. Acad. Sci. U.S.A.* **1998**, *95*, 1460–1465.
(14) Leslie, D. C.; Sohrabi, A.; Ikonomi, P.; McKee, M. L.; Landers, J. P. *Electrophoresis* **2010**, *31*, 1–8.
(15) Kuhn, H.; Frank-Kamenetskii, M. D. *FEBS J.* **2005**, *272*, 5991–6000.
(16) Hill, A. V. *J. Physiol.* **1910**, *40*, iv–vii.
(17) Weiss, J. N. *FASEB J.* **1997**, *11*, 835–841.
(18) Kim, J.; Hu, J.; Sollie, R. S.; Easley, C. J. *Anal. Chem.* **2010**, *82*, 6976-6982.
(19) Heyduk, E.; Dummit, B.; Chang, Y.-H.; Heyduk, T. *Anal.Chem* **2008**, *80*, 5152-5159.

CHAPTER 4

The Electrochemical Proximity Assay (ECPA)

4.1 Introduction

Diagnostics is one of the most critical steps in health care and medical treatment.[1] Specific protein detection is of great importance in this realm, since it is currently one of the predominant methods to diagnose the onset or progression of disease states.[2,3] Unless specialized point-of-care assays are available for the protein of interest, quantitation is typically performed in a centralized laboratory by technicians.[4] This process is expensive and could waste time that is critical to patient care. Over the years, clinical approaches for point-of-care testing have addressed this challenge for select analytes,[5-9] yet these assay formats are highly specialized to the particular target molecule, thus inflexible to apply to other targets. To keep pace with expectations in future point-of-care testing, there is a need for more flexible, yet highly sensitive, quantitative, and easy-to-use methods.[4]

Although point-of-care devices are welcome in clinical and research laboratories, the existence of surrounding infrastructure places fewer constraints on methodology. Based on their inherent flexibility, sandwich enzyme-linked immunosorbent assays (ELISA) have emerged as the method of choice for protein quantitation in clinical and

research laboratories.[3] Unfortunately, these heterogeneous assays require expert users with dedicated instrumentation, and they are time-consuming, laborious, and expensive. Quantitative, point-of-care protein analysis is thus not possible with standard sandwich ELISA formats. Nonetheless, the flexibility of the dual-antibody recognition concept is highly valuable and has served as a guide to various alternative strategies in recent years.[10-16]

Proximity immunoassays such as the proximity ligation assay (PLA)[11,12] or the molecular pincer assay[13] can overcome some of the limitations of ELISA. PLA, for example, is one of the most simple-to-use and sensitive protein assays developed to date.[17] The assay is homogeneous (no washing steps), and detection limits rival or outperform ELISAs, even with much smaller sample volumes. A key concept in PLA is the "proximity effect," which relies on simultaneous recognition of a target molecule by a pair of affinity probes. The bound probes can then be covalently linked by enzymatic ligation of their oligonucleotide tails, and qPCR is used as the readout, with products proportional to target protein concentration. PLA has been shown functional with aptamer pairs[11] and with a variety of antibody pairs.[12] Although nucleic acid aptamers have garnered significant attention in the analytical and biosensing communities based on their many potential advantages,[18-24] the use of aptamers as affinity probes in PLA is severely limited. PLA requires two aptamers binding at separate sites on the same protein target, but aptamer pairs unfortunately do not yet exist against most targets. In PLA[12] or in the pincer assays,[13] this limitation was overcome by employing antibody-oligonucleotide conjugates as probes, since the popularity and success of sandwich methodology (ELISA, Western blots) has afforded a large, commercially available library

of antibody pairs against many proteins. These assays thus provide simpler and less expensive alternatives to ELISA.

Nonetheless, limitations in current proximity assays impede their use in a point-of-care setting. Although the use of qPCR gives PLA its high sensitivity, this readout requires that each sample be added to a tube with ligation and PCR reagents, and then be inserted into a qPCR instrument followed by 1-2 hours of amplification and analysis. The molecular pincer assays are simpler and more rapid (<20 min),[13] making them more amenable to point-of-care measurements by fluorescence readout; however, the limit of detection of these assays is several orders of magnitude higher than PLA. Thus, there is a need for a more sensitive yet simpler readout for proximity assays that is amenable to point-of-care testing.

Electrochemical detection is of particular interest in the development of biosensors because it offers great signal stability, simple instrumentation, high sensitivity, and ease of calibration compared to fluorescence, as well as excellent compatibility with miniaturization technologies.[25,26] Here, we present the marriage of the proximity assay concept with electrochemical detection to give a simple, highly sensitive, flexible strategy for specific protein quantitation, termed the electrochemical proximity assay (ECPA). ECPA uses the proximity effect to move an electrochemically active label, methylene blue (MB),[27] closer to a gold electrode upon binding of two probes to a protein target, an approach akin to electrochemical DNA sensing[28,29] or specialized aptamer-based protein sensing[30-32] reported by others. In the presence of protein targets, the redox current in ECPA is quantified using square wave voltammetry (SWV) and is found to depend directly on the concentration of target. This detection strategy is based largely

upon pioneering work by the Plaxco group,[33-37] in using MB-labeled DNA for biosensing. Building upon this work and on aptamer-based protein sensing by Zhang et al.,[32] we have added the antibody-based proximity assay concept. We used a DNA-based experimental model to optimize signal-to-background ratios, ultimately providing a direct insulin detection limit that is lower than most commercially available ELISAs, with a dynamic range >40-fold wider than these ELISAs. These results were achieved with direct electrochemical readout, i.e., without requiring washing steps, which bodes well for the future of ECPA in point-of-care settings. In contrast to other approaches for electrochemical protein sensing,[24,30] ECPA should be useful for any protein with available antibody pairs.

4.2 Reagents and Experimental Methods

4.2.1 Reagents and Materials

All solutions were prepared with deionized, ultrafiltered water (Fisher Scientific). The following reagents were used as received: insulin antibodies (clones 3A6 and 8E2; Fitzgerald Industries), 4-(2-hydroxyethyl)-1-piperazineethanesulfonic acid (HEPES) (99.5%), tris-(2-carboxyethyl) phosphine hydrochloride (TCEP), (Sigma-Aldrich, St. Louis, MO), bovine serum albumin (BSA, 98%; EMD Chemicals Inc.), human thrombin, immunoglobulin E (IgE), and insulin (Sigma Aldrich). Methylene blue-conjugated DNA (MB-DNA) was purchased from Biosearch Technologies (Novato, CA), purified by RP-HPLC. Oligonucleotides were obtained from Integrated DNA Technologies (IDT; Coralville, Iowa), with purity and yield confirmed by mass spectrometry and HPLC, respectively. Sequences (listed 5′ to 3′) for aptamer based ECPA were as follows.

Thrombin aptamer A (THRaptA): AGTCCGTGGTAGGGCAGGTTGGGGTGA-CTTTTTTTTTTTTTTTTTATATTTTTTTTTTCTCGCGGATTTGAACCCTAACG;

Table 4-1. Single-Stranded DNA Sequences Used in the ECPA Model Systems (Strategies 1 and 2)[a]

name	(abbreviation)	DNA sequence, listed 5′ to 3′
ECPA-loop	(loop)	TAG GAA AAG GAG GAG GGT GGC CCA CTT AAA CCT CAA TCC ACC CAC TTA AAC CTC AAT CCA CGC GGA TTT GAA CCC TAA CG
ECPA-MB-10	(MB-DNA)	CCA CCC TCC TCC TTT TCC TAT CTC TCC CTC GTC ACC ATG C/MB-C7/
ECPA-gold-10	(G10)	/5ThioMC6-D/GCA TGG TGA CAT TTT TCG TTC GTT AGG GTT CAA ATC CGC G
ECPA-gold-7	(G7)	/5ThioMC6-D/GCA TGG TAT TTT TCG TTC GTT AGG GTT CAA ATC CGC G
ECPA-gold-5	(G5)	/5ThioMC6-D/GCA TGA ATT TTC GTT CGT TAG GGT TCA AAT CCG CG
ECPA-Comp-9	(C9)	TCA CCA TGC
ECPA-Comp-8	(C8)	CAC CAT GC
ECPA-Comp-7	(C7)	ACC ATG C

[a]MB-DNA, G10, and C9 were employed in the optimized detection system. Abbreviations: /MB-C7/ = methylene blue modification (Biosearch), /5ThioMC6-D/ = disulfide bond flanked by two six-carbon spacers (IDT).

Thrombin aptamer B (THRaptB): TAGGAAAAGGAGGAGGGTGGG-ATTGGTGTGTGTTTTTTTTTTTTTTTTTTTTTTTTTTTTTTTTTTGGTTGGTGTGGT TGG. Sequences (listed 5′ to 3′) for antibody-based ECPA were as follows. Insulin antibody arm 1 (AbArm1): /5AmMC6//iSp18/CCCACTTAAACCTC-AATCCACGCGGATTTGAACCCTAACG; Insulin antibody arm 2 (AbArm2): TAGGAAAAGGAGGAGGGTGGCC-CACTTAAACCTCAATCCA/iSp18//3AmMC6/. Sequences of ssDNA strands used in the experimental model are given in Table 4-1.

4.2.2 Preparation of the Electrode and DNA Monolayer Assembly

ECPA sensors for the model system, for thrombin detection, and for insulin detection were fabricated using a gold working electrode (Bioanalytical Systems Inc., r =

0.75 mm). The gold electrode was polished carefully to a mirror surface with an aqueous slurry of 0.05 μm diameter alumina particles and then successively washed in an ultrasonic cleaner with water. The electrode was then immersed into fresh piranha solution (H_2SO_4/H_2O_2, 3:1) for 5 min, rinsed with D. I. water, and dried under a stream of nitrogen gas. (Caution: piranha solution is dangerous to human health and should be used with extreme caution and handled only in small quantities). Finally, the gold electrode was electrochemically polished by scanning the potential from −0.5 to +1.5 V in 0.1 M H_2SO_4 at a scan rate of 0.1 V s^{-1} for 50 cycles. The cleaned gold electrode was thoroughly washed with D. I. water and ethanol and dried under flowing nitrogen.

Prior to modification of the electrode, 1 μL of 200 μM thiolated-DNA and 1 μL of 200 μM MB-DNA were each separately mixed with 2 μL of 10 mM TCEP in two 200-μL PCR tubes. These tubes were incubated for 90 min at room temperature (21 ℃) for reduction of disulfide bonds in the thiolated-DNA and to reduce the MB-moiety of the MB-DNA. Both of these solutions were then diluted to a total volume of 200 μL in HEPES/$NaClO_4$ buffer (10 mM HEPES and 0.5 M $NaClO_4$, pH 7.0)[29] to a final concentration of 1 μM. Unless otherwise noted, all solutions used in the experiments to follow were carried out at pH 7.0. For immobilization, the previously cleaned gold electrode was transferred directly to the diluted and reduced thiolated-DNA solution and incubated for 16 h at room temperature in the dark. Following the formation of a self-assembled monolayer (SAM), excess thiolated-DNA physically adsorbed on the electrode surface was removed via a room temperature-deionized water rinse (~ 20 s). For all assay strategies employing the competitor DNA strands, this same process was followed, except after reduction by 10 mM TCEP, the reduced thiolated-DNA solution was diluted

to a total volume of 200 µL in HEPES/$NaClO_4$ buffer and incubated with 2 µM competitor DNA sequence (C9) for 60 min at room temperature in the dark. For immobilization in competitor systems, the cleaned gold electrode was transferred directly to this equilibrated thiolated-DNA/competitor solution then incubated for 16 h at room temperature in the dark.

4.2.3 ECPA Probe Assembly and Electrochemical Measurements

Electrochemical measurements were performed using an Epsilon electrochemistry workstation (Bioanalytical Systems, Inc.) with a standard three-electrode configuration consisting of a Ag|AgCl(s)|KCl(sat) reference electrode (Bioanalytical Systems, Inc.), a homemade platinum gauze flag (0.77 cm^2) counter electrode, and a gold working electrode. All potentials are reported relative to the saturated Ag|AgCl reference electrode. Electrochemical measurements were performed in HEPES/$NaClO_4$ buffer using square wave voltammetry (SWV) with a 50 mV amplitude signal at a frequency of 60 Hz, over the range from −0.45 to 0.00 V versus Ag|AgCl reference. The characteristic voltammetric peak of MB was detected by SWV at −210 mV (vs Ag/AgCl). MB was chosen as the redox tag due to its excellent shelf life and robust electrochemical response in serum compared to other redox tags, such as ferrocene.[29,31] The electrochemical response of each sensor was measured as follows: (1) reference and measurement SWV data sets were collected; (2) both raw data sets were smoothed using a 21-point boxcar function and baseline corrected (all data corrected with B-spline generated baseline in Origin 8 using two regions: −0.40 to −0.35 V and −0.08 to 0.00 V); and (3) difference traces were generated. Signal (with target) and background (no target) voltammograms

were treated in this manner and are presented as difference traces. To prepare calibration graphs and calculate standard deviations, traces were integrated from −0.330 to −0.100 V. In the case of the aptamer-based system, we report the average of three measurements, while in the case of the antibody-based system the average of two measurements is reported.

Model System Strategy 1: Decreasing Binding Affinity by Reducing the Number of Complementary Bases. The electrode was modified as described above and was placed into a glass electrochemical cell with HEPES/$NaClO_4$ buffer. Three different thiolated DNA sequences, G5, G7, and G10 (Table 4-1), were used in strategy 1 of the model system. In this way, the affinity of thiolated DNA and MB-DNA were adjusted through changes in the number of complementary bases between them. For modeling signal, the sensor was immersed in 10 nM ECPA-loop and 15 nM MB conjugated DNA sequences in 3 mL of HEPES/$NaClO_4$ buffer. For modeling background, the sensor was immersed in 15 nM MB conjugated DNA in 3 mL of HEPES/$NaClO_4$ buffer. Both signal and background currents were measured at the 15-min time point.

Model System Strategy 2: Use of a Short DNA Competitor. The electrode was modified as described above and was placed into a glass electrochemical cell with HEPES/$NaClO_4$ buffer. Three different competitor DNA sequences, C7, C8, and C9, were used in strategy 2 of the model system (Table 4-1). The sensor was allowed to equilibrate in 3 mL HEPES/$NaClO_4$ buffer with various concentrations of competitors for 6 h. For modeling background in the competitor systems, redox current was measured at each 10 min of the first hour, then at 90 and 120 min. Once C9 was chosen, 1:3, 1:7,

1:10, and 1:25 molar ratios of MB-DNA:C9 were tested at a fixed concentration of 15 nM MB-DNA.

Aptamer-Based ECPA System. The sensor was allowed to equilibrate in 3 mL of HEPES/$NaClO_4$ buffer with 100 nM C9 for 6 h. Thrombin aptamers (THRaptA and THRaptB) were first folded by heating to 95 ℃ and cooled rapidly by immersion in ice water to promote intramolecular interactions. Thrombin of various concentrations (from 50 pM to 50 nM) was incubated with folded 10 nM THRaptA and 15 nM THRaptB in HEPES/$NaClO_4$ buffer for 90 min prior to measurements. The thrombin/aptamer incubations were then added into the glass electrochemical cell. Before conducting voltammetric measurements, the sensor surface was allowed to react with analytes for 90 min. Selectivity tests with other proteins (IgE, insulin, or BSA) were made under the same conditions.

Antibody-Based ECPA System. The sensor was equilibrated in 500 μL of HEPES/$NaClO_4$ buffer with 300 nM C9 for 6 h. Prior to measurements, HEPES/$NaClO_4$ buffer was supplemented with 0.5% BSA (w/v) (to minimize antibody adsorption), 10 nM Ab1, 10 nM Ab2, and 10 nM MB (for background measurements), and various concentrations of insulin (from 128 fM to 2 nM). Before conducting voltammetric measurements, the sensor surface was allowed to react with analytes for 40 min. Selectivity tests were performed in the same manner by substituting 2 nM C-peptide or insulin-like growth factor 1 (IGF-1) for insulin.

4.2.4 Preparation of Antibody-Oligonucleotide Conjugates

The antibody-oligonucleotide conjugates used in the insulin ECPA, AbArm1−3A6 and AbArm2−8E2, were prepared by conjugating AbArm1 to insulin antibody 3A6 ($K_d \approx 1$ nM) and AbArm2 to insulin antibody 8E2 ($K_d \approx 0.1$ nM), respectively (antibodies obtained from Fitzgerald Industries). Conjugation reactions and purification steps were accomplished using an Antibody-Oligonucleotide All-In-One Conjugation Kit (Solulink), according to the manufacturer’s instructions. Briefly, the oligonucleotides were first activated with sulfo-S-4FB, and their quantities and qualities were confirmed using absorbance, specifically A260 nm of unmodified activated oligonucleotides and the A260 nm to A360 nm ratio after the modification of activated oligonucleotides. Antibodies were also activated with S-HyNic. Activated oligonucleotides and antibodies were then mixed and incubated at room temperature for 2 h. Once the conjugation reaction was stopped, conjugates were further purified using the supplied magnetic affinity matrix. (Figure 4-1) The final concentrations of the conjugates were determined by the Bradford protein assay. AbArm1−3A6 and AbArm2−8E2 were synthesized with 45% and 86% recovery from the initial amount of antibodies (100 μg).

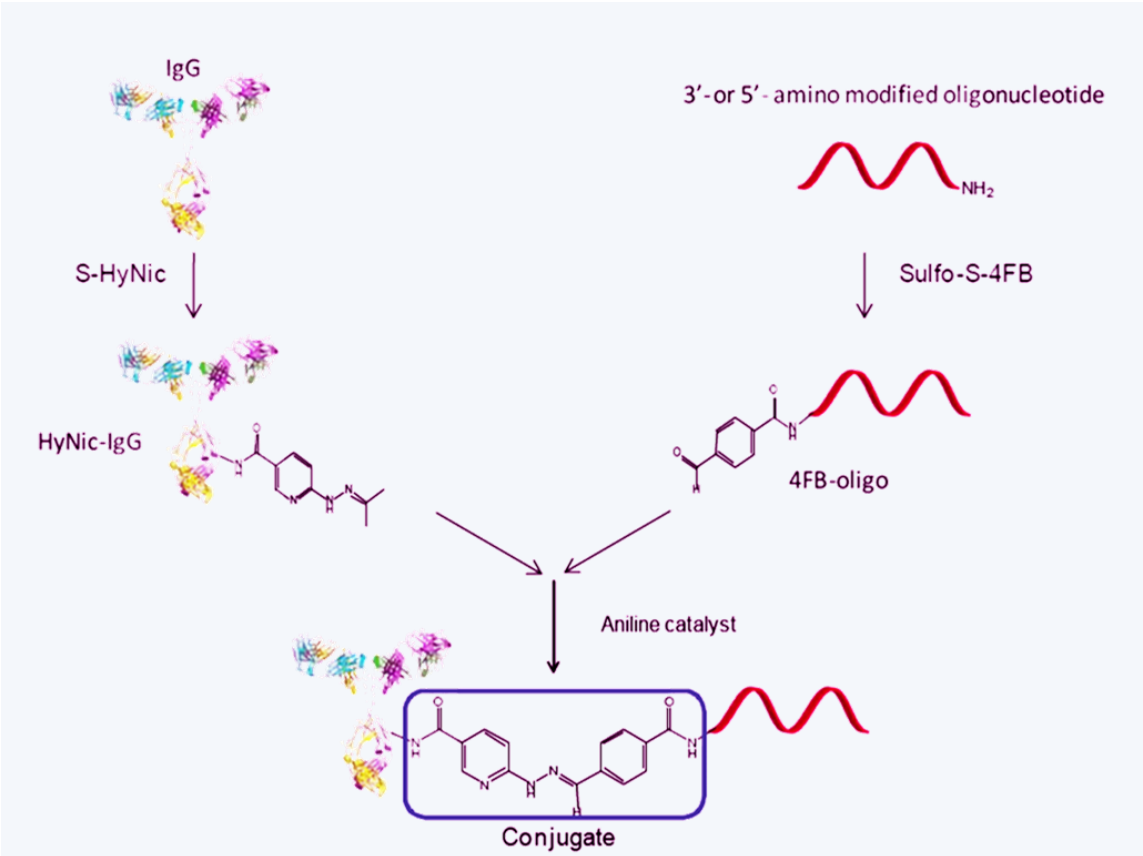

Figure 4-1: Reaction of a HyNic-modified IgG with a 4FB-modified oligo leads to the rapid formation of a stable antibody-oligonucleotide conjugate.
Image from Solulink technical manual: *Antibody-oligonucleotide all-in-one conjugation kit*.

4.3 Signal and Background in ECPA

The principle of the electrochemical proximity assay (ECPA) is shown in Figure 4-2. The sensor is prepared by self-assembly of thiolated DNA strands onto a gold electrode via the alkanethiol moiety at the 5′ terminus. The quantitative capacity of

ECPA stems from cooperative hybridization of the five-part complex shown in Figure 4-2A: thiolated DNA−DNA conjugated antibody 1−target protein−DNA conjugated antibody 2−MB conjugated DNA. The five-part complex forms a circular structure on the sensor surface through proximity-dependent hybridization of the thiolated DNA and MB-DNA, which is the step that brings MB close enough to the gold electrode surface for electrochemical current enhancement. This process results in a quantity of electrons transferred from MB to the electrode that is proportional to the original amount of protein analyte (“signal”), albeit with some analyte-independent current generated by hybridization of thiolated DNA and MB-DNA only (“background”). Although SWV does not differentiate signal and background currents, under optimized conditions, the signal will greatly exceed the background to allow highly sensitive, direct electrochemical quantitation of the protein analyte. Similar to what has been observed in PLA[11,17] or the molecular pincer assays,[13] signal enhancement over background in ECPA is based on the proximity effect, that is, the marked increase in the effective concentrations of the MB-DNA and thiolated DNA due to the simultaneous binding of the two probes to the same protein. This allows the MB-DNA/thiolated DNA interaction to be weak in the absence of protein (“background”) yet strong in the presence of the protein (“signal”). Finally, it should be noted that the detection limits of proximity assays are often well below the K_d values of the individual probes, which can be attributed to the chelate-like effect of utilizing two probes in a cooperative fashion, often termed the “proximity effect.”

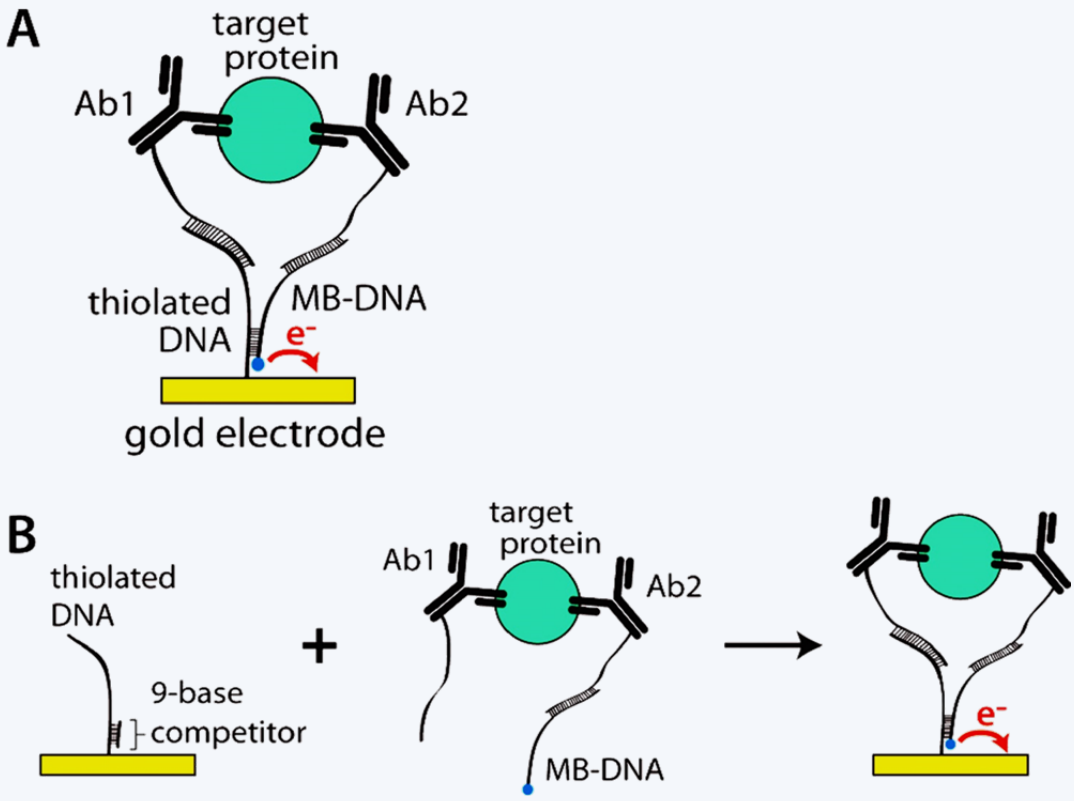

Figure 4-2: Principle of the electrochemical proximity assay (ECPA). (A) the final, five-part cooperative complex and (B) the stepwise operation of the assay, in which the electrode with a preassembled DNA/competitor monolayer is immersed into a premixed solution of EPCA probes (two Ab-oligos and MB-DNA) and target protein to generate current.

Through binding equilibria, a fraction of thiolated DNA will always hybridize with the MB-DNA sequences, even in the absence of target analyte, resulting in target-independent hybridization, recruitment of MB to the gold surface, and an increase in current. A portion of this background current could also result from nonspecific adsorption of MB-DNA to the surface, although our results suggest that specific binding is the major cause. The presence of this background current is obviously detrimental to the assay. We applied two strategies in attempt to lower the background using our model system, as discussed below.

4.4 DNA-Based Experimental Model of ECPA

In chapter 3, I introduced the model systems of ECPA. As shown in Figure 4-3, a 80-nucleotide DNA loop mimics formation of the ECPA complex (Figure 4-2A), moving MB-conjugated oligonucleotide close to the gold surface, where it participates in oxidation and reduction reactions facilitated by a regenerator in solution. Thus, electrical current is increased in proportion to the concentration of loop strands.

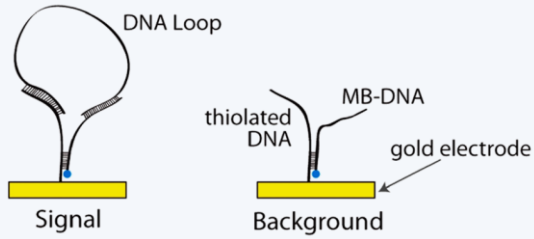

Figure 4-3: DNA-based model for ECPA.

In the first strategy, binding affinity between thiolated DNA and MB-DNA was decreased by reducing the number of complementary bases in the thiolated DNA (Figure 4-4A). The hypothesis was that the amount of background hybridization between thiolated DNA and MB-DNA would be greatly reduced, thereby reducing background

current greatly without a large decrease in signal current. Figure 4-4B compares the signal and background responses of the system with 5, 7, and 10 complementary bases (G5, G7, and G10 strands). Comparing G10 to G7, as hypothesized, the background current was reduced by 2-fold while signal current was reduced by only 1.6-fold. Furthermore, compared to a background peak current of 54 nA with G10, it was indeed possible to reduce the background current to baseline using G5. However, the background reduction was accompanied by a large decrease in signal peak current from 104 nA down to 38 nA, since the weakened connection also weakened hybridization of the DNA Loop (model of signal).

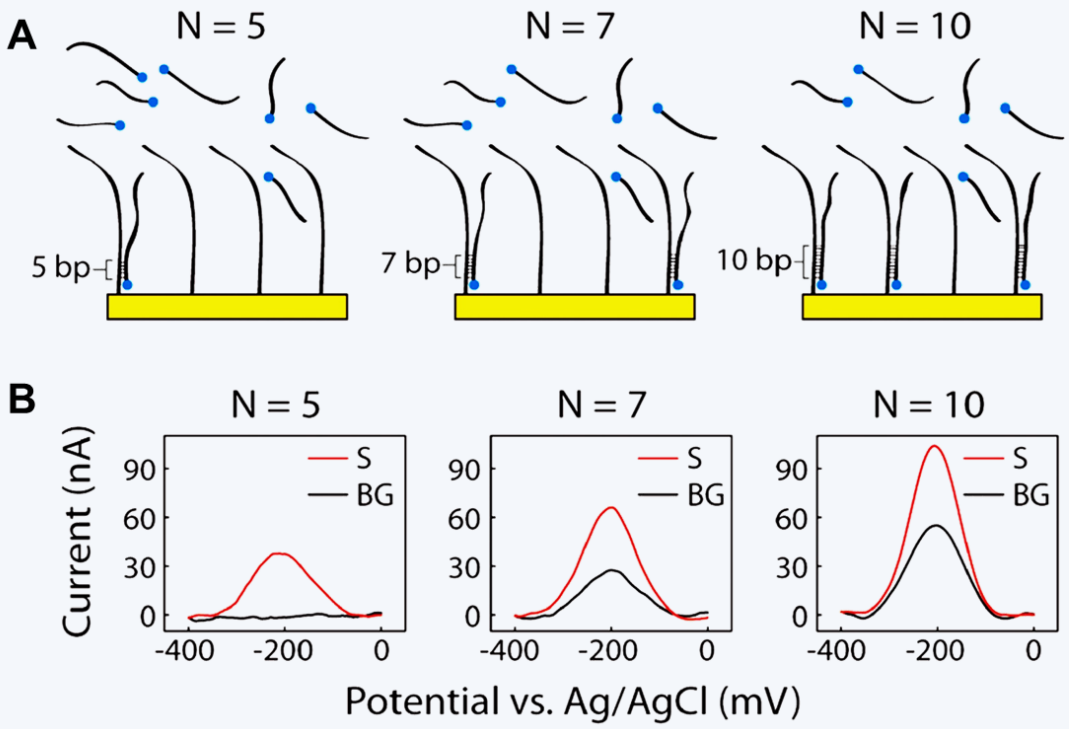

Figure 4-4: Model system strategy 1: Decreasing binding affinity by reducing the number of complementary bases. (A) Fewer base pairs (weaker hybridization) between thiolated DNA and MB-DNA results in lower background current. (B) Experimental confirmation of strategy 1, with both signal and background currents reduced in the voltammograms as the number of base pairs (N) is reduced. At N = 5, background is minimized, but signal is reduced significantly.

So in order to reduce background without such a large signal reduction, a short DNA competitor with the G10 system was utilized in the second strategy. The hypothesis is background hybridization would occur more slowly than signal hybridization, since both signal and background complexes must displace the short competitor prior to current enhancement by the MB-DNA strand. Figure 4-5A shows a representation of the delayed

background formation over time, mediated by competition with competitor strands. This way, signal of similar magnitude to that in the N = 10 case above should form rapidly, while background would be delayed kinetically by the competitor. Figure 4-5B shows signal and background responses of the system with 7-, 8-, and 9-base competitors (C7, C8, and C9). As hypothesized, the hybridized competitor sequences blocked access of MB-DNA to the thiolated DNA, thereby slowing background formation. Figure 4-5B shows that with C7 and C8, background currents of 47 and 24 nA were detected even 10 min after addition of MB-DNA, while no background was detected for as long as 40 min using C9. Since C9 allowed a 40-min time window for detection, we chose C9 as the competitor for further experiments. Upon addition of the Loop (model of signal), significant signal current of 81 nA was possible after 30 min, while C9 prevented background formation (Figure 4-5C). Optimal conditions were determined to be 15 nM MB-DNA and 100 nM C9, and these were applied in the aptamer-based ECPA system, below.

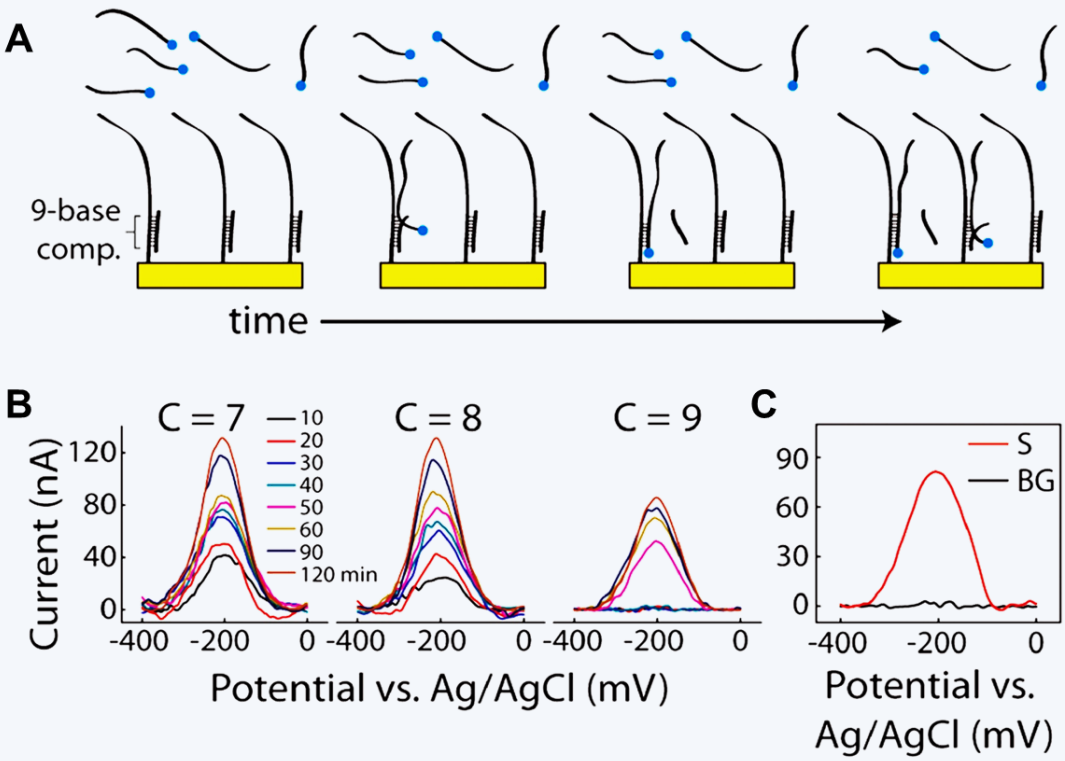

Figure 4-5: Model System Strategy 2: Use of a Short DNA Competitor. (A) Depiction of background reduction in strategy 2, where a competitor strand prevents or slows background formation over a given time window. (B) Experimental confirmation of strategy 2. The 9-base competitor (C9) was the only one to show baseline current for up to 40 min. (C) Signal and background voltammograms are shown with C9 under optimal conditions, showing more than double the signal current and equal background current compared to N = 5 from strategy 1.

4.5 Aptamer-Based ECPA

A schematic of aptamer-based ECPA is shown in Figure 4-6A (upper right). Two thrombin aptamers (THRaptA, THRaptB) that bind thrombin at different sites were applied as affinity probes, and competitor C9 was used to minimize background. Using

conditions optimized by the model system, background levels were measured in the absence of target protein (human thrombin). Similar to the model system, background remained at baseline current for up to 90 min, after which an increasing peak current at −210 mV was detected, indicating that MB-DNA was beginning to displace the competitors. This 90-min detection window was actually wider than the 40-min window observed in the model system. This difference is attributed to the decreased diffusion coefficient38 of the MB-DNA (40-base; ~70 $\mu m^2\ s^{-1}$) when hybridized with THRaptB (120-bases; ~30 $\mu m^2\ s^{-1}$), which would slow the kinetics of the competitor displacement process by ~2.3-fold in comparison to the model system. This estimation agrees very well with the 2.25-fold increase in time required for background formation. The lower right plot in Figure 4-6A shows the background with no thrombin (black trace) and a typical MB oxidation peak appearing at −210 mV (red trace) in the presence of 2.5 nM thrombin after the 90 min incubation. As expected, the saturated peak current at 10 nM thrombin (52 nA) was of lower magnitude than the model system (81 nA), which had assumed probes with infinite affinity. This aptamer-based ECPA system calibrated versus thrombin concentration (Figure 4-6A, left plot), with sensor responses recorded in triplicate as integrated MB peak areas from −330 to −100 mV. ECPA was capable of detecting thrombin levels as low as 50 pM using a direct electrochemical readout, with a dynamic range up to 10 nM at these probe concentrations.

To demonstrate specificity, the aptamer-based ECPA was challenged with nonspecific proteins including human IgE, insulin, and BSA. Figure 4-6B shows that essentially no response was observed in the presence of 10 nM insulin or IgE; even with 4-fold lower thrombin (2.5 nM), the signal was ~ 40-fold larger than that of IgE or

insulin. In addition, baseline current was observed in the presence of 2% BSA, while the signal from 2.5 nM thrombin was recovered by 93% in 2% BSA. This result is encouraging for future application of ECPA to biological samples and point-of-care settings.

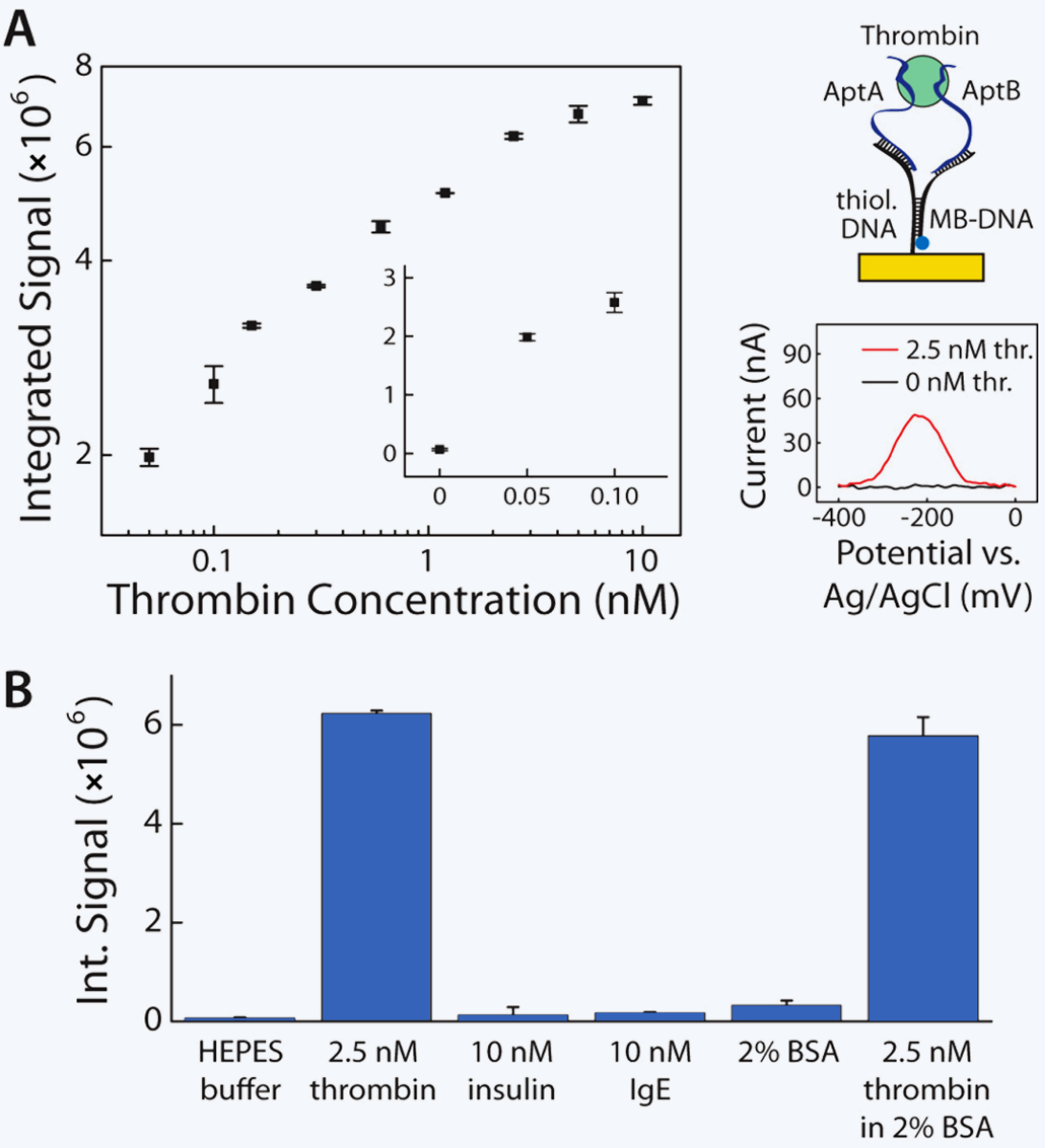

Figure 4-6: Aptamer-based ECPA. (A) With a direct readout, a human thrombin detection limit of 50 pM was achieved, with a dynamic range up to 10 nM. Upper right image shows the principle of the assay, with the lower right plot showing example voltammagrams for the blank (black) and in the presence of 2.5 nM thrombin (red). (B) The dual probe assay shows high selectivity, as expected, with 93% recovery of signal in the presence of 2% BSA.

4.6 Antibody-Based ECPA

The flexibility of the aptamer-based approach is limited because of the requirement of two aptamers for the target protein, since aptamer pairs exist only for a few select proteins. As noted above, the use of antibody-oligonucleotide conjugates as probes can overcome this challenge. [12,13] With the success of sandwich immunoassays, there exists a large, commercially available library of antibody pairs against many proteins. As proof of concept that ECPA can be applied to a wide variety of protein targets, we show herein that insulin can be directly detected using two antibody-oligonucleotide conjugates as ECPA probes.

A schematic of antibody-based ECPA is shown in Figure 4-7A (upper right), again employing the short DNA competitor strategy. With this new assay format, a different set of conditions were determined as optimal, including the addition of 0.5% BSA to reduce nonspecific antibody adsorption and a C9 concentration of 300 nM. Using 10 nM of each antibody-oligo and 10 nM MB-DNA, the assay showed a 40-min detection window before competitor began to be displaced by MB-DNA. Since the antibody-oligo conjugates will significantly alter the diffusion rates of most components, we did not expect the kinetics of signal and background formation to follow trends observed in the model system or aptamer-based ECPA; nonetheless, the detection time window was similar to the other systems. The lower right plot in Figure 4-7A shows the background with no insulin (black trace) and a typical MB oxidation peak appearing at −210 mV (red trace) in the presence of 2 nM insulin after 40 min. This antibody-based ECPA system was then calibrated versus insulin concentration (Figure 4-7A, left plot), with sensor response recorded in duplicate as integrated MB peak areas from −330 to −100 mV.

Remarkably, using a direct electrochemical readout, ECPA was capable of detecting insulin levels as low as 128 fM (7.43×10^{-4} ng mL^{-1}) with a dynamic range extending to 2 nM (11.6 ng mL^{-1}). The selectivity of antibody-based ECPA was tested against insulin-like growth factor 1 (IGF-1), which has similar structure to insulin, and against C-peptide, which is consecrated with insulin into the bloodstream. As expected, the sensor did not respond to higher concentrations of either IGF-1 or C-peptide (Figure 4-7B). The drastically improved performance of the antibody-based ECPA compared to the thrombin aptamer ECPA was expected, since the aptamer K_d values[44] are several orders of magnitude higher than the typical antibody K_d.

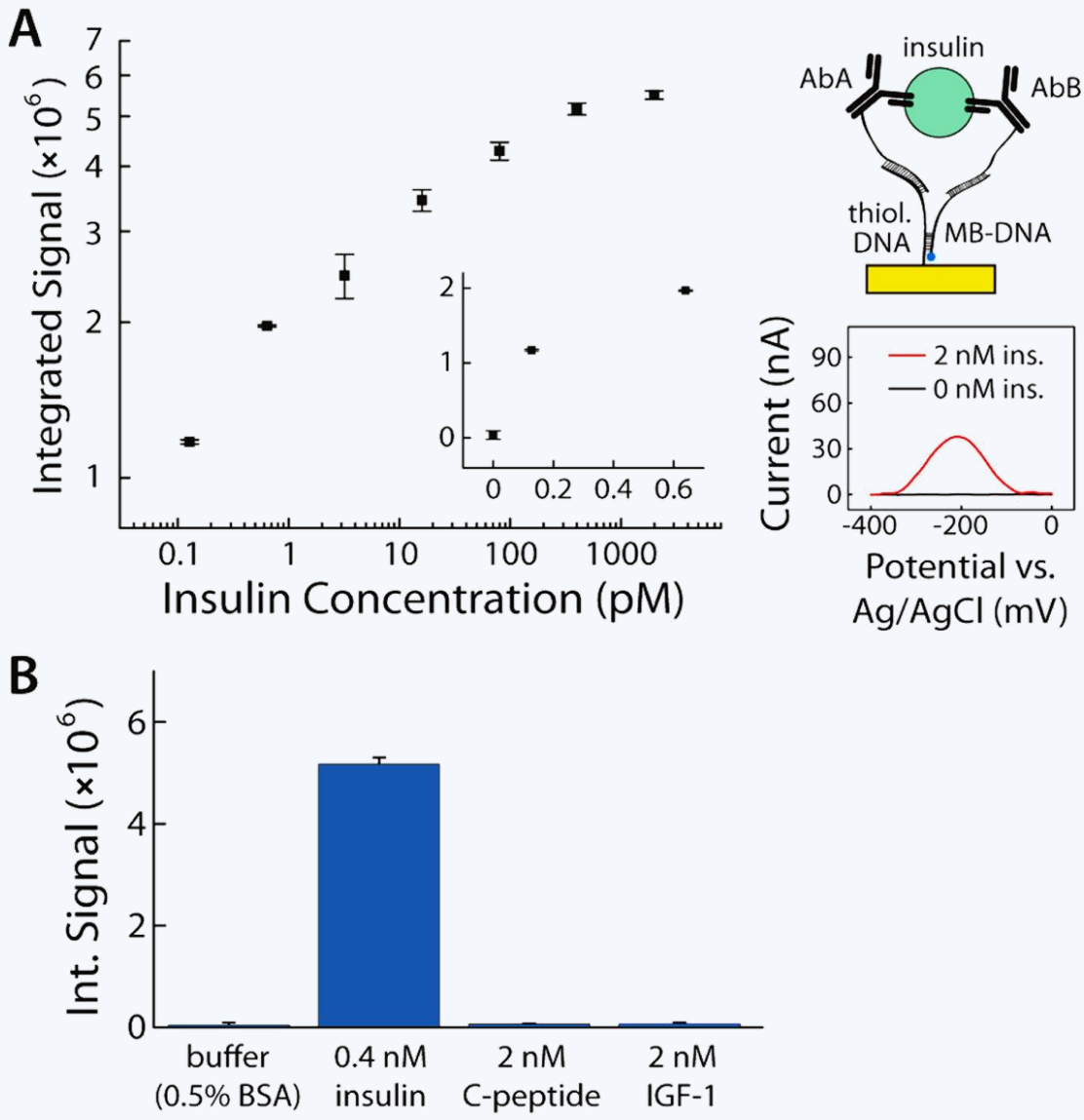

Figure 4-7: Success of antibody-based ECPA greatly improves the flexibility of the assay, since a large variety of protein targets could be quantified this way. (A) Insulin as low as 128 fM was detected with direct readout, with a dynamic range up to 2 nM. Upper right image shows the principle of the assay, with the lower right plot showing example voltammagrams for the blank (black) and in the presence of 2 nM insulin (red). (B) The dual-antibody assay also shows high selectivity, as expected.

Finally, Table 4-2 shows a comparison of our antibody-based ECPA to commercially available sandwich ELISAs for insulin detection.[45-50] In order to facilitate equal comparison of the direct-readout ECPA with various heterogeneous ELISAs, the concentrations of insulin in the incubation solution of each ELISA is reported in Table 4-2. ECPA outperforms all of the kits in terms of assay dynamic range (from 43- to 312-fold wider range). The impressive ECPA dynamic range of 15 600 (from 128 fM to 2 nM) should provide enhanced flexibility in sample preparation. Only one of the "ultrasensitive" versions of ELISA (25-μL sample volume) has an essentially equal detection limit (1.1-fold higher) compared to ECPA. Compared to "standard" ELISA kits, ECPA shows between 15.6- and 60.9-fold lower limit of detection for insulin. In fact, using the noise level of the blank, the linearly extrapolated LOD for insulin was calculated to be 20 fM, lower than all ELISAs shown in Table 4-2. These performance improvements come with the additional benefit of a direct-readout format, making ECPA amenable to point-of-care analysis. To our knowledge, ECPA represents the highest performing direct-readout insulin assay reported to date. Looking toward future application in point-of-care insulin measurements in human serum, if we leverage the pioneering efforts of the Plaxco group using similar DNA-based electrochemical sensors,[28,29,33-37] it should be possible to detect a variety of proteins in undiluted serum. Of course, since the ECPA detection limit for insulin (128 fM) is over 400-fold lower than the normal human serum insulin levels (~60 − 80 pM), serum samples could be simply diluted to minimize interferences in this case.

Table 4-2. Performance Comparisons between ECPA and Various Commercially Available ELISA Kits[a]

assay	analyte	LOD (fM)	relative LOD (LOD_{ELISA}/LOD_{ECPA})	dynamic range	relative range ($range_{ECPA}/range_{ELISA}$)
ECPA	human insulin	128	1	15 600	1
ELISA[b]	human insulin standard	5200	41	100	160
		2000	16	200	80
		7800	61	75	210
	ultrasensitive	140	1.1	290	50
	mouse insulin standard	3100	24	50	310
	ultrasensitive	820	6.4	360	40

[a]ECPA has a lower detection limit than five of the six kits in the table (as much as 60-fold lower), with a comparable detection limit to one 'ultrasensitive' human insulin ELISA. The dynamic range of ECPA is >40-fold wider than all ELISAs shown in the table (as much as 300-fold wider). These improvements shown by ECPA come with the added benefit of a direct electrochemical readout, i.e., without requiring washing steps. Abbreviations: ECPA = electrochemical proximity assay, ELISA = enzyme-linked immunosorbent assay, LOD = limit of detection. [b]To provide valid method comparisons, LODs and dynamic ranges for ELISAs are defined by the concentrations in the incubation mixture, prior to the washing step and secondary antibody incubation.

4.7 Conclusions

In this chapter, I described the development of the electrochemical proximity assay (ECPA), which leverages two aptamer or antibody-oligonucleotide probes and proximity-dependent DNA hybridization to move a redox active molecule near a gold electrode. A DNA-based experimental model was used to optimize the assay format, and aptamer- and antibody-based ECPA were shown functional with high sensitivities and low detection limits, employing a short DNA competitor to limit background current. This background-reduced ECPA was shown to match or outperform currently used ELISA kits for insulin detection.

Of particular importance is the proof-of-concept provided by antibody-based ECPA. Judging from to the successes of other proximity immunoassays,[12,13] it is reasonable to assume that ECPA should perform well in quantifying any other protein with an available antibody pair. Combining the assay's flexibility and high sensitivity with the simplicity of direct electrochemical readout, ECPA should be useful in a variety of settings in the future, including medical diagnostics, biological research, and point-of-care testing.

4.8 References

(1) Martinez, A.; Phillips, S. T.; Whitesides, G. M.; Carrilho, E. *Anal. Chem*. **2010**, *82*, 3−10.

(2) Burtis, C. A.; Ashwood, E. R. Tietz Textbook of Clinical Chemistry; Saunders: Philadelphia, PA, **1999**.

(3) Rusling, J. F.; Kumar, C. V.; Gutkind, J. S.; Patel, V. *Analyst* **2010**, *135*, 2496−2511.

(4) von Lode, P. *Clin. Biochem.* **2005**, *38*, 591−606.

(5) Sorell Go´mez, L.; Rojas, G. *Clin. Chim. Acta* **1997**, *260*, 65−71.

(6) Jung, K.; Zachow, J.; Lein, M.; Brux, B.; Sinha, P.; Lenk, S.; Schnorr, D.; Loening, S. A. *Urology* **1999**, *53*, 155−160.

(7) Stivers, C. R.; Baddam, S. R.; Clark, A. L.; Ammirati, E. B.; Irvin, B. R.; Blatt, J. M. *Diabetes Technol. Ther.* **2000**, *2*, 517−526.

(8) Davies, S; Byrn, F; Cole, L. A. *Clin. Lab. Med.* **2003**, *23*, 257−264.

(9) Seamark, D. A.; Backhouse, S. N.; Powell, R. *Ann. Clin. Biochem*. **2003**, *40*, 178−180.

(10) Haab, B. B.; Dunham, M. J.; Brown, P. O. *Genome Biol*. **2001**, *2*, 1−5.

(11) Fredriksson, S.; Gullberg, M.; Jarvius, J.; Olsson, C.; Pietras, K.; Gustafsdottir, S. M.; Ostman, A.; Landegren, U. *Nat. Biotechnol*. **2002**, *20*, 473−477.

(12) Gullberg, M.; Gustafsdottir, S. M.; Schallmeiner, E.; Jarvius, J.; Bjarnegård, M.; Betsholtz, C.; Landegren, U.; Fredriksson, S. *Proc. Natl. Acad. Sci. U.S.A.* **2004**, *101*, 8420−8424.

(13) Heyduk, E.; Dummit, B.; Chang, Y. H.; Heyduk, T. *Anal. Chem*. **2008**, *80*, 5152−5159.

(14) Konry, T.; Hayman, R. B.; Walt, D. R. *Anal. Chem*. **2009**, *81*, 5777−5782.

(15) Kim, D.; Daniel, W. L.; Mirkin, C. A. *Anal. Chem*. **2009**, *81*, 9183−9187.

(16) Luminex Corporation, Technologies and Science, http://www.luminexcorp.com/TechnologiesScience/index.htm; accessed December 2011.

(17) Kim, J.; Hu, J.; Sollie, R. S.; Easley, C. J. *Anal. Chem*. **2010**, *82*, 6976−6982.

(18) Osborne, S. E.; Ellington, A. D. *Chem. Rev.* **1997**, *97*, 349−370.

(19) Famulok, M. Curr. Opin. Struct. *Biol.* **1999**, *9*, 324−329.

(20) Drummond, T. G.; Hill, M. G.; Barton, J. K. *Nat. Biotechnol.* **2003**, *21*, 1192−1199.

(21) The Aptamer Handbook. Functional Oligonucleotides and Their Applications; Klussmann, S., Ed.; WILEY-VCH Verlag GmbH & Co. KGaA: Weinheim, Germany, 2006.

(22) Herr, J. K.; Smith, J. E.; Medley, C. D.; Shangguan, D.; Tan, W. *Anal. Chem*.

2006, *78*, 2918−2924.
(23) Shangguan, D.; Li, Y.; Tang, Z.; Cao, Z. C.; Chen, H. W.; Mallikaratchy, P.; Sefah, K.; Yang, C. J.; Tan, W. *Proc. Natl. Acad. Sci. U.S.A.* **2006**, *103*, 11838−11843.
(24) Liu, Y.; Tuleouva, N.; Ramanculov, E.; Revzin, A. *Anal. Chem.* **2010**, *82*, 8131−8136.
(25) Hianik, T.; Wang, J. *Electroanalysis* **2009**, *21*, 1223-1235.
(26) Sassolas, A.; Blum, L. J.; Leca-Bouvier, B. D. *Electroanalysis* **2009**, *21*, 1237-1250.
(27) Kelley, S. O.; Barton, J. K.; Jackson, N. M.; Hill, M. G. *Bioconjug. Chem.* **1997**, *8*, 31−37.
(28) Fan, C.; Plaxco, K. W.; Heeger, A. J. *Proc. Natl. Acad. Sci. U.S.A.* **2003**, *100*, 9134−9137.
(29) Kang, D.; Zuo, X.; Yang, R.; Xia, F.; Plaxco, K. W.; White, R. J. *Anal. Chem.* **2009**, *81*, 9109−9113.
(30) Zhang, Y. L.; Huang, Y.; Jiang, J. H.; Shen, G. L.; Yu, R. Q. *J. Am. Chem. Soc.* **2007**, *129*, 15448−15449.
(31) Ferapontova, E. E.; Olsen, E. M.; Gothelf, K. V. *J. Am. Chem. Soc.* **2008**, *130*, 4256−4258.
(32) Zhang, Y. L.; Pang, P. F.; Jiang, J. H.; Shen, G. L.; Yu, R. Q. *Electroanalysis* **2009**, *21*, 1327−1333.
(33) Bonham, A. J.; Hsieh, K.; Ferguson, B. S.; Valle´e-Be´lisle, A.; Ricci, F.; Soh, H. T.; Plaxco, K. W. *J. Am. Chem. Soc.* **2012**, *134*, 3346−3348.
(34) Valle´e-Be´lisle, A.; Ricci, F.; Plaxco, K. W. *J. Am. Chem. Soc.* **2012**, *134*, 2876−2879.
(35) Xia, F.; Zuo, X.; Yang, R.; White, R. J.; Xiao, Y.; Kang, D.; Gong, X.; Lubin, A. A.; Valle´e-Be´lisle, A.; Yuen, J. D.; Hsu, B. Y.; Plaxco, K. W. *J. Am. Chem. Soc.* **2010**, *132*, 8557−8559.
(36) Rowe, A. A.; Chuh, K. N.; Lubin, A. A.; Miller, E. A.; Cook, B.; Hollis, D.; Plaxco, K. W. *Anal. Chem.* **2011**, *83*, 9462−9466.
(37) Lubin, A. A.; Plaxco, K. W. *Acc. Chem. Res.* **2010**, *43*, 496−505.
(38) Nkodo, A. E.; Garnier, J. M.; Tinland, B.; Ren, H.; Desruisseaux, C.; McCormick, L. C.; Drouin, G.; Slater, G. W. Electrophoresis 2001, 22, 2424−2432.
(39) Hu, J.; Easley, C. J. *Analyst* **2011**, *136*, 3461−3468.
(40) Millipore Corportation, Human Insulin ELISA, http://www.millipore.com/catalogue/item/ezhi-14k; accessed December 2011.
(41) Mercodia AB, Insulin ELISA, http://www.mercodia.se/index.php?page=productview2&prodId=9; accessed December 2011.
(42) AbCam plc., Insulin Human ELISA Kit − 1 ×96 Well Plate (ab100578), http://www.abcam.com/Insulin-Human-ELISA-Kit-1-x-96-Well-Plate-ab100578.html; accessed December 2011.

(43) Mercodia AB, Insulin, Ultrasensitive ELISA, http://www.mercodia.se/index.php?page=productview2&prodId=11; accessed December 2011.
(44) Millipore Corporation, Rat/Mouse Insulin ELISA, http://www.millipore.com/catalogue/item/ezrmi-13k; accessed December 2011.
(45) ALPCO Diagnostics, Mouse Ultrasensitive Insulin ELISA, 80-INSMSU-E01, http://www.alpco.com/products/Insulin_Ultrasensitive_Mouse_ELISA.aspx; accessed December 2011.

CHAPTER 5

The Reusable Electrochemical Proximity Assay (ECPA)

5.1 Abstract of ECPA

We previously developed an electrochemical proximity assay (ECPA) format for direct detection of a wide variety of target proteins (Chapter 4). The first generation of ECPA was composed of two aptamers or antibody-oligo conjugates that form a cooperative complex only in the presence of target protein molecules. Electrochemical current was thus increased in proportion to protein concentration, and detection limits were in the fM range with direct readout.

We have further improved ECPA towards reusable protein quantitation. Regeneration of the base DNA monolayer was accomplished enzymatically. First, we incorporated uracils (U) into selected probe strands, then these strands were enzymatically cleaved using a uracil-DNA excision mix. After reducing complementary bases of thiolated DNA, assembled on gold electrode surface, to methylene blue (MB)-conjugated oligonucleotide, this allowed measurement time to be reduced 30-fold, from 90 min to 3 min, without significant loss of sensitivity. A single electrode could be enzymatically regenerated and reused at least 17 times without loss of signal, even when detecting picomolar concentrations of thrombin or femtomolar concentrations of insulin.

Selectivity was again confirmed against IgE and insulin in aptamer-based, and against IGF-1 and C-peptide in antibody-based reusable ECPA systems. This technique was also proven useful for hormone secretion measurements in vitro from murine pancreatic islets, and it was validated for insulin quantitation in murine blood serum. The reusable format of ECPA is faster and easier to implement than standard ECPA, while maintaining high sensitivity and selectivity. It is feasible to envision that ECPA could be easily integrated with portable electronic devices and applied in point-of-care settings and that reusable ECPA could be expanded upon and used in clinical laboratories and basic research settings.

5.2 Introduction

Early medical diagnosis of critical health changes could enable the prevention of fatal events because it can ensure appropriate and timely care and treatment to patients.[1-3] Highly sensitive detection and accurate analysis of diseases-associated proteins is demanded for early diagnosis.[4-6] Current standard detection methods such as Western blots and enzyme-linked immunosorbent assays (ELISA) are usually slow, cumbersome, laboratory-bound processes that require hours to days to obtain clinical information[5]. Point of care approaches could overcome those drawbacks and speed implementation of treatment processes and improve patient outcomes.[3,7-11]

There are some challenges that must be surmounted from laboratory sensor development to point of care application.[12,13] First, the technology must be sufficiently selective to reject false signals; second, it must operate continuously and cannot rely on

batch process steps such as separations; and third, it should be reversible. Reversibility is a very important factor, since it could greatly reduce the cost of the product.

With the development of biosensing techniques, DNA based electrochemical sensors become more and more promising towards point of care applications because they are rapid, low-cost, suitable for miniaturized devices, and ideal for application in chemically complex environments such as blood serum.[13,14] Types of designs that are published include electrochemical DNA (E-DNA), traditional sandwich/supersandwich assays, competition-type assays, electrochemical aptamer-based sensors (E-AB), double-antibody sandwich assay, and aptamer-based sandwich assays.[15-20] Generally, DNA based electrochemical sensors are engineered by attaching an electro-active reporter to one position of DNA sequence which transfers electrons to or from the electrode surface, thus inducing electrochemical signal change at a detector. The principle can be based on target-induced strand displacement mechanisms, analyte-induced conformational changes, or combinations with sandwich and competitive assays, by forcing redox-labeled DNA into proximity with the electrode surface.[16]

Motivated by the point of care application,s the first generation of standard electrochemical proximity assay (ECPA) was successful developed.[21] The sensor used the proximity effect[22,23] to move an electrochemically active label, methylene blue (MB), closer to a gold electrode upon binding of two probes to a protein target with high sensitivity and selectivity. Using antibody-oligo probes in standard ECPA, the detection limit for insulin was 20 fM, which is lower than most commercially available ELISAs, with a much wider dynamic range. These improvements come with the added benefit of direct electrochemical readout.

Although standard ECPA has great achievements, the limitations are also obvious. First, it is not reusable, meaning that repeated preparation of the electrode and DNA monolayer assembly (many hours) is required after every measurement. Secondly, probes and target are needed to be incubated for a long time before measurement either in aptamer-based or antibody-based assays. The popular way to make a DNA-based surface assay reusable is using a water rinse.[17,24,25] However, this reusable method has some deficiencies. First, it is only useful for small numbers of base pairs of dsDNA. If two DNA strands have a significant number of complementary bases—such as with hairpin structures or complex structures formed by proximity effect making three or more DNA strands binding together—a water rinse may not be a good way to impart reusability. Second, a water rinse results in a signal decrease, but a signal decrease is not sufficient basis to prove the sensor is regenerated, it can only explain the reporter molecules are not near the sensor surface; the dsDNA may not be denatured, or target molecules may still be attached on the surface. Here, regeneration was accomplished enzymatically by incorporating uracils into selected probe DNA strands, where these strands could be cleaved into small pieces using a uracil-DNA excision mix. Following enzymatic cleavage, the leftover short DNA strands were less than six oligonucleotides, which will easily denature at 37 ℃, or even at room temperature. This reusable version of ECPA performed as well as standard ECPA, in categories such as optimized signal-to-background ratios and an equal direct insulin detection limit. Reusable ECPA even showed a 4-fold wider dynamic range than standard ECPA, meaning that it has >160-fold wider range than ELISAs, and we also proved its utility in endocrine tissue sampling tests

and blood serum tests. These achievements further prove the reusable ECPA should be useful in medical research or clinical measurements.

5.3 Reagents and Experimental Methods

5.3.1 Reagents and Materials

All solutions were prepared with deionized, ultrafiltered water (Fisher Scientific). The following reagents were used as received: insulin antibodies (clones 3A6 and 8E2; Fitzgerald Industries), 4-(2-hydroxyethyl)-1-piperazineethanesulfonic acid (HEPES) (99.5%), tris-(2-carboxyethyl) phosphine hydrochloride (TCEP), (Sigma-Aldrich, St. Louis, MO), bovine serum albumin (BSA, 98%; EMD Chemicals Inc.), human thrombin, immunoglobulin E (IgE), and insulin (Sigma Aldrich). Methylene blue-conjugated DNA (MB-DNA) was purchased from Biosearch Technologies (Novato, CA), purified by RP-HPLC. Oligonucleotides were obtained from Integrated DNA Technologies (IDT; Coralville, Iowa), with purity and yield confirmed by mass spectrometry and HPLC, respectively. Sequences (listed 5′ to 3′) for aptamer based ECPA were as follows. Thrombin aptamer A (THRaptA): AGTCCGTGGTAGGGCAGGTTGGGGTGA-CTTTTTTTTTTTTTTTTTATATTTTTTTTTCTCGCGGA**UUU**GAACCC**U**AACG; Thrombin aptamer B (THRaptB): TAGGAAAAGGAGGAGGGTGGG-ATTGGTGTGTGTTTTTTTTTTTTTTTTTTTTTTTTTTTTTTTTTGGTTGGTGTGGT TGG. Sequences (listed 5′ to 3′) for antibody-based ECPA were as follows. Insulin antibody arm 1 (AbArm1): /5AmMC6//iSp18/CCCACTTAAACCTC-AATCCACGCGGA**UUU**GAACCC**U**AACG; Insulin antibody arm 2 (AbArm2):

TAGGAAAAGGAGGAGGGTGGCC-CACTTAAACCTCAATCCA/iSp18//3AmMC6/.

Sequences of ssDNA strands used in the experimental model are given in Table 5-1.

Table 5-1. Single-Stranded DNA Sequences Used in the Reusable ECPA Model Systems[a]

name	(abbreviation)	DNA sequence, listed 5′ to 3′
dU_ECPA-loop	(loop)	TAG GAA AAG GAG GAG GGT GGC CA**U** CTT AAA CCT CAA TCC ACC CAC TTA AAC CTC AAT CCA CGC GGA **UUU** GAA CCC **U**AA CG
dU_ECPA-MB-10	(MB-DNA)	CCA CCC TCC TCC TTT TCC TAT CTC TCC CTC G**U**C ACC A**U**G C/MB-C7/
dU_ECPA-gold-10	(G10)	/5ThioMC6-D/GCA TGG TGA CAT TTT TCG TTC GTT AGG GTT CAA ATC CGC G
dU_ECPA-gold-7	(G7)	/5ThioMC6-D/GCA TGG TAT TTT TCG TTC GTT AGG GTT CAA ATC CGC G
dU_ECPA-gold-5	(G5)	/5ThioMC6-D/GCA TGA ATT TTC GTT CGT TAG GGT TCA AAT CCG CG
dU_ECPA-Comp-9	(C9)	TCA CCA TGC

[a] MB-DNA, G10, and C9 were employed in the optimized detection system. Abbreviations: /MB-C7/ = methylene blue modification (Biosearch), /5ThioMC6-D/ = disulfide bond flanked by two six-carbon spacers (IDT).

5.3.2 Preparation of Sensor Surface

Reusable ECPA sensors for the model system, for thrombin detection, for insulin detection, for measurement of hormone secretion, and for insulin measurement of blood serum were fabricated using a gold working electrode (2 mm diameter, CH instruments, Inc., Austin, TX). Gold electrodes were polished using a previously reported protocol (JACS) with minor alterations. In brief, the gold electrodes were first polished with a slurry of 0.05 μm aluminum oxide in water (Buehler, Lake Bluff, IL) followed by sonication in ethanol for 10 min. This was followed by pipetting fresh piranha solution (H_2SO_4/H_2O_2, 3:1) on gold surface for 10 min, rinsed with D. I. water. (Caution: piranha solution is dangerous to human health and should be used with extreme caution and handled only in small quantities). The gold electrodes were further cleaned by a series of

oxidative and reductive scans in 0.5 M H_2SO_4 as previously described. The cleaned gold electrodes were thoroughly washed with D. I. water and ethanol and dried under flowing nitrogen.

The volume for preparation of electrode-immobilized probe is dependent upon the number of electrodes to be prepared and is intended to conserve reagents. We will provide info for our conditions when preparing 7 electrodes. 14 μL (2 μL per electrode) of 200 μM thiolated-DNA was mixed with 28 μL (4 μL per electrode) of 10 mM TCEP in a 1.5-mL microcentrifuge tubes. This tube was incubated for 120 min at room temperature (21 ℃) in the dark for reduction of disulfide bonds in the thiolated-DNA. This solution was then diluted to a total volume of 1400 μL in HEPES/$NaClO_4$ buffer (10 mM HEPES and 0.5 M $NaClO_4$, pH 7.0)[16,21] to a final concentration of 2 μM thiolated DNA.

The MB-DNA must also be reduced in a similar way, but less volume is needed. To generate sufficient reduced MB-DNA for 20-30 measurements, 3 μL of 200 μM MB-DNA was mixed with 6 μL of 10 mM TCEP in a 1.5-mL microcentrifuge tubes. This tube was incubated for 120 min at room temperature (21 ℃) in the dark for reduction of the MB-moiety of the MB-DNA. This solution was then diluted to a total volume of 600 μL in HEPES/$NaClO_4$ buffer to a final concentration of 1 μM MB-DNA. (Critical step: Thiolated-DNA should be reduced with TCEP immediately before immobilization on a clean electrode. MB-DNA is mildly light-sensitive, so it is preferable to perform reduction step in the dark.) Unless otherwise noted, all solutions used in the experiments to follow were carried out at pH 7.0.

For immobilization, the previously cleaned electrode was directly transferred to the reduced thiolated-DNA solution and Incubated overnight (~12-16 h) at room temperature in the dark. Following incubation and SAM formation, remove any excess probe DNA physically adsorbed on electrode surface via a room temperature-deionized water rinse (~20 s). The stream of deionized water should flow over the modified electrode. And then the modified electrode was immediately transferred to 3 mM 6-mercaptohexanol solution for 40 min at room temperature in the dark. (Figure 5-1) (Critical step: 6-Mercaptohexanol solution should be prepared immediately before use. It's better to do it in the hood.)

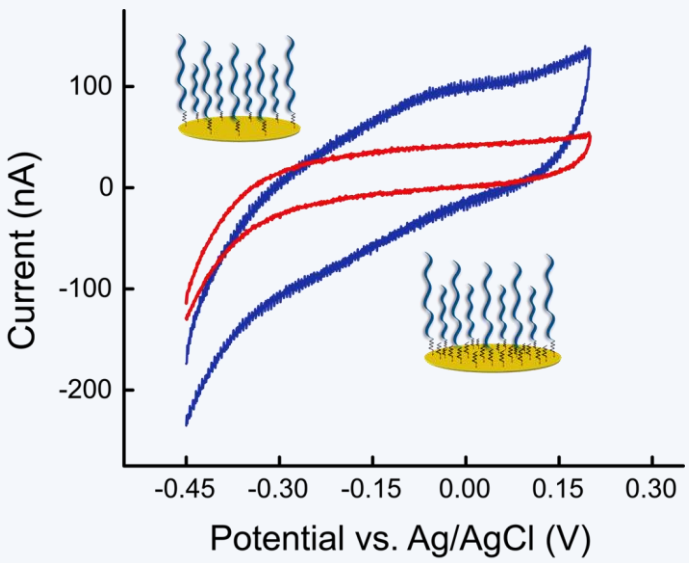

Figure 5-1: Cyclic voltammetric response of modified gold electrode before transferred to 3 mM 6-mercaptohexanol solution (blue trace) and after (red trace).

5.3.3 ECPA Probe Assembly and Electrochemical Measurements

Electrochemical measurements were performed as described previously[21] using an GAMRY Reference 600 electrochemistry workstation with a standard three-electrode configuration consisting of a Ag|AgCl(s)|KCl(sat) reference electrode (Bioanalytical Systems, Inc.), a homemade platinum gauze flag (0.77 cm^2) counter electrode, and a gold

working electrode. All potentials are reported relative to the saturated Ag|AgCl reference electrode. Electrochemical measurements were performed in HEPES/$NaClO_4$ buffer using square wave voltammetry (SWV) with a 50 mV amplitude signal at a frequency of 60 Hz, over the range from −0.45 to 0.10 V versus Ag|AgCl reference.

Model system. The electrode was modified as described above and was placed into a glass electrochemical cell with HEPES/$NaClO_4$ buffer. For modeling signal, the sensor was immersed in 10 nM ECPA-loop and 15 nM MB- DNA in 500 µL of HEPES/$NaClO_4$ buffer. For modeling background, the sensor was immersed in 15 nM MB-DNA in 500 µL of HEPES/$NaClO_4$ buffer. Both signal and background currents were measured at the 3-min time point.

Aptamer-Based reusable ECPA System. Seven gold working electrodes were used for signal measurement of each thrombin concentration. Thrombin of seven different concentrations (from 0 to 10 nM) was incubated with 10 nM THRaptA and 15 nM THRaptB in HEPES/$NaClO_4$ buffer prior to measurements. The thrombin/aptamer incubations were then added into the glass electrochemical cell. Before conducting voltammetric measurements, the sensor surface was allowed to react with analytes for 3 min. After measurement, each sensor was regenerated by immersing in 2 unit uracil DNA excision mix in 100 µl uracil excision enzyme buffer (50 mM Tris-HCl (pH 9.0), 20 mM $[NH_4]_2SO_4$ and 10 mM EDTA) for 7 min at 37 ℃. Removing the enzyme solution and cleaved DNA pieces physically adsorbed on electrode surface via a room temperature-deionized water rinse (~20 s), the stream of deionized water should flow over the modified electrode, and then electrodes were dried by using nitrogen gas. After that, the

sensor was ready for next measurement. Regeneration and selectivity tests with other proteins (IgE, insulin, or BSA) were made under the same conditions.

Antibody-Based Reusable ECPA System. Antibody-oligonucleotide conjugates were prepared using the same method as described.[21] The measurements of insulin secretions from pancreatic islets were performed with our novel cyclic methodology (see Figure 5-7). The sensor was incubated with 50 nM Ab1 (DNA conjugated antibody 1: AbArm1−3A6) for 3 min by dropping 10 μL solution on the sensor surface, and then washed within HEPES/$NaClO_4$ buffer for ~15-second. Next, the sensor was transferred to a tube with live pancreatic islets in solution (300 μL), which was kept at 37 ℃ by heat block. After 3 min incubation in the sample solution, the electrode was washed by HEPES/$NaClO_4$ buffer for ~15-second, and then was incubated with 50 nM Ab2 (DNA conjugated antibody 2: AbArm2−8E2) for 3 min by dropping 10 μL solution on the gold surface. Finally, the sensor was transferred to 500 μL of HEPES/$NaClO_4$ buffer with 50 nM MB-DNA. Both signal and background currents were measured at the 3-min time point. For insulin calibration, we also used seven gold working electrodes for signal measurement of each insulin concentration by adopting the same protocol as measurement of secretions from pancreatic islets.

5.4 Principle of reusable ECPA

The principle of the reusable electrochemical proximity assay (ECPA) is shown in Figure 5-2. The sensor is prepared by self-assembly of thiolated DNA strands onto a gold electrode via the alkanethiol moiety at the 5’ terminus, and also treated by 3 mM 6-mercaptohexanol solution, ensuring monolayer formed on the whole gold surface. The

five-part complex is shown in Figure 5-2A: thiolated DNA−Ab1−target protein−Ab2−MB conjugated DNA. Uracils are incorporated into Ab1 oligo and MB-conjugated DNA, so that the Ab1 and MB conjugated DNA will be enzymatically cleaved using a uracil-DNA excision mix into three and two small DNA pieces, respectively. Thus, after rinsing, only thiolated-DNA and 6-mercapto-1-hexanol are left on the sensor surface. Uracil-DNA excision mix contains two enzymes, HK-UNG (Heat-Killable Uracil N-Glycosylase [UNG]) and Endonuclease IV. HK-UNG cleaves the uracil base from a uracil-deoxynucleotide in any DNA, creating an abasic site at the location of dUTP incorporation. Endonuclease IV then cleaves the phosphodiester bond at this abasic site, generating a series of digestion fragments. (Figure 5-2B)

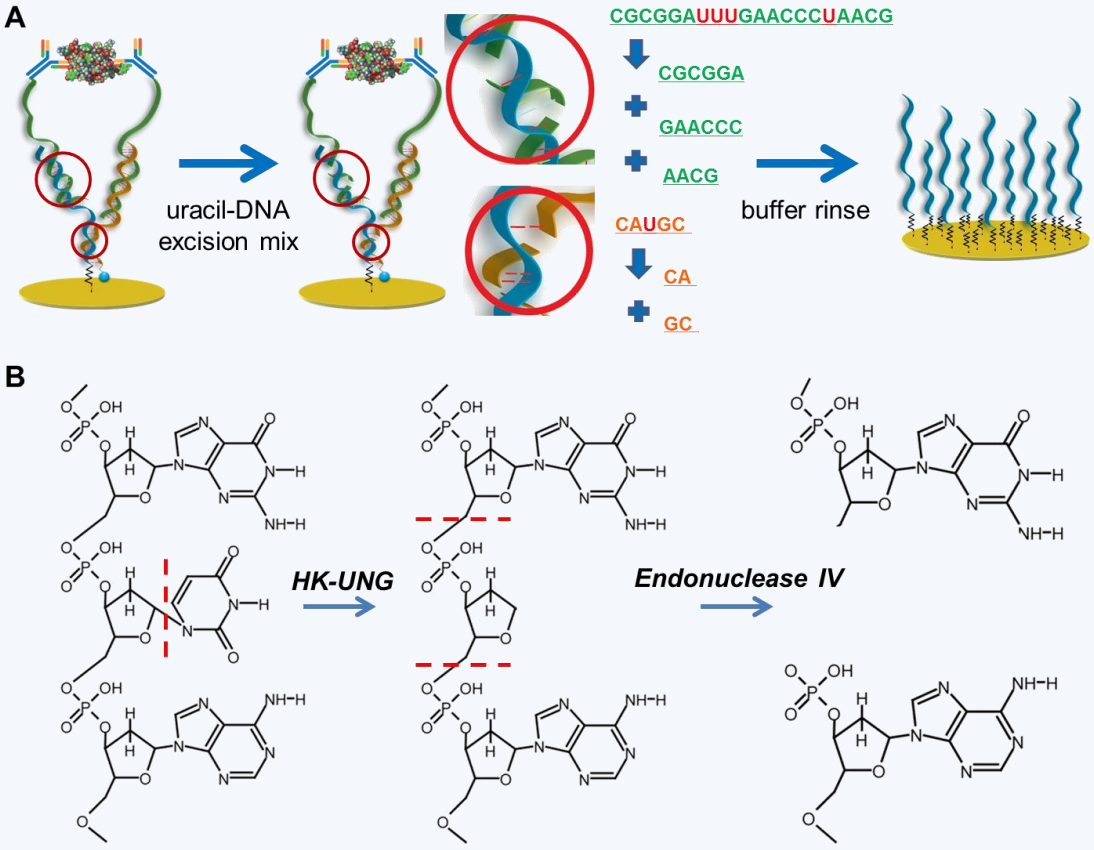

Figure 5-2: Principle of reusable ECPA. (A) Stepwise operation of the assay. Electrode was immersed into uracil enzyme solution, the selected probe strands were enzymatically cleaved by uracil-DNA excision mix, the base DNA monolayer was regenerated. (B) Illustration of uracil-DNA excision mix mechanism.

5.5 DNA-Based Experimental model of reusable ECPA

The same ssDNA strands are utilized as in our previous work ,[21] except DNA loop and MB-DNA strands incorporated with uracils (Table 5-1). In standard ECPA, the signal measurement time of DNA-based experimental model is 40 min. Here, the purpose of this experimental model is to shorten the measurement time. As we know, in standard ECPA, we compared the signal and background responses of the system with 5, 7, and 10 complementary bases (G5, G7, and G10 strands), and G10-competitor system. The advantages and disadvantages of G5 system and G10-competitor system are as follows. In the G5 system, measurements could be made quickly, and the background current was reduced to baseline, but with a large signal reduction. In the G10-competitor system, there was a large signal current and a baseline level background; however, both signal and background currents were necessarily measured at the 40-min time point.

In an attempt to increase signal and reduce the measurement time, a higher concentration of MB-DNA was adopted in G5, G7, and G10-competitor systems. Previously, in standard ECPA, the concentration of MB-DNA used was 15 nM, but here we utilized 50 nM MB-DNA. The hypothesis was that the higher amount of MB-DNA would not greatly affect the background current in the G5 system, due to the restriction of fewer base pairs where the binding between G5 and MB-DNA was very weak at room temperature. However, forsignal current, the proximity effect (discussed in our previous work with both PLA and ECPA[21,23]) should provide even more enhancement. Figure 5-3 compares the signal and background responses of the G5, G7, and G10-competitor systems. As hypothesized, the background current of G5 system still kept at the baseline level while signal current was increased to the same current level as in G7 and G10

systems. For G7 and G10 systems, because of more complementary bases in the thiolated DNA than G5, the background current of G7 was above baseline level. Even with the short DNA competitor utilized in G10 system, at higher concentration of MB-DNA, both signal and background formed rapidly. After comparing G5, G7, and G10 systems, we choose G5 for further experiments, since G5 allowed a short measurement time without sacrificing signal current. Furthermore, the G5 system is simpler to implement than the G10 system, since a short DNA competitor was not required.

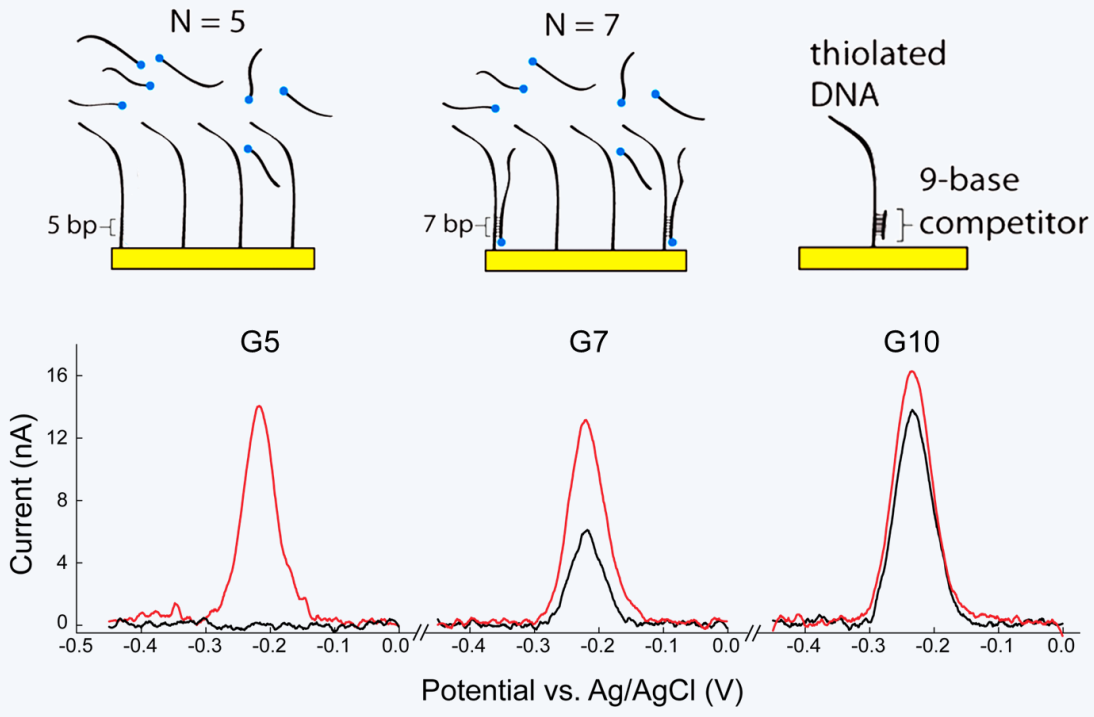

Figure 5-3: Comparisons of the signal and background responses of the G5, G7, and G10 with C9 competitor systems in DNA-based model for reusable ECPA. Experiments confirmed that the background current of G5 system could keep at the baseline level, while the signal current could be increased at high concentration of MB-DNA.

5.6 Regeneration comparisons between uracil enzyme and several general methods

Before making the decision of using the uracil excision enzymes as a regeneration reagent, we compared it with other methods such as water rinse and water or HEPES/$NaClO_4$ buffer bath at 37 ℃. Figure 5-4 shows the comparison results. The red line in Figure 5-4 shows the signal current of 10 nM thrombin measured with 10 nM THRaptA, 15 nM THRaptB and 50 nM MB-DNA in HEPES/$NaClO_4$ buffer at the 3-min time point. The pink curve shows the result after a 7-min soak in HEPES/$NaClO_4$ buffer at 37 ℃. The signal current went down to 80% of original value. In work by the Plaxco group, E-AB sensors could be regenerated by washing for ~30s in room temperature-deionized water[24]. However, this water flow method was not sufficient for our ECPA system. The regeneration result of water rinse in our experiment is shown by the blue curve, where the current value was about 35% of the original one, which means only about 65% of the five-part cooperative complex was denatured. The green curve shows the result of immersing the sensor in 37 ℃ warm water for 7 min, which can denature 80% of cooperative complex. The black line shows the electrode regeneration

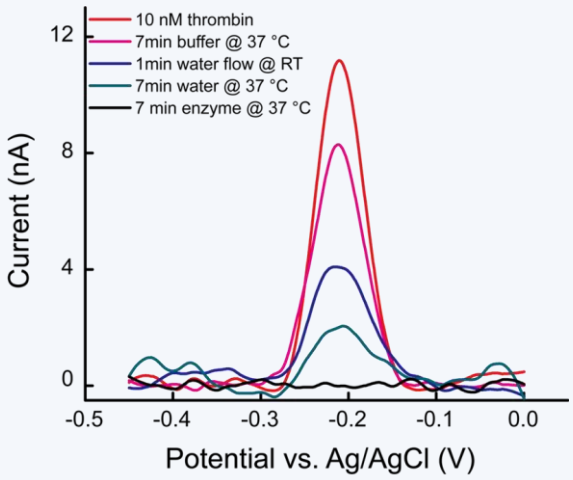

Figure 5-4: Regeneration comparisons between uracil enzyme and several general methods.

result using uracil-DNA excision mix, indicating that this approach is far superior to the other approaches for regenerating the biosensor surface in ECPA.

5.7 Aptamer-Based reusable ECPA

A schematic of aptamer-based reusable ECPA is shown in Figure 5-5A (inside figure). Two thrombin aptamers (THRaptA, THRaptB) that bind thrombin at different sites were applied as affinity probes. Using conditions optimized by the model system, background levels were measured in the absence of target protein (human thrombin). Similar to the model system, background remained at baseline current at the 3 min time point. Figure 5-5A shows the background with no thrombin (black trace) and typical MB oxidation peaks appearing at −210 mV in the presence of various amount of thrombin measured at 3 min time point. Seven current signals of various concentration of thrombin (from 0 to 10 nM) were measured by seven sensors, which were prepared under the same condition. Each sensor was regenerated seven times, so signal currents of 7 different concentrations of thrombin were measured by every sensor. Figure 5-5B shows this reusable aptamer-based ECPA system calibrated versus thrombin concentration with each sensor response recorded as integrated MB peak areas from −330 to −100 mV. The curve with error bars is the average value of 7 sensors (dash line). It is noteworthy that 150 pM is clearly not at the detection limit of the reusable ECPA. This result was also very promising in that electrode surface preparation proved to be highly consistent. Calibrations from seven differently-prepared electrodes were statistically equal.

The next step was to test how many times the sensor can be regenerated with reusable ECPA. In order to ensure reliability, two sensors with two different

concentrations of thrombin were chosen to test this experiment. The signal of both sensors starts to decrease after 19 times regeneration by uracil-DNA excision enzyme (Figure 5-5C).

To demonstrate specificity and sustainable signal reproducibility, the reusable ECPA was challenged with nonspecific proteins including human IgE, insulin, and BSA by using only one sensor. In Figure 5-5D, the signal of four measurements (first, second, ninth, and tenth) was 5 nM thrombin, the signal of four measurements (fifth, sixth, thirteenth, and fourteenth) was 5 nM thrombin in 3% BSA. Figure 5-5D shows that essentially no response was observed in the presence of 15 nM IgE (eleventh, twelfth) or insulin (fifteenth, sixteenth); even with 3-fold lower thrombin (5 nM), the signal was ~ 65 – 95-fold larger than that of IgE or insulin. In addition, the signal of ninth and tenth measurements of thrombin was 94% of the first and second measurements, the same situation for 5 nM thrombin in 3% BSA, showing good signal recovery. Furthermore, baseline current was observed in the presence of 3% BSA, while the signal from 5 nM thrombin was recovered by 92% in 3% BSA. This result is encouraging for future application of reusable ECPA to continuous measurement of biological samples and possibly for point-of-care settings.

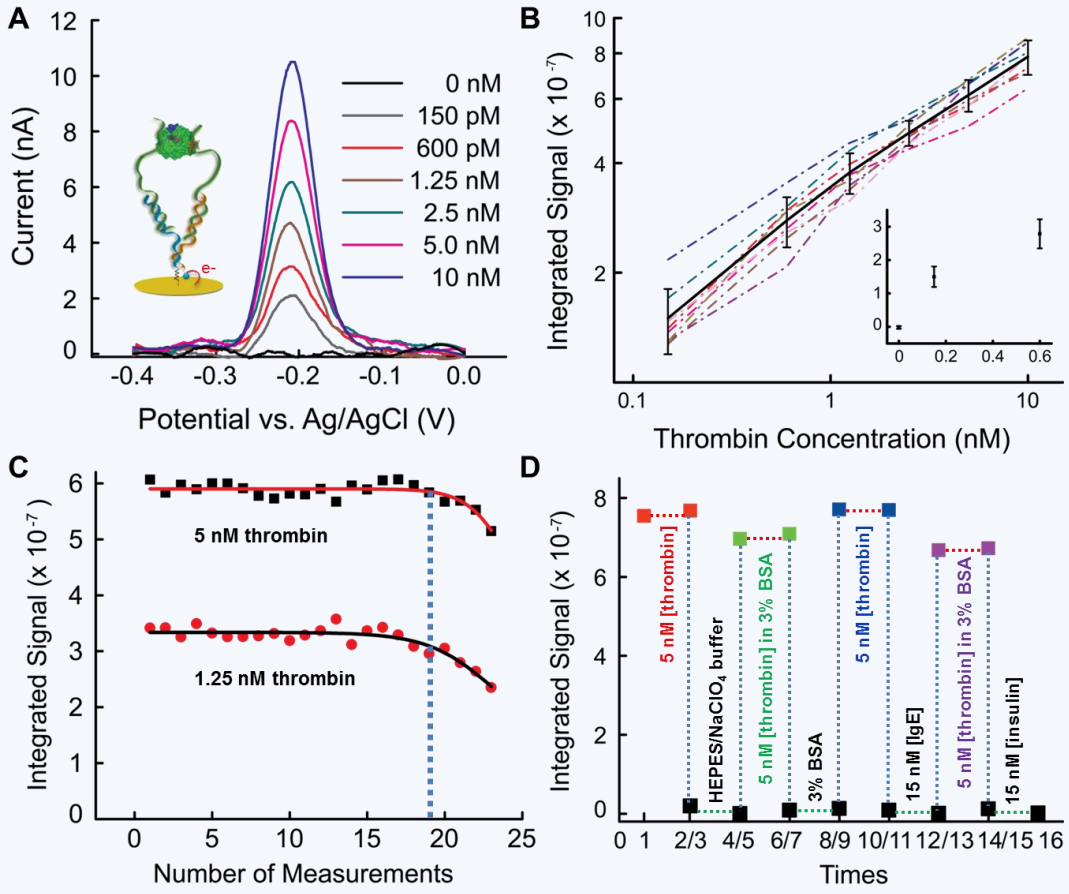

Figure 5-5: Aptamer based reusable ECPA. (A) Current changes under different concentrations of thrombin in pM to nM range. (B) Seven different electrodes generated similar calibration curves. The thrombin limit of detection was 150 pM with reusable ECPA. (C) 1.25 and 5 nM thrombin were chosen to test regeneration. A single electrode can be reused 18 times without loss of signal. (D) A single electrode test shows high selectivity throughout regeneration steps.

5.8 Antibody-Based reusable ECPA

The flexibility of the aptamer-based approach is limited because of the requirement of two aptamers for the target protein, since aptamer pairs exist only for a few select proteins. The use of antibody-oligonucleotide conjugates as probes can overcome this challenge.[26,27]

A schematic of antibody-based reusable ECPA is shown in Figure 5-6A (inside figure). A different set of conditions were determined for this antibody-based assay. We adopted a cyclic protocol, and insulin standard solutions were incubated at 37 ℃ to ensure relevance to secretion sample measurements from pancreatic islets. Since we used 50 nM of each antibody-oligo and 50 nM MB-DNA, the assay showed a higher signal than the model system (10 nM loop and 50 nM MB-DNA). Figure 5-6A shows the background with no insulin (black trace) and typical MB oxidation peaks appearing at −210 mV in the presence of various amount of insulin measured at 3 min time point (at 37 ℃). This antibody-based reusable ECPA system was then calibrated versus insulin concentration (Figure 5-6B), with response recorded in 7 sensors as integrated MB peak areas from −330 to −100 mV. Remarkably, using a direct electrochemical readout, ECPA was capable of detecting insulin levels as low as 100 fM with a dynamic range extending to 6.25 nM. The number of possible regenerations of antibody-based reusable ECPA is 17 times (Figure 5-6C). The selectivity of antibody-based reusable ECPA was tested against insulin-like growth factor 1 (IGF-1), which has similar structure to insulin, and against C-peptide, which is co-secreted with insulin into the bloodstream. As expected, the sensor did not respond significantly to higher concentrations of either IGF-1 or C-peptide (Figure 5-6D).

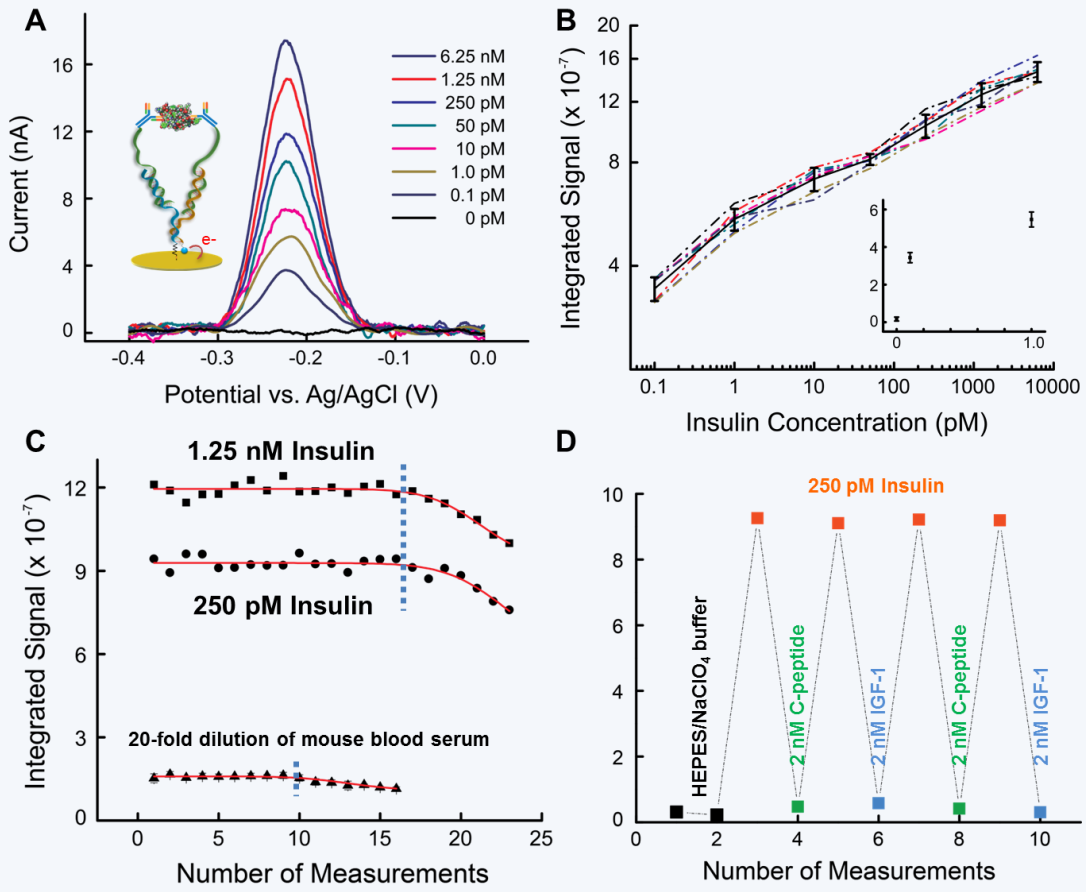

Figure 5-6: Antibody based reusable ECPA. (A) Current changes under different concentrations of insulin in fM to nM range. (B) Seven different electrodes generated similar calibration curves. The insulin limit of detection was 100 fM with reusable ECPA. (C) 1.25 and 0.25 nM insulin were chosen to test regeneration. A single electrode can be reused 17 times without loss of signal. (D) A single electrode test shows high selectivity throughout regeneration steps.

5.9 Temporal Measurement of Hormone Secretion from Endocrine Tissue

In order to monitor secretions from pancreatic islets, we cannot add antibody-oligonucleotide conjugates into the same solution with pancreatic islets as we did in the aptamer-based reusable ECPA system. First, the insulin antibodies have been shown to bind pancreatic islets, not just insulin in solution, which can affect the function of the cells. Second, we want to continuously monitor the secretion changes from pancreatic islets in real-time, not just make a one-time measurement. A schematic of the cyclic methodology of antibody-based reusable ECPA used for measurement of secretions from pancreatic islets is shown in Figure 5-7A. In this cycle, 10 μL of oligo-modified Ab1 solution was first dropped on the gold surface of the pre-fabricated sensor and incubated for 3 min. After washing, the sensor was loaded into a tube containing pancreatic islets at 37 ℃ (using a heat block). At this time, some of the secreted insulin molecules would bind with Ab1, staying on the sensor surface. Next, the electrode was washed briefly in HEPES/$NaClO_4$ buffer. The third step included pipetting 10 μL of oligo-modified Ab2 solution onto the sensor surface and incubating for 3 min. The sensor was then placed into 50 nM MB-DNA solution, at which time the signal current was measured after 3 min. Finally, after measurement, the sensor was enzymatically regenerated in uracil-DNA excision mix solution to prepare for the next time measurement.

Figure 5-7B shows quantitation of insulin secretion from living pancreatic islets (two different mice) using antibody-based reusable ECPA, during basal (3 mM) and stimulatory (11 mM) glucose levels. The reported signal here is integrated current change versus time. Sensor responses were recorded as integrated MB peak areas from −330 to −100 mV, then each point was subtracted from its subsequent measurement in time. The

first 3 measurements were made at 37 ℃ with islets experiencing basal glucose levels (3 mM). Immediately following the 3rd measurement, glucose was increased to 11 mM. As expected, an increase was observed on the 4th measurement after changing from 3 to 11 mM glucose. This "spike" in insulin was expected and is shown as the third current difference data point in all data sets shown in Figure 5-7B. With the group of 5 islets, the integrated signal increased from 132 to 212 nA(80 nA spike). With the groups of 15 islets, the integrated signal spike was from 266 to 505 nA (239 nA spike) and 272 to 491 nA (219 nA spike), respectively. The integrated signal current of control measurements of 50 pM insulin in the buffer with 3 mM glucose was 239 nA, which falls between the signals measured from 5 islets and 15 islets.

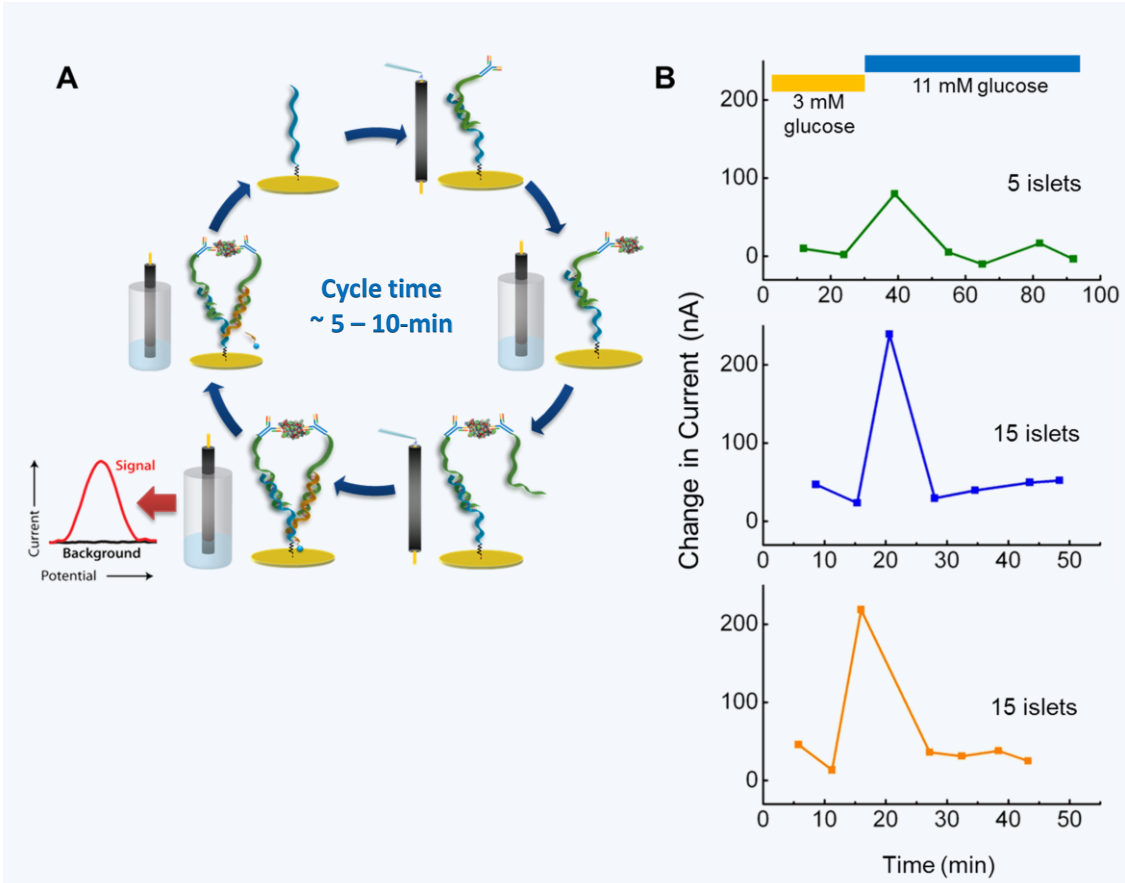

Figure 5-7: Temporal measurement of hormone secretion from endocrine tissue via reusable ECPA. (A) This cyclic protocol allowed insulin secretion measurements from pancreatic islets at 37 °C. (B) Insulin secretion measurements by antibody based reusable ECPA from living pancreatic islets (2 different mice), during basal (3 mM) and stimulatory (11 mM) glucose levels.

5.10 Measurement of Insulin from Murine Blood Serum

The same cyclic methodology as used in measurement of hormone secretions was also adopted in the insulin measurement from murine blood serum. Since various enzymes are present in serum, especially DNases, we need to inhibit the enzymes' activities to avoid degradation of DNA strands used in our assay. For this reason, the second step of loading the sensor into the blood serum sample in the cyclic protocol was performed on ice, keeping the temperature around 0 ℃. Figure 5-8A shows that a single electrode can be reused ~9 times without loss of signal in 20-fold dilution of blood serum. Figure 5-8B shows insulin quantitation in blood serum from two different mice (C57BL/6J), in 20-fold diluted serum samples. The concentration of insulin in blood serum was measured by standard addition of fixed amounts of insulin into the serum sample. This way, the measured insulin concentrations were 120 and 140 pM, separately for the two blood samples. The published result of insulin concentration in the blood of normal C57BL/6J mice was 16.4 ± 4.5 mU/ml (113.8 ± 31.2 pM).[28] This result proved that our reusable ECPA approach could be used successfully to quantify proteins in complex biological samples such as serum. The results bode well for the possible use of ECPA in clinical research or integrated with medical devices applied in point-of-care settings.

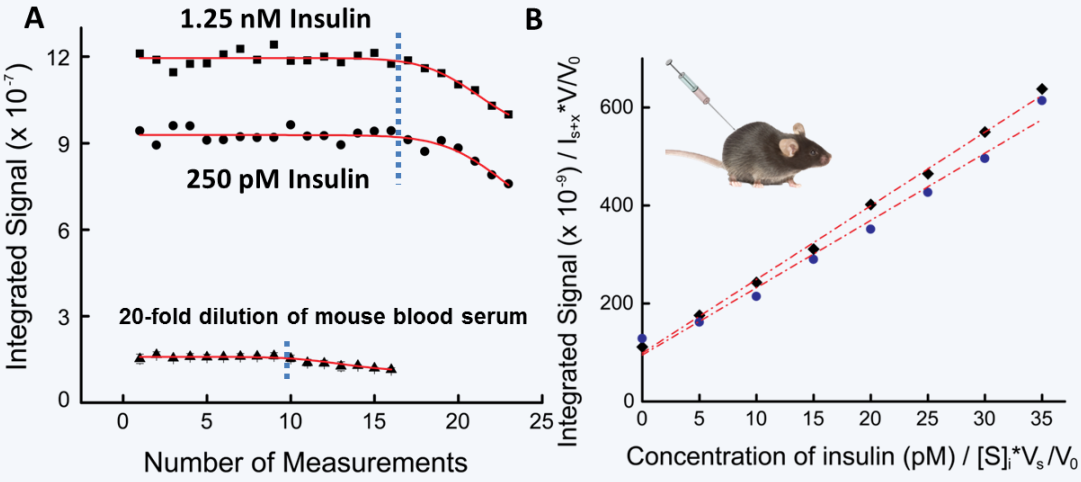

Figure 5-8: Insulin measurements from murine blood serum. (A) single electrode can be reused 9 times without loss of signal in 20-fold dilution of blood serum performed on ice (0 - 4 ° C) (B) Insulin measurements of blood serum from two different mice (C57BL/6J), 20-fold dilution in HEPES/$NaClO_4$ buffer. The measured insulin concentrations were 120 and 140 pM separately.

5.11 Characterization by surface plasmon resonance

We have begun characterization of our electrochemical proximity assay with surface plasmon resonance (SPR). SPR has several advantages that the electrochemical detection method does not have, such as real-time sensing and label free nature. As noted, to make our ECPA biosensor, we first need to prepare DNA monolayers on the gold electrode surface. We hypothesized that monolayer formation of thiolated-DNA on gold surface would be faster in a flowing system. Using an SPR system with our collaborator, Dr.

Simonian (Materials Engineering, Auburn University), the flow rate was first set at 2 μL min^{-1} for 60 min of continuous flow of running buffer through flow cell for stabilization of the gold surface. When the signal of gold surface was stable, we then switched to the sample channel, and the thiolated-DNA solution was pumped into the flow cell. Figure 5-9A shows real-time interrogation of self-assembled monolayer (SAM) formation at the gold surface at different concentrations of thiolated-DNA. As we expected, the self-assembled monolayer was formed faster than that under static mode. Usually in ECPA, for DNA monolayer assembly on the gold electrode surface, the electrode was incubated for 16 h at room temperature in the dark, since optimization experiments had not been peformed. In Figure 5-9A, after 500 s continuous flow of 1 μM thiolated-DNA, 95% of gold surface was covered. For 0.3, 0.1, and 0.03 μM thiolated-DNA, coverage required 2000 s, 2500 s, and 5000 s respectively. For saving reagents yet maintaining rapid SAM formation, we chose the 0.1 μM thiolated-DNA for future monolayer formation. The total amount of thiolated-DNA used to cover 95% of the surface was ~ 8.3 pmol at 2 μL min^{-1} flow rate. However, the total amount of thiolated-DNA used in ECPA was 200 pmol. In the experiments shown by Figure 5-9B, 0.1 μM thiolated-DNA was flowed through first to form a monolayer on the gold surface, and after reaching equilibrium, we switched to the buffer channel for rinsing physically absorbed thiolated-DNA. This rinsing resulted in aslightly reduced response. The DNA Loop model of ECPA signal, consisting of 15 nM loop and 15 nM MB-DNA, was then added. The figure clearly shows the response values increased in the presence of the loop model solution. These preliminary results are encouraging for future experiments in optimizing the timing and kinetics of ECPA, as well as for fundamental characterization of the electrode surface preparation in ECPA.

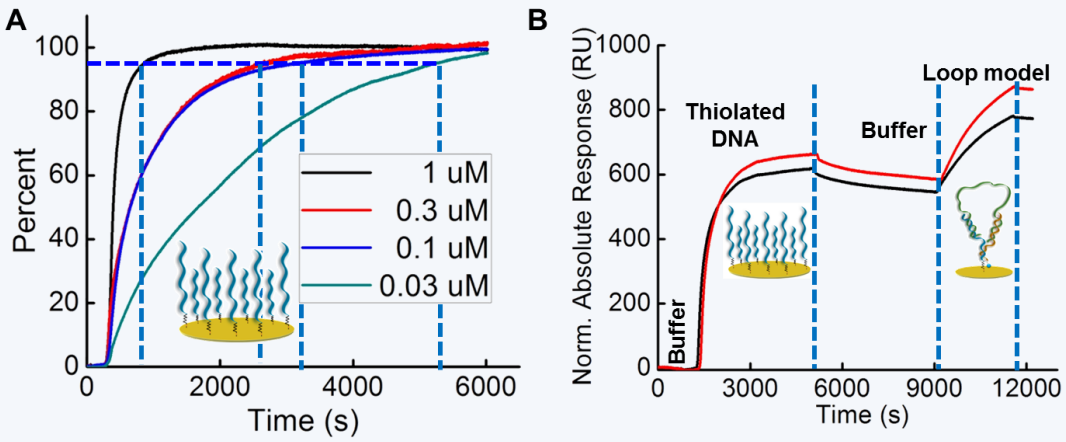

Figure 5-9: Characterization of ECPA with surface plasmon resonance (SPR). (A) The figure shows real-time interrogation of self-assembled monolayer (SAM) formation at the gold surface at different concentrations of thiolated-DNA. (B) Real-time sensing of SAM forming, buffer rinsing, and loop model binding with thiolated-DNA.

5.12 Conclusions

In this chapter, I described the development of reusable ECPA, which overcomes limitations of standard ECPA, namely the slow measurement time and the slow electrode regeneration steps. A DNA-based experimental model was used to optimize the assay format, and uracils were incorporated into selected probe strands, making the assay reusable after a simple enzymatic surface "cleaining." Aptamer-based reusable ECPA clearly showed faster measurement without significant loss of sensitivity, and selectivity was again confirmed for thrombin against IgE, insulin, and BSA. Furthermore, the faster measurement with antibody-based reusable ECPA made it possible to monitor secretions from pancreatic islets in near real-time. Finally, insulin quantitation in murine blood serum further proved this assay could be highly useful in clinical research.

Due to its high sensitivity, direct-readout format, and flexibility to assay multiple targets, ECPA has good potential for quantitation of a variety of proteins in clinical laboratories, research laboratories, or at the point-of-care. Reusable ECPA is faster and easier to implement than standard ECPA, while maintaining high sensitivity and selectivity. The reusable version of ECPA should be more useful in research settings, such as secretion sampling or high-throughput screening applications.

5.13 References

(1) Hay Burgess, D.; Wasserman, J.; Dahl, C. *Nature* **2006**, *444*, 1-2.
(2) Yager, P.; Domingo, G. J.; Gerdes, J. *Annual Review of Biomedical Engineering* **2008**, *10*, 107-144.
(3) Martinez, A.; Phillips, S. T.; Whitesides, G. M.; Carrilho, E. *Anal. Chem.* **2010**, *82*, 3−10.
(4) Burtis, C. A.; Ashwood, E. R. Tietz Textbook of Clinical Chemistry; Saunders: Philadelphia, PA, **1999**.
(5) Rusling, J. F.; Kumar, C. V.; Gutkind, J. S.; Patel, V. *Analyst* **2010**, *135*, 2496−2511.
(6) Wang, J. *Biosensors and Bioelectronics* **2006**, *21*, 1887-1892.
(7) Sorell Go´mez, L.; Rojas, G. *Clin. Chim. Acta* **1997**, *260*, 65−71.
(8) Jung, K.; Zachow, J.; Lein, M.; Brux, B.; Sinha, P.; Lenk, S.; Schnorr, D.; Loening, S. A. *Urology* **1999**, *53*, 155−160.
(9) Stivers, C. R.; Baddam, S. R.; Clark, A. L.; Ammirati, E. B.; Irvin, B. R.; Blatt, J. M. *Diabetes Technol. Ther.* **2000**, *2*, 517−526.
(10) Davies, S; Byrn, F; Cole, L. A. *Clin. Lab. Med.* **2003**, *23*, 257−264.
(11) Seamark, D. A.; Backhouse, S. N.; Powell, R. *Ann. Clin. Biochem.* **2003**, *40*, 178−180.
(12) Drummond, T.; Hill, M. G.; Barton, J. K. *Nature Biotechnol.* **2003**, *21*, 1192-1199.
(13) Plaxco, K. W.; Soh, H. T. *Trends in Biotechnology* **2011**, *29*, 1-5.
(14) Cagnin, S.; Caraballo, M.; Guiducci, C.; Martini, P.; Ross, M.; SantaAna, M.; Danley, D.; West, T.; Lanfranchi, G. *Sensors* **2009**, *9*, 3122-3148.
(15) Xia, F.; White, R. J.; Zuo, X.; Patterson, A.; Xiao, Y.; Kang, D.; Gong, X.; Plaxco, K. W.; Heeger, A. J. *J. Am. Chem. Soc.* **2010**, *132*, 14346-14348.
(16) Kang, D.; Zuo, X.; Yang, R.; Xia, F.; Plaxco, K. W.; White, R. J. *Anal. Chem.* **2009**, *81*, 9109-9113.
(17) Zuo, X.; Xiao, Y.; Plaxco, K. W. *J. Am. Chem. Soc.* **2009**, *131*, 6944-6945.
(18) Baker, B. R.; Lai, R. Y.; Wood, M. S.; Doctor, E. H.; Heeger, A. J.; Plaxco, K. W. *J. Am. Chem. Soc.* **2006**, *128*, 3138-3139.
(19) Xiao, Y.; Lubin, A. A.; Baker, B. R.; Plaxco, K. W.; Heeger, A. J. *Proc. Natl. Acad. Sci. USA* **2006**, *103*, 16677-16680.
(20) Liu, Y.; Tuleouva, N.; Ramanculov, E.; Revzin, A. *Anal. Chem.* **2010**, *82*, 8131–8136.
(21) Hu, J.; Wang, T.; Kim, J.; Shannon, C.; Easley, C. J. *J. Am. Chem. Soc.* **2012**, *134*, 7066-7072.
(22) Fredriksson, S.; Gullberg, M.; Jarvius, J.; Olsson, C.; Pietras, K.; Gústafsdóttir, S. M.; Östman, A.; Landegren, U. *Nature Biotechnol.* **2002**, *20*, 473-477.
(23) Kim, J.; Hu, J.; Sollie, R. S.; Easley, C. J. *Anal. Chem.* **2010**, *82*, 6976-6982.

(24) Xiao, Y.; Lai, R. Y.; Plaxco, K. W. *Nat. Protocols* **2007**, *2*, 2875-2880.
(25) Rowe, A. A.; Chuh, K. N.; Lubin, A. A.; Miller, E. A.; Cook, B.; Hollis, D.; Plaxco, K. W. *Anal. Chem.* **2011**, *83*, 9462-9466.
(26) Gullberg, M.; Gustafsdottir, S. M.; Schallmeiner, E.; Jarvius, J.; Bjarnegård, M.; Betsholtz, C.; Landegren, U.; Fredriksson, S. *Proc. Natl. Acad. Sci. U.S.A.* **2004**, *101*, 8420−8424.
(27) Heyduk, E.; Dummit, B.; Chang, Y. H.; Heyduk, T. *Anal. Chem.* **2008**, *80*, 5152−5159.
(28) Surwit, R. S.; Kuhn, C. M.; Cochrane, C.; McCubbin, J. A.; Feinglos, M. N. *Diabetes* **1988**, *37*, 1163-1167.

CHAPTER 6

Future Directions

6.1 Future Portable Electronic Device

Based on the electrochemical proximity assay (ECPA) presented in Chapters 4 and 5, it is feasible to envision that ECPA could be integrated with portable electronic devices and applied in point-of-care settings. In terms of protein quantitation, a standard antibody-based ECPA has been proven to detect insulin as low as 20 fM by introducing a short DNA competitor. The reusable version of ECPA has proven that a single electrode can be regenerated and reused 18 times without loss of signal. Selectivity tests based on thrombin aptamers in reusable ECPA again showed high selectivity and high signal recovery. The signal of 5 nM thrombin was ~ 65 to 100-fold larger than that of 15 nM IgE or insulin. And the signal of 5 nM thrombin was recovered by over 90% in 3% BSA. These results strongly encouraged future applications to biological samples and blood serum tests. It was shown that it is possible to build a cyclic protocol for insulin secretion measurements from pancreatic islets on a chip. With this in mind, Figure 6-1 shows a proposed integrated electronic device including 10 sensor sets, each set containing one reference electrode, one counter electrode, and three gold working electrodes. Each set stays in a reservoir for 3 min, then is clockwise rotated to the next reservoir. Based on the

result of regeneration test from aptamer based reusable ECPA, a single electrode could be regenerated and reused for 18 times. Thus, the proposed chip could complete 180 individual measurements, each results being an average of signal from the 3 electrodes shown in the inset at the top right of the figure.

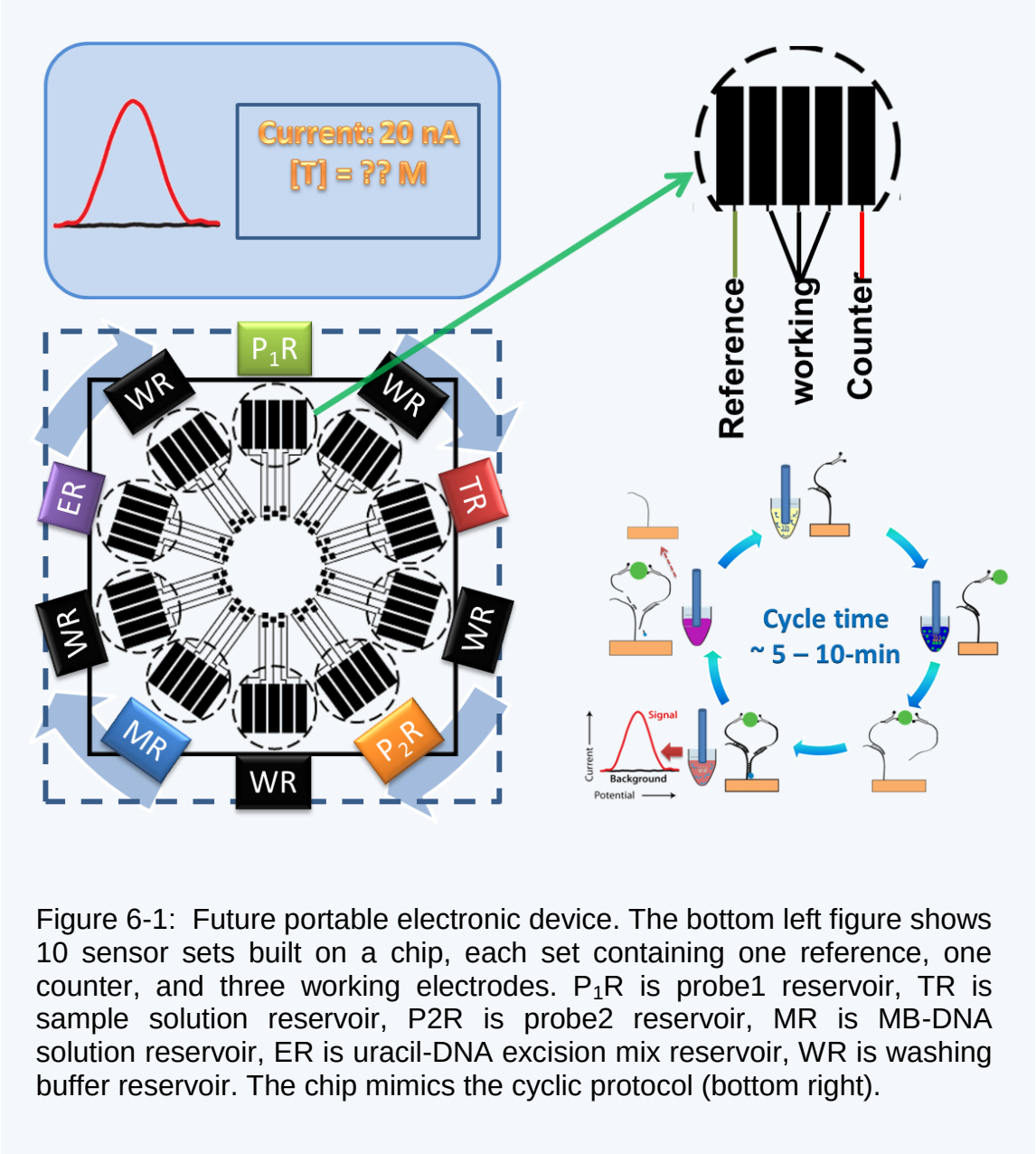

Figure 6-1: Future portable electronic device. The bottom left figure shows 10 sensor sets built on a chip, each set containing one reference, one counter, and three working electrodes. P_1R is probe1 reservoir, TR is sample solution reservoir, P2R is probe2 reservoir, MR is MB-DNA solution reservoir, ER is uracil-DNA excision mix reservoir, WR is washing buffer reservoir. The chip mimics the cyclic protocol (bottom right).

6.2 Prospect of Detection Technology

Besides integrated with portable electronic devices, the reusable version of ECPA could also be useful in high-throughput screening applications, such as conjugating with HPLC fraction collectors or for drug discovery applications using 96-well plates with cells treated with different drugs (Figure 6-2).

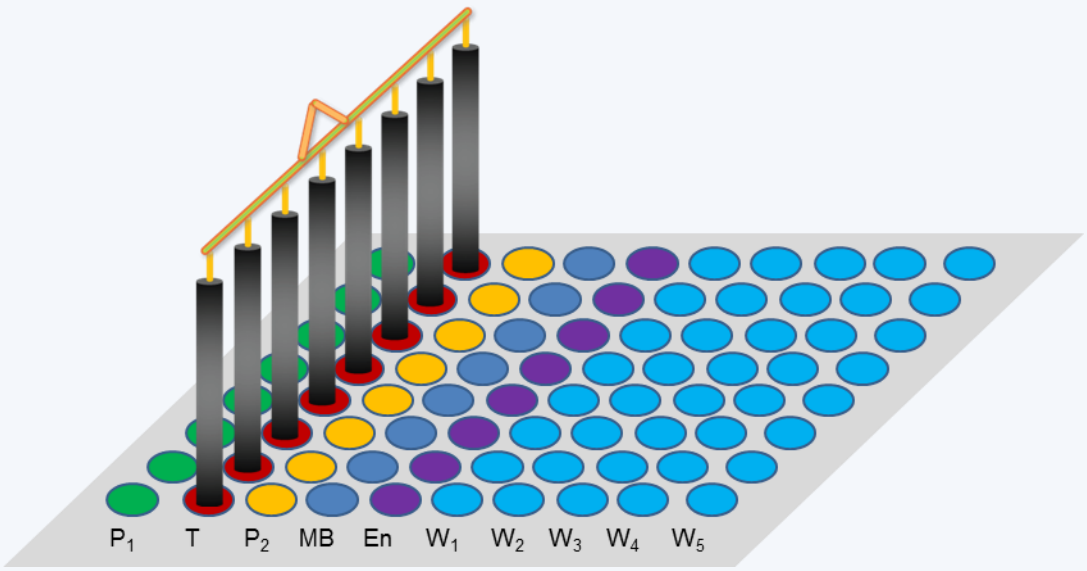

Figure 6-2: Reusable ECPA integration with high throughput well-plate formats: P_1 (probe1 well), T (collection sample wells), P_2 (probe2 wells), MB (MB-DNA & signal measurement wells), En (uracil-DNA excision mix wells), W_1 – W_5 (washing buffer wells).